SYNTHESIS, CHARACTERIZATION AND OPTIMIZATION OF TITANIUM PHOSPHATES DERIVED FROM SRI LANKAN ILMENITE BEACH SAND ENHANCED YIELD AND INDUSTRIAL-SCALE PRODUCTION

By

Kulathunga Malliyawadu Ushan Sameera

SYNTHESIS AND CHARACTERIZATION OF TITANIUM PHOSPHATES DERIVED FROM SRI LANKAN ILMENITE BEACH SAND FOR ENHANCED YIELD AND INDUSTRIAL SCALE PRODUCTION

DOCTORAL DISSERTATION

Submitted by

KULATHUNGA MALLIYAWADU USHAN SAMEERA
[Student ID No: 55145017]

Under the guidance of

ATUSHI KUBONO

(Professor, Department of Optoelectronics and Nanostructure Science, Shizuoka University, Hamamatsu Campus, Japan)

in partial fulfillment for the award of the degree
in
Doctor in Philosophy
In Engineering
of
Department of Optoelectronics and Nanostructure Science
Graduate School of Science and Technology
Shizuoka University

National University Corporation
Shizuoka University

2024

DECLARATION

The work described in this dissertation was carried out by me under the supervision of Prof. Atusushi Kubono and a report on this has not been submitted in whole or in part to any university or any other institution for anther Degree/Diploma.

Kulathunga Malliyawadu Ushan Sameera

TABLE OF CONTENTS

LIST OF FIGURES

ACKNOWLEDGMENTS

I would like to express my deepest gratitude to my supervisor; Prof. Atshushi Kubono sensei, and all the other co-supervisors, for their valuable guidance, consistent encouragement, personal caring, and timely help, and for providing me with an excellent atmosphere for doing research. All through the work, despite his busy schedule, they have extended cheerful and cordial support to me for completing this research work.

I specially extend my deepest gratitude to my first advisor, Prof. Masaru Shimomura sensei, for his continuous guidance, encouragement, and support throughout my doctoral journey at Shizuoka University. His wise advice and mentorship shaped my research and helped me complete this dissertation. Shimomura Sensei leadership and optimism have profoundly influenced me both academically and personally. And special thanks are due to Professor Nakamura sensei for his invaluable assistance and encouragement.

I would also like to thank, Prof. Pradeep Jayaweera, for their help and guidance during the course of my research work. I would also like to express my gratitude to my colleagues at Shimomura laboratory, Nakamura laboratory for their support and corporation during the past three years.

I would also like to express my sincere appreciation to the staff of the International Student Unit at Shizuoka University for their unwavering support in facilitating my PhD program. My heartfelt gratitude also goes to the SPRING fellowship for providing me with the opportunity to pursue my studies comfortably in Japan.

Lastly, I am deeply grateful to my family, especially my mother, past teachers, and friends for their boundless love and support throughout my academic journey.

Kulathunga Malliyawadu Ushan Sameera

ABSTRACT

This study investigates two methods for the synthesis of α-titanium phosphate (α-TiP) from ilmenite ($FeTiO_3$) ore: a direct digestion method using conc. H_3PO_4 and an alkali roasting method involving KOH treatment followed by an acid reaction step. The α-TiP products were characterized using X-ray Diffraction (XRD), Energy Dispersive X-ray Analysis (EDAX), Thermogravimetric Analysis (TGA), and Differential Scanning Calorimetry (DSC).

The direct digestion method yielded α-TiP with a low recovery of 17% and purity of 93 wt%. The alkali roasting method achieved a significantly higher α-TiP yield of 99.6 wt% but lower initial purity of 87 wt% due to higher iron impurities. Various purification strategies using concentrated H_3PO_4, HCl, and $H_2C_2O_4$ were explored to remove iron from the α-TiP obtained via alkali roasting.

H_3PO_4 washing effectively reduced the iron content from 3.5% to 0.4%, increasing the α-TiP purity to 99.8 wt% with a yield of 92.5 wt%. HCl washing showed lower iron removal efficiency (2.5% residual iron) and leached titanium into the solution, decreasing the yield to 76.6 wt%. $H_2C_2O_4$ washing achieved 85.7% iron removal but induced a chemical transformation of α-TiP to titanyl pyrophosphate $(TiO)_2P_2O_7$.

Thermal analysis revealed a two-stage decomposition of α-TiP, involving dehydration and pyrophosphorization to form TiP_2O_7, except for the $H_2C_2O_4$-washed sample, which exhibited a three-stage process. XRD confirmed the phase evolution from α-TiP to TiP_2O_7 upon heating and the formation of $(TiO)_2P_2O_7$ for the $H_2C_2O_4$-washed sample.

The fabrication of α-TiP on stainless steel mesh was successfully done in a very simple and cost-effective way which needs very lesser and inexpensive chemicals with less preparation time.

The fabrication of α-TiP on stainless steel mesh, particularly with the addition of a TiO_2 layer, represents a significant advancement in materials science and engineering. Its unique combination of properties, including robust adhesion, resistance to extreme conditions, and high surface area, position it as a versatile material with potential applications across numerous industries.

This comprehensive study provides insights into the synthesis, purification, and thermal behavior of titanium phosphate materials derived from ilmenite, highlighting the advantages and limitations of different approaches for efficient titanium recovery and product optimization and its applications.

CHAPTER 1
INTRODUCTION

1.1   Titanium Phosphates and their applications

1.1.1   Titanium Phosphates (TiPs)

Titanium phosphates (TiPs) constitute an intriguing class of inorganic compounds characterized by their notable structural versatility and multifaceted properties.[1] These materials exhibit a diverse array of structural configurations, ranging from layered to framework architectures, which significantly influence their overall functionality and potential applications.[2]

The layered structures of TiPs can be primarily classified into two categories based on the phosphorus-to-titanium ratio.[3]

(i)   Classical TiP

- alpha-TiP [α-TiP, $Ti(HPO_4).H_2O$]

- gamma-TiP [γ-TiP, $Ti(H_2PO_4)(PO_4).2H_2O$]

- beta-TiP [β-TiP, $Ti(H_2PO_4)(PO_4)$]

(ii)   Hydroxotitanium/titanyl type

- $Ti_2O_3(H_2PO_4)_2.2H_2O$

- $Ti(OH)_{1.2}(HPO_4)_{1.28}(H_2PO_4)_{0.24}.2.5H_2O$

- $Ti(OH)_{1.2}(HPO_4)_{1.4}.H_2O$

- $TiO(OH)(H_2PO_4).2H_2O$

- $TiO_{1.25}(OH)_{0.47}(H_2PO_4)_{0.77}(HPO_4)_{0.13}.2.3H_2O$

- $TiO_{0.11}(OH)_{0.58}(H_2PO_4)_{0.8}(HPO_4)_{0.2}.0.64H_2O$

The first category comprises the 2:1 compounds, wherein the structure consists of two phosphorus atoms per titanium atom.[4] An exemplary compound in this group is $Ti_2O_3(H_2PO_4)_2.2H_2O$, which features $TiO_3(H_2PO_4)_2$ layers separated by intercalated water molecules.[5] Thermal analysis of this material reveals a three-step weight loss pattern, indicative of the presence of distinct types of water molecules within the structural framework.[5,6]
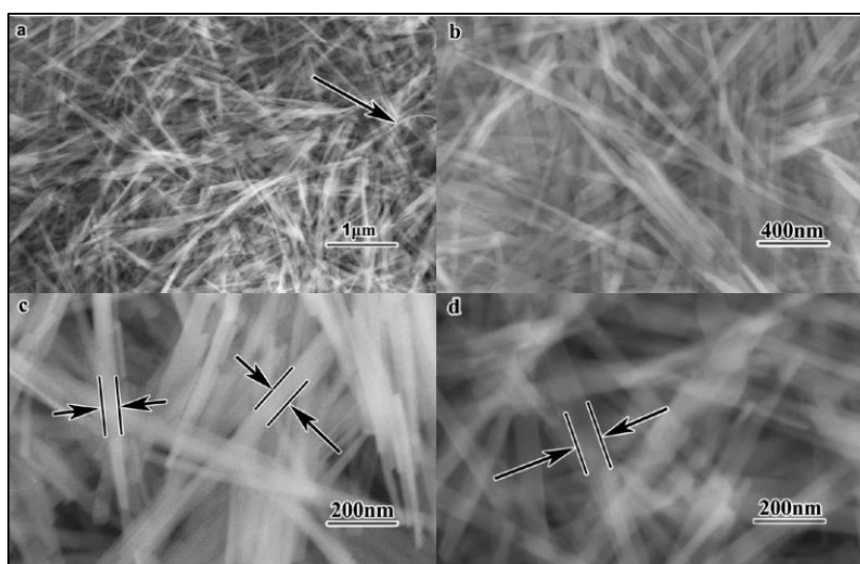
Figure 1.1: SEM images of $Ti_2O_3(H_2PO_4)_2 \cdot 2H_2O$ with different magnifications.

Source: Li, Wen, and Lin (2016)

In contrast, the 1:1 layered TiPs contain one phosphorus atom per titanium atom. A prominent representative of this class is the $TiO(OH)(H_2PO_4).H_2O$ (TiHP) phase, which exhibits a structure constructed from TiO_6 octahedra interconnected by phosphate groups.[7] This particular phase has garnered significant attention due to its exceptional sorption capacity towards Cs^+ and Sr^{2+} ions, rendering it a promising candidate for the remediation of complex radioactive liquid waste streams.[8]
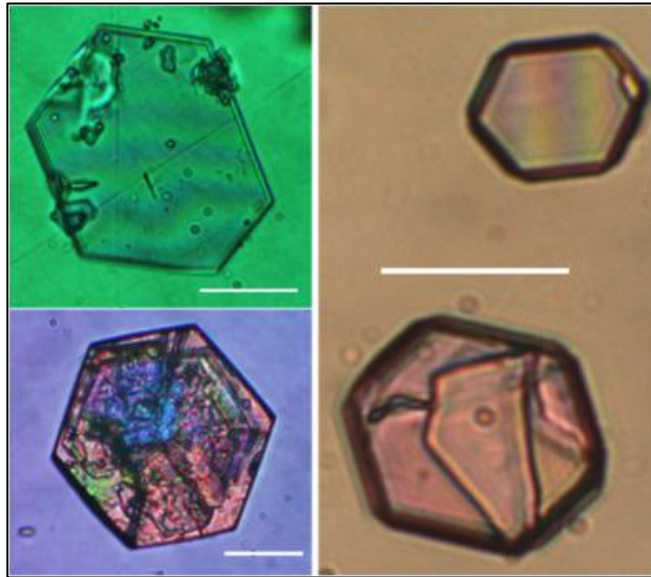
Figure 1.2: Polarization optical microscopy images for single crystals of α-Ti(HPO$_4$)2H$_2$0.

Source: Amghouz, Mendoza and Adawy (2023)

Beyond the layered structures, TiPs can also adopt framework configurations, which can be further classified as fibrous or three-dimensional in nature.[9] These framework architectures often involve the intricate linkage between the oxygen atoms of the phosphate groups and the titanium centers, resulting in a diverse range of structural motifs.[10]
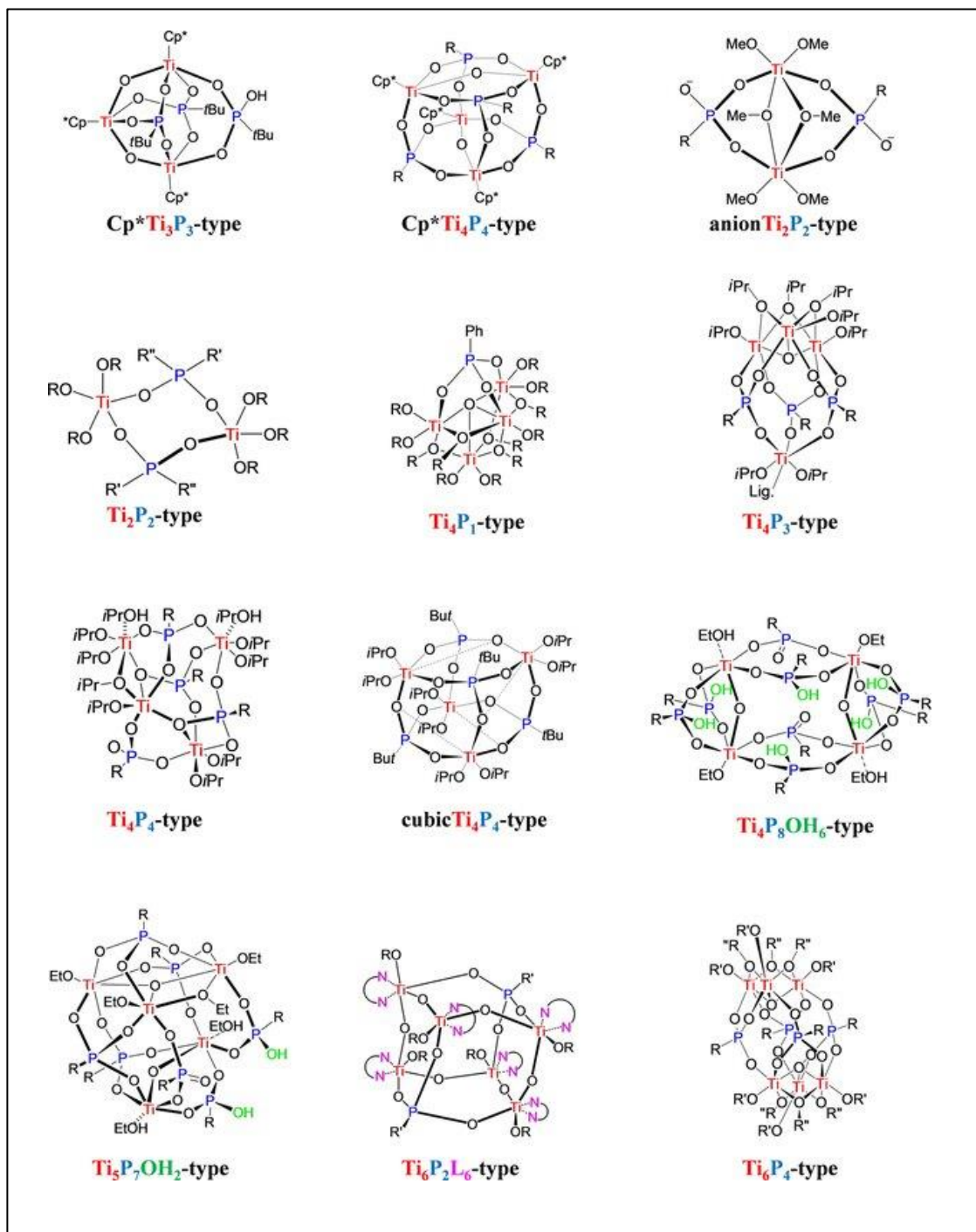
Figure 1.3: Structures of titanium phosphonate clusters.

Source: Hayami and Gunji (2021)

The structural versatility of TiP does not end there, as the incorporation of additional elements, such as copper, can lead to the formation of composite materials with enhanced properties. For instance, titanium phosphate copper hexacyanoferrate composites have been synthesized and demonstrated their potential for the efficient removal of metal ions from aqueous solutions.[5,8]

The synthesis of TiPs typically involves the reaction between H_3PO_4 or phosphate salts and titanium-based precursors, including titanium oxides, alkoxides, or salts like $TiCl_4$. These synthetic approaches have undergone continuous refinement to improve efficiency and reduce production costs, making TiP materials more accessible for various applications.[12]

An intriguing aspect of TiPs is their amphoteric behavior, with the ion exchange process primarily driven by the protons within the phosphate groups.[3] This property has led to the exploration of TiPs as selective sorbents for transition metal ions in aqueous environments, highlighting their potential in wastewater treatment and metal recovery applications.[3,13]

1.1.2 Applications of TiPs

The structural complexity and versatility of TiPs encompass layered, framework, and composite architectures. These inorganic materials have attracted significant attention due to their unique ion exchange and sorption properties and have demonstrated their utility across various fields, including wastewater remediation, ion exchange, sorbents for radioactive waste, electrochemical applications, catalysis, and proton conductors.

(i)   Wastewater Remediation:

TiPs-based composites have been extensively studied for their ability to selectively adsorb and sequester a range of heavy metal ions, making them valuable tools for wastewater treatment and environmental remediation. For example, phosphate-modified TiO_2 (TiPh) synthesized from titanium (IV) isopropoxide in aqueous H3PO4 solution adsorbed onto the TiPh surface followed the sequence $Cu^{2+} > Co^{2+} > Ni^{2+}$ in different media such as water, alcoholic solutions, and aqueous-alcoholic solutions. The adsorption equilibrium between the metal species and the TiPh matrix occurs after 10-40 minutes.[14] Additionally, titanium oxide has been used as a solid-state catalyst in the synthesis of titanium phosphate copper hexacyanoferrate composites, which have shown potential for the removal of metal ions from aqueous solutions.[2]

(ii)   Ion Exchange:

These inorganic compounds have demonstrated a high affinity towards transition metal ions in aqueous solutions, highlighting their potential applications in ion exchange processes, water purification, and metal recovery.[2] Furthermore, spherically granulated TiPs have been utilized for commercial production in liquid radioactive waste treatment systems, with its ion-exchange capacity studied in detail and exhibiting high-performance properties for the removal of toxic heavy metals such as Pb^{2+} and Zn^{2+}.[15,16]

(iii)   Sorbents for Radioactive Waste:

Certain TiP phases, such as $TiO(OH)(H_2PO_4).H_2O$ (TiHP), have exhibited remarkably high sorption capacities towards radioactive cesium (Cs^+) and strontium (Sr^{2+}) ions. This unique characteristic makes them promising candidates for the treatment of complex liquid radioactive waste streams.[2,15]

(iv)   Electrochemical Applications:

TiPs have been investigated for their electrochemical properties, potentially useful as electrode materials in batteries.[2] These thin films of titanium TiPs can be synthesized through the spin coating of colloidal solutions, and these films might find applications in various fields such as electro-optic materials, optical fibers coatings, or ionic conductors for microionic applications.[17]

(v)   Catalysts:

TiP-based materials have been explored as solid-state catalysts, demonstrating their versatility in facilitating a range of chemical reactions.[18] For instance, titanium phosphate copper hexacyanoferrate composites have been synthesized using titanium oxide as a catalyst, showcasing their potential in catalytic applications.[2]

(vi)   Proton Conductors:

Certain TiP compositions have been identified as potential candidates for proton-exchange membranes, highlighting their possible applications in energy-related technologies, such as fuel cells. Structural and conductivity studies of fibrous π-$Ti_2O(PO_4)_2.2H_2O$ have further expanded the understanding of TiP materials as proton conductors, with applications in chitosan-based composite membranes.[7, 15]

The diverse applications of TiPs are a testament to their structural complexity and the ability to tailor their properties through careful synthesis and compositional modifications. As research in this field continues to evolve, the full potential of these remarkable inorganic compounds is expected to be further explored and exploited across a wide range of industries and technological domains.

1.1.3 Advantages of TiPs

(i) Ease of Preparation

TiPs can be easily prepared using various methods, including, (a) hydrolysis reaction of H_3PO_4 or phosphate salts with titanium or titanium-based materials; (b) hydrothermal synthesis using use of titanium sources, such as titanium sulfate, and reacting them under controlled temperature and pressure in an aqueous solution to form nanocrystalline anatase, brookite, and layered titanium phosphate; (c) solid-state synthesis using a liquid titanium source, such as aqueous titanium oxysulfate $[TiOSO_4(H_2SO_4)_x]$, and H_3PO_4; (d) bottom-up approach by reacting titanium isopropoxide (TIP), H_3PO_4, and ammonium hydroxide (NH_4OH) in aqueous sols. This adaptability in synthesis routes allows for the production of these materials using relatively straightforward and accessible techniques.[2,12,19]

(ii) Amphoteric Behavior and Ion Exchange Capacity

TiPs exhibit amphoteric behavior due to the presence of protons within the phosphate groups, which are responsible for the ion exchange process.[20] This property enables TiPs to be used as effective inorganic ion exchangers and sorbents, with high ion exchange capacity which applies in various fields, such as solid-state catalysts,

cathode materials in rechargeable batteries, or potential candidates for proton-exchange membranes in fuel cells.[4,20]

(iii)   Versatile Synthesis and Modification

TiPs can be synthesized using a range of precursors, such as titanium isopropoxide and H_3PO_4, and can be further modified by the addition of other materials to enhance their properties. This flexibility in synthesis and modification allows for the tailoring of titanium phosphates to meet specific application requirements. [12,19]

(iv)   Characterization Techniques

TiPs can be thoroughly characterized using various analytical techniques, including X-ray diffraction (XRD), high-resolution Transmission Electron Microscopy (TEM), Fourier-Transform Infrared Spectroscopy (FTIR), Thermogravimetric Analysis (TGA), Electron Paramagnetic Resonance (EPR), and 31P solid-state Nuclear Magnetic Resonance (NMR), to determine their composition and structure.[12,21,22,23,24,25] This comprehensive characterization enables a deeper understanding of the materials' properties and performance.

1.1.4   Drawbacks and Disadvantages of TiPs

(i)   High Energy Consumption and Preparation Cost

The preparation of TiPs often involves long procedures and harsh conditions, such as high pressure and temperatures. These requirements can lead to high energy consumption and increased production costs. For example, the synthesis of TiPs may require annealing at temperatures up to 800 °C to form the desired Ti^{3+}, which can significantly impact the overall energy usage and economic feasibility of the process.[4,26]

(ii)   Structural Complexity and Variability

TiPs can display a range of different structures, including amorphous, fibrous, layered (α-TiP and γ-TiP), and three-dimensional forms.[2,3] This structural complexity and variability can affect the materials' properties, such as ion exchange capacity, adsorption behavior, and stability. The specific structure obtained during the synthesis process can be challenging to control, leading to potential inconsistencies in the final product's performance. For instance, annealing the TiP samples at high temperatures (up to 1000 °C) resulted in the formation of a mixture of different phases, including TiO_2 and titanium oxide phosphate, further demonstrating the complexity of controlling the final structure.[12,27]

(iii)   Limited Adsorption Capacity

The adsorption capacity of TiPs can be influenced by their specific surface area and total pore volume.[12] Variations in these physical characteristics can result in inconsistent or suboptimal adsorption performance, limiting their effectiveness as sorbents for certain applications. Optimizing the synthesis conditions to achieve the desired surface area and pore structure can be a challenging task.[2,28]

(iv)   Influence of Crystal Structure

The crystal structure of TiPs can have a significant impact on their properties, such as conductivity and stability. Achieving the desired crystal structure during the synthesis process can be challenging, as it may require specific conditions, such as annealing to form the appropriate titanium cations. Variations in the crystal structure can lead to inconsistencies in the materials' performance, which can be a drawback for applications that require precise and predictable properties.[4, 12]

1.2   Enhanced Stability and Durability of Stainless-Steel Mesh Coatings

Stainless steel meshes are commonly used in a wide range of applications, from filtration systems to architectural design elements. The use of mesh structures offers several advantages, including increased surface area, improved fluid flow, and enhanced mechanical properties.[29, 30] Stainless steel is a widely used material in a variety of industries due to its excellent corrosion resistance, mechanical properties, and aesthetic appeal. However, even stainless steel can be susceptible to corrosion in certain harsh environments. To enhance the corrosion protection of stainless steel, researchers have explored the use of surface coatings and treatments.[30, 31] One promising approach is the incorporation of titanium into stainless steel mesh coatings, which has been shown to significantly improve the material's corrosion resistance.[32]

Titanium is a class of coatings that can significantly enhance the corrosion resistance of stainless-steel mesh.[32] These coatings are based on the formation of a layer on the surface of the stainless steel, which provides a protective barrier against corrosive elements.[33, 34]

Titanium coatings on stainless steel mesh can be applied using various methods, including immersion, spraying, or sponging.

Hydrothermal treatment: This method involves placing titanium discs into a mixed solution containing H_2O_2 and H_3PO_4 with different mass ratios and water content in a Teflon liner, which is then tightly sealed in an autoclave followed by hydrothermal treatment at different temperatures for 24 hours.[35]

Soaking process: This method involves improving the titanium implant surface roughness and chemistry by optimizing the surface preparation and the soaking process.[36] The titanium substrates are first prepared by sandblasting and acid etching to create a roughened surface. The prepared titanium substrates are then soaked in a phosphate solution, typically a 0.5 M solution of sodium phosphate ($Na_3PO_4 \cdot 12H_2O$), for 30 minutes at 37 °C. During the soaking process, a calcium phosphate coating is formed on the titanium surface. This coating helps improve the surface roughness and chemistry of the titanium implant. In some cases, a centrifugation step is included after the soaking process to create a more uniform phosphate coating on the titanium surface.[35,36,37]

Pulsed electrodeposition: This method involves synthesizing strontium-substituted calcium phosphate coatings by pulsed electrodeposition on titanium alloy (Ti_6Al_4V) with experimental conditions optimized to obtain a coating with a 5% atomic substitution of calcium by strontium.[38]

The application process typically involves the following steps:

Surface preparation: The stainless-steel mesh is first cleaned and prepared to ensure proper adhesion of the coating. This may involve removing any contaminants or oxides from the surface.[39]

Application of the phosphate solution: A dilute solution of H_3PO_4, possibly with soluble titanium or zinc salts, is applied to the stainless-steel mesh. The solution can be applied by immersion, spraying, or sponging.[39]

Reaction and coating formation: The phosphate solution reacts with the iron, zinc, or manganese in the stainless steel, forming a thin layer of iron, zinc, or manganese phosphates on the surface. This layer provides corrosion resistance and can serve as a foundation for subsequent coatings or painting.[39]

Adjustment of the coating: The coating can be adjusted by varying the bath concentration, composition, temperature, and time to achieve the desired crystal structure and thickness. A dense microcrystalline structure with a low porosity is usually best for corrosion resistance or subsequent painting.[39]

Post-treatment: After the coating has formed, the stainless-steel mesh can be subjected to additional treatments, such as annealing or heat treatment, to improve its properties and performance.[39]

The choice of application method and post-treatment depends on the specific requirements of the stainless-steel mesh and its intended use.[39]

The addition of TiO_2 to these coatings can further improve their corrosion resistance. The enhancement of anti-corrosion performance of Chemically Bonded Phosphate Ceramic (CBPCs) coatings reinforced by nano-TiO_2 particles is based on three main mechanisms: Increased bonded phase ($AlPO_4$) formation: The addition of nano-TiO_2 particles allows for the formation of a more bonded phase ($AlPO_4$), which can help CBPCs to get a more compact microstructure. $AlPO_4$ particles possess low density and good corrosion resistance, leading to an increase in the corrosion resistance of CBPCs.[40,41]

Strengthened compactness: Increasing the content of nano-TiO$_2$ can also strengthen the compactness of CBPCs, protecting the substrates from the penetration of aggressive electrolytes and prolonging electrolyte diffusion path. [40]

Improved hydrophobic performance: Through the analysis of microstructure, it is found that most of the hydrophobic nano-TiO$_2$ particles homogeneously distribute on the surface of CBPCs. This leads to well-hydrophobic performance, which can further improve the anti-corrosion property of CBPCs. [40, 41]

Moreover, titanium coatings can be enriched with copper, which is known for its excellent corrosion resistance, particularly in marine environments.[42] The incorporation of titanium into the coatings can be achieved through various methods, such as the DC-PEO process, which involves the use of concentrated orthoH3PO4 with the addition of copper(II) nitrate(V) trihydrate. The resulting coatings can display different structures, such as amorphous, fibrous, layered α-TiP and γ-TiP, or three-dimensional TiPs.[42, 43]

1.2.1 Advantages of Titanium-Enhanced Stainless-Steel Mesh Coatings

(i) Improved Corrosion Resistance

TiP layer forms a robust, passive barrier that effectively shields the stainless-steel mesh from corrosive environments, such as those encountered in marine, industrial, or chemical processing applications.[44] For Instance, in a study conducted by researchers at the University of Science and Technology in Beijing, stainless steel mesh samples coated with titanium exhibited significantly higher corrosion resistance compared to uncoated samples when exposed to a saline solution. The coated meshes displayed a lower corrosion rate and a more stable

passive film, demonstrating the effectiveness of the titanium phosphate coating in enhancing the material's protection against corrosion.[45]

(ii)   Enhanced Durability

Titanium coating not only provides corrosion protection but also enhances the overall durability of the stainless-steel mesh. The strong adhesion and chemical stability of the coating contributes to its resistance to mechanical wear, abrasion, and thermal stress. For example, researchers at Tsinghua University in China investigated the performance of titanium-coated stainless steel meshes under prolonged exposure to high-temperature environments. The coated meshes exhibited superior thermal stability and maintained their structural integrity, even after extended periods at elevated temperatures, compared to uncoated counterparts, which showed signs of deterioration.[46]

(iii)   Versatility and Customization

Titanium coating can be tailored to specific application requirements by adjusting the composition, thickness, and deposition method. This flexibility allows for the optimization of the coating's properties, such as corrosion resistance, wettability, or electrical conductivity, to meet the demands of various industries. For example, a research team at the National University of Singapore developed a novel approach to incorporate functional additives, such as nanoparticles or organic inhibitors, into the titanium phosphate coating. The resulting coatings demonstrated enhanced corrosion protection and additional functionalities, such as self-healing or anti-fouling properties, making them suitable for specialized applications in marine environments or chemical processing plants.[44]

(iv)   Environmentally Friendly

Titanium coatings are generally considered environmentally friendly, as they do not rely on the use of harmful or toxic materials during the coating process. This aligns with the increasing emphasis on sustainable and eco-friendly technologies in various industries. For instance, a study conducted by researchers at the Harbin Institute of Technology in China compared the environmental impact of titanium-based coatings to traditional chrome-based coatings. The results showed that the titanium phosphate coatings had a significantly lower carbon footprint and reduced the generation of hazardous waste, making them a more sustainable option for corrosion protection.[44]

1.2.2   Disadvantages of Titanium Enhanced Stainless Steel Mesh Coatings

(i)   Complex synthesis process

The synthesis of titanium phosphate coatings can involve high pressure and temperatures, as well as the use of specialized equipment and materials.[44, 47.]

(ii)   Limited adhesion

Titanium coatings may not adhere well to certain substrates, such as stainless-steel mesh, due to differences in surface chemistry or topography. [44, 47]

(iii)   Potential for cracking

Titanium coatings can be prone to cracking due to the formation of internal stresses during the synthesis process or due to exposure to external stressors, such as mechanical loads or temperature changes. [44, 47]

(iv)   High cost

The high cost of titanium phosphate coatings can make them less economically viable for some applications compared to other coating materials, such as zinc phosphate coatings.[44, 47]

(v)   Limited availability

Titanium coatings may not be readily available or widely used in certain industries, such as the automotive industry, which can limit their accessibility and applicability.[44, 47]

1.3   Ilmenite as a TiO₂ Source

TiO_2 is a highly valued industrial material with diverse applications spanning white pigments, UV protection, catalysis, photovoltaics, and more. With annual global production exceeding 9 million tonnes, ensuring adequate supplies of TiO_2 from abundant and cost-effective mineral sources is of critical importance.[51]

In 2023, the global TiO_2 market was estimated to be worth USD 26.9 billion.[1] The market is expected to grow at a compound annual growth rate (CAGR) of 5.80% during the forecast period, reaching a projected market size of USD 34.47 billion by 2032.[2] The Lomon Billions Group is highlighted as one of the top three producers of high-performance TiO_2 pigments globally and the largest producer in Asia.[3] Key global players in the TiO_2 market include Chemours Titanium Technologies, Huntsman Corporation, Cristal, and Kronos.[1] The report from Polaris Market Research also lists other significant players like The Chemours Company, Tronox Holdings plc, LB Group, Venator Materials PLC, and KRONOS Worldwide Inc.[52]

Asia Pacific is leading the global TiO_2 market, driven by significant consumption and production in the region. North America and Europe also represent substantial markets, with detailed analyses available for country-level and regional impacts.[52] The market dynamics are influenced by factors such as the economic impact of the COVID-19 pandemic and geopolitical events like the Russia-Ukraine war.[1]Despite a downturn in the industry with a projected 5-8% drop in demand in 2023, long-term projections remain positive, with expectations of a return to the long-term trend line of demand growth later in the decade. The industry faces challenges such as overcapacity, particularly in China, and structural market changes. Companies like LB Group and Chemours are adjusting their strategies, focusing on optimizing production capacity and diversifying into related sectors like battery materials to mitigate risks associated with the TiO_2 market.[53, 54]

The three primary naturally occurring mineral concentrates used as feedstocks for TiO_2 production are ilmenite ($FeTiO_3$), rutile (TiO_2), and leucoxene (an alteration product of ilmenite). Ilmenite is the most abundant titanium-containing mineral, but it has a low titanium dioxide content and contains iron along with other impurities.[55] Concentrated ilmenite ore generally has a TiO_2 content of at least about 40%, and generally in the range of 45% to 65% TiO_2.[6] While rutile deposits are less common, they have the advantage of containing over 95% TiO_2, allowing for more direct processing routes.[55, 56] Leucoxene typically occurs intermixed with ilmenite in mineral sand deposits, containing over 65% TiO_2.[57]

However, ilmenite represents the most abundant and widely utilized source for TiO_2 production globally. As an iron titanium oxide mineral containing around 50% TiO_2, ilmenite requires additional chemical processing to separate the titanium and iron components compared to rutile.[56, 58] Despite this added complexity, ilmenite's widespread availability and lower production costs have made it the dominant feedstock for the TiO_2 industry. i.e., ilmenite supplies about 91% of the world's demand for titanium minerals.[58]

1.3.1 Ilmenite Characteristics and Occurrence

Ilmenite is an iron-black, opaque mineral that crystallizes in the hexagonal system. It commonly forms thick tabular crystals with a metallic to sub-metallic luster and a black streak (Figure 1.4). Ilmenite has a Mohs hardness of 5-6 and a specific gravity of 4.68-4.76 g/cm^3.[59, 60] It is brittle with a conchoidal to sub-conchoidal fracture.[9] Ilmenite is weakly magnetic or non-magnetic, which helps distinguish it from magnetite.[60, 61]

Figure 1.4: Ilmenite ore.

Source: Encyclopedia Britannica; 2020.

In its pure form, ilmenite's composition is $FeTiO_3$, containing 31.6% titanium by weight. However, in nature, ilmenite forms a solid solution series with the minerals geikielite ($MgTiO_3$) and pyrophanite ($MnTiO_3$), resulting in variable titanium content. This solid solution results in ilmenite deposits having variable titanium content, as the magnesium and manganese substitute for iron in the mineral structure.[10, 11] The composition of ilmenite deposits can range from around 40-80% TiO_2, with the remainder being other metal oxides like FeO, Fe_2O_3, MnO, and MgO.[58]
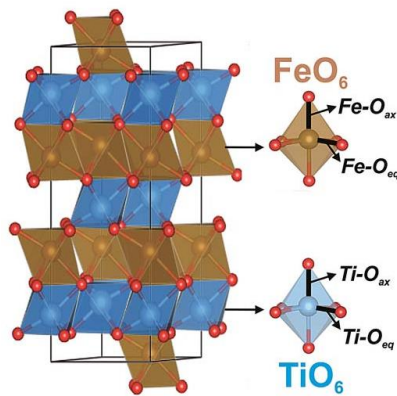
Figure 1.5: Structure of Ilmenite.

Source: Ribeiro and Lazaro (2014)

Amghouz, Mendoza and Adawy (2023)

The variable titanium content in natural ilmenite deposits is an important consideration, as it affects the processing and extraction of titanium from the mineral. Higher titanium content is generally desirable, as it leads to higher yields and efficiency in producing titanium metal or titanium dioxide pigment.[8, 11]

While ilmenite is a common accessory mineral in many igneous and metamorphic rock types, the principal economic sources of ilmenite are derived from heavy mineral sand deposits.[58, 62] These coastal sand deposits are formed through the concentration of

dense, erosion-resistant minerals like ilmenite by longshore wave and current action over geologic timescales.[62] Major locations of these heavy mineral sand deposits containing significant ilmenite resources include Australia, India, Mozambique, Madagascar, and others. The ilmenite in these heavy mineral sand deposits is more economically viable to extract and process compared to ilmenite found dispersed in igneous and metamorphic rock types.[62, 63]

1.3.2   Natural TiO$_2$ Deposits in Sri Lanka

Sri Lanka's complex geological history, spanning billions of years, has played a pivotal role in the formation and distribution of TiO$_2$ deposits. The island's geology is characterized by the presence of the Precambrian highland complex, composed of metamorphic and igneous rocks, as well as sedimentary basins and coastal plains.[64] The TiO$_2$ deposits are primarily associated with the heavy mineral sand deposits found along the island's coastal regions, particularly in the northwestern and eastern provinces. The Pulmoddai mineral sand deposit, located on the northeast coast, stands out as the main source of TiO$_2$ in Sri Lanka (Figure 2.2).[64, 65] It is estimated to cover an area of 3.2 km^2, with an even thickness of 6 m.[66] It is a very high-grade deposit, with no overburden. This deposit contains over 80% heavy minerals, with the main components being ilmenite (70-72%), zircon (8-10%), and rutile (8%).[67]
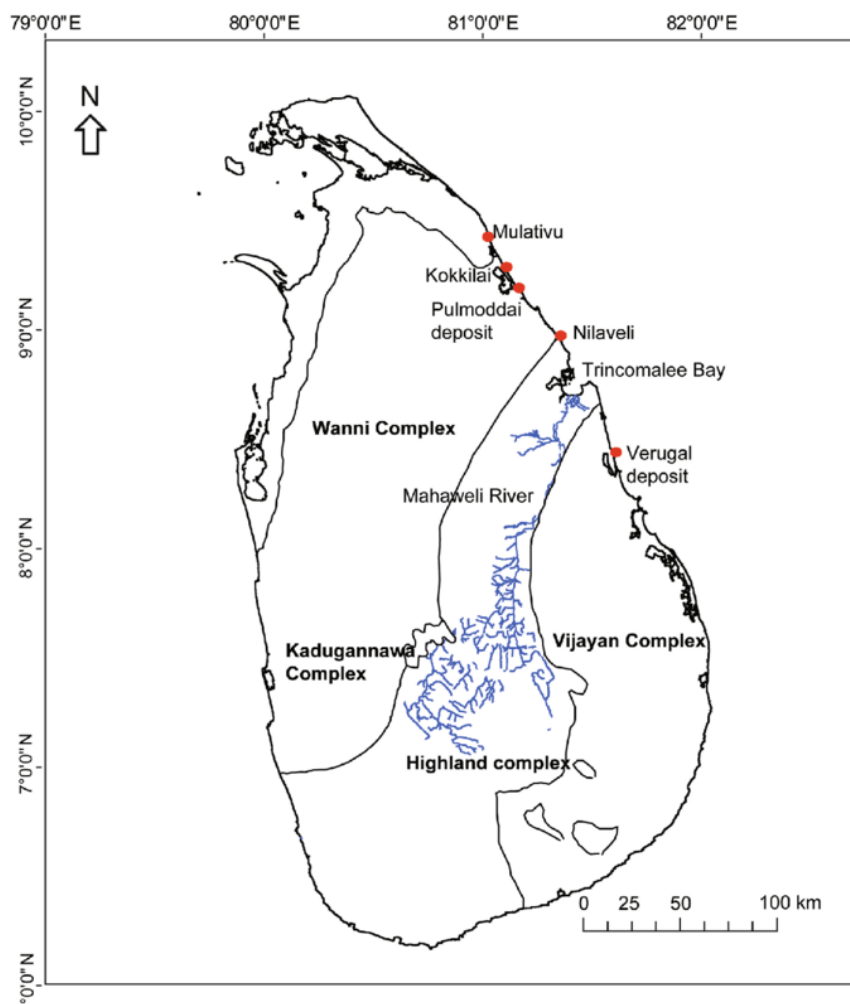
Figure 1.6: Simplified geological map of Sri Lanka.

Source: Wijewrdena et al. (2014)

The exploration and mining of natural TiO_2 deposits in Sri Lanka have a long history, dating back to the early 20th century. Initial efforts focused on the extraction of ilmenite from coastal placer deposits, primarily for export purposes. The Pulmoddai mineral sand deposit, discovered in the 1960s, quickly became the primary focus of exploration and mining activities due to its rich TiO_2 content. Over time, more advanced exploration techniques, such as geophysical surveys and drilling, have been employed to identify and evaluate new deposits, including potential extensions of the Pulmoddai deposit.[69, 70]

Sri Lanka exports large quantities of raw ilmenite from the Pulmoddai deposits every year. However, converting the ilmenite to value-added TiO_2 could increase the revenue by up to 15 times, as TiO_2 sells for around \$2,250 per ton compared to \$150 per ton for ilmenite.[67] Maldives is the main destination for titanium dioxide exports from Sri Lanka, accounting for approximately 60% of total exports. Other than that export market expands to its neighboring countries in the region, such as Pakistan, and Bangladesh. Sri Lanka also exports some TiO_2 to more distant markets like the United States.[69, 71]

1.3.3 Ilmenite Processing Routes for TiO_2

Traditionally, TiO_2 has been extracted from ilmenite through the sulfate and chloride processes, which involve high temperatures up to 1000 °C and the use of hazardous concentrated acids. These conventional methods are costly and have a high environmental impact.[67]

In the production of TiO_2 from ilmenite, the mineral concentrate first undergoes extensive physical processing, including electrostatic and magnetic separation, to remove impurities and concentrate the ilmenite fraction.[72] The enriched ilmenite is then reacted with concentrated sulfuric acid and subjected to high-temperature roasting, causing it to undergo a phase transformation. This produces water-soluble ferrous sulfates that can be leached away, leaving behind a solid TiO_2 residue.[72]

This TiO_2 residue then requires further processing steps involving hydrochloric acid leaching, purification, calcination, and milling to manufacture the final pigment-grade TiO_2 product. Depending on the desired properties and end-use, the TiO_2 may be finished as either an anatase or rutile polymorph.[72]

The multistage sulfate and chloride processing required to upgrade ilmenite to pigment-grade TiO_2 is chemically intensive and generates significant acidic waste streams and CO_2 emissions from the calcination stages. Consequently, there have been concerted research efforts aimed at developing more sustainable and direct processing routes from ilmenite and other titanium mineral sources.[68, 72]

1.4   Objectives and Scope of the Study

The primary objective of this research is to develop a novel, efficient, and cost-effective synthetic procedure for the production of high-purity titanium phosphate materials from Sri Lankan ilmenite beach sand, a readily available and abundant titanium-bearing ore,[48] and to evaluate their potential as corrosion-resistant coatings for stainless steel mesh. Ilmenite, a naturally occurring titanium-iron oxide mineral, is widely distributed globally, but extracting and purifying titanium compounds from it can be challenging due to the presence of iron.[49] Conventional methods often involve complex and energy-intensive processes, resulting in low conversion rates and purity levels.[48, 50] This research aims to address these challenges by designing a synthetic approach that can efficiently convert ilmenite into high-purity titanium phosphate precursors, which can then be further processed and utilized as corrosion-resistant coatings for stainless steel mesh.

Specifically, the study will focus on the synthesis of alpha titanium bis(hydrogen phosphate) monohydrate [α-Ti(HPO$_4$).H$_2$O], a versatile precursor material with a wide range of industrial applications, including ion-exchange chromatography, chemical catalysis, and energy storage. The research will also investigate the calcination of the synthesized α-Ti(HPO$_4$).H$_2$O to produce stable titanium pyrophosphate (TiP$_2$O$_7$) and explore methods to remove residual iron from the materials. Additionally, the study will synthesize and characterize the titanyl pyrophosphate (TiO)$_2$P$_2$O$_7$, obtained from the calcination of the iron-free α-Ti(HPO$_4$).H$_2$O. The ultimate goal is to evaluate the potential of these titanium phosphate materials as corrosion-resistant coatings for stainless steel mesh, which could find applications in various industries, such as water filtration, catalytic reactors, and protective barriers.

The scope of this research encompasses the development of a novel synthetic procedure to convert Sri Lankan ilmenite beach sand into high-purity titanium phosphate materials, with a focus on maximizing the conversion rate and purity. The study will explore the optimization of reaction parameters, such as temperature, time, and reagent ratios, to achieve the targeted conversion and purity levels. The characterization of the synthesized materials, including α-Ti(HPO$_4$).H$_2$O, TiP$_2$O$_7$, and (TiO)$_2$P$_2$O$_7$, will be conducted using a range of analytical techniques, including XRD, X-ray fluorescence (XRF), thermogravimetric analysis (TGA), and Raman spectroscopy. The research will also investigate the removal of residual iron from the α-Ti(HPO$_4$).H$_2$O through multiple washing steps using different chelating acids, and evaluate the effectiveness of the iron removal process.

Furthermore, the study will assess the potential of the synthesized titanium phosphate materials as corrosion-resistant coatings for stainless steel mesh. This will involve evaluating the physical and chemical properties of the coatings, as well as their ability to enhance the corrosion resistance of the stainless-steel substrate. The research will also explore potential applications of titanium phosphate materials in other areas, such as ion-exchange chromatography, chemical catalysis, and energy storage, based on their characteristics. Finally, a techno-economic analysis will be performed to estimate the cost-effectiveness and scalability of the developed synthetic process for potential industrial-scale production and application of the corrosion-resistant stainless steel mesh coatings.

References

[1] Zhu, Y.-P.; Ma, T.-Y.; Liu, Y.-L.; Ren, T.-Z.; Yuan, Z.-Y. Metal Phosphonate Hybrid Materials: From Densely Layered to Hierarchically Nanoporous Structures. *Inorg. Chem. Front.* **2014**, *1* (5), 360–383. https://doi.org/10.1039/c4qi00011k.

[2] Trublet, M. Titanium(IV) Phosphates the next Generation of Wastewater Sorbents, 2018.

[3] Amghouz, Z.; Mendoza, R.; Adawy, A. Nucleation & Growth of α-Ti(HPO$_4$)$_2$.H$_2$O Single-Crystal and Its Structure Determination from X-ray Single—Crystal Data. *Journal of Solid State Chemistry* **2023**, *327*, 124251–124251. https://doi.org/10.1016/j.jssc.2023.124251.

[4] Petersen, H.; Stegmann, N.; Fischer, M.; Zibrowius, B.; Radev, I.; Philippi, W.; Schmidt, W.; Weidenthaler, C. Crystal Structures of Two Titanium Phosphate-Based Proton Conductors: Ab Initio Structure Solution and Materials Properties. *Inorganic Chemistry* **2021**, *61* (5), 2379–2390. https://doi.org/10.1021/acs.inorgchem.1c02613.

[5] Zhu, Y.; Hasegawa, G.; Kanamori, K.; Nakanishi, K. Comprehensive Studies on H$_3$PO$_4$ Treatment of Porous Titania toward Titanium Phosphate and Pyrophosphate Monoliths with Pore Hierarchy and a Nanostructured Pore Surface. *Inorganic Chemistry Frontiers* **2018**, *5* (6), 1397–1404. https://doi.org/10.1039/C8QI00146D.

[6] Li, P.; Wen, X.-G.; Lin, S.-X. Synthesis and Adsorption Properties of $Ti_2O(PO_4)_2.2H_2O$ Nanobelts. In *Proceedings of the 2nd Annual International Conference on Advanced Material Engineering (AME 2016)*; Atlantis Press, 2016; pp. 244–249.

[7] Amghouz, Z.; García, J. R.; Adawy, A. A Review on the Synthesis and Current and Prospective Applications of Zirconium and Titanium Phosphates. *Eng* **2022**, *3* (1), 161–174. https://doi.org/10.3390/eng3010013.

[8] Maslova, M.; Ivanenko, V.; Gerasimova, L.; Larsson, A.-C.; Antzutkin, O. N. Synthesis of Titanium Phosphates from Unconventional Solid Precursor and Their Ion-Exchange and Electrochemical Properties. *Journal of materials science* **2021**, *56* (16), 9929–9950. https://doi.org/10.1007/s10853-021-05876-4.

[9] Raptopoulou, C. P. Metal-Organic Frameworks: Synthetic Methods and Potential Applications. *Materials* **2021**, *14* (2), 310. https://doi.org/10.3390/ma14020310.

[10] Ban, T.; Asano, K.; Takai-Yamashita, C.; Ohya, Y. Bottom-up Synthesis of Titanophosphate Nanosheets by the Aqueous Solution Process. *Nanoscale Advances* **2020**, *2* (8), 3542–3549. https://doi.org/10.1039/D0NA00376J.

[11] Hayami, R.; Gunji, T. A Review of Phosphorus(V)-Substituted Titanium-Oxo Clusters. *Journal of Sol-Gel Science and Technology* **2021**, *100* (2), 205–223. https://doi.org/10.1007/s10971-021-05652-5.

[12] EL-Mekkawi, D. M.; Othman, S. A.; Rasha; Selim, M. M. Easily Prepared Titanium Phosphate-Based Composites for the Remediation of Synthetic and Real Wastewaters. *Water, air and soil pollution (Print)* **2023**, *234* (4). https://doi.org/10.1007/s11270-023-06256-1.

[13] Baby, R.; Hussein, M. Z.; Abdullah, A. H.; Zainal, Z. Nanomaterials for the Treatment of Heavy Metal Contaminated Water. *Polymers* **2022**, *14* (3), 583. https://doi.org/10.3390/polym14030583.

[14] Pipi, A.; Neto, S. A.; Fernanda, P.; Devaney. The Use of Titanium (IV) Phosphate for Metal Removal from Aqueous and Alcoholic Samples. *SN applied sciences (Print)* **2019**, *1* (8). https://doi.org/10.1007/s42452-019-0968-4.

[15] Onoda, H.; Yamaguchi, T. Synthesis of Titanium Phosphates with Additives and Their Powder Properties for Cosmetics. *Materials Sciences and Applications* **2012**, *03* (01), 18–23. https://doi.org/10.4236/msa.2012.31003.

[16] Маслова, М. В.; Иваненко, В. И.; Yanicheva, N. Yu.; Mudruk, N. Comparison of the Sorption Kinetics of Lead(II) and Zinc(II) on Titanium Phosphate Ion-Exchanger. *International Journal of Molecular Sciences* **2020**, *21* (2), 447–447. https://doi.org/10.3390/ijms21020447.

[17] Schmutz, C.; Basset, E.; Barboux, P.; Maquet, J. Study of Titanium Phosphate Gels and Their Application to the Synthesis of $KTiOPO_4$ Films. *Journal of Materials Chemistry* **1993**, *3* (4), 393. https://doi.org/10.1039/jm9930300393.

[18] *Bibliographies: "Titanium Phosphate" — Grafiati*. www.grafiati.com. https://www.grafiati.com/en/literature-selections/titanium-phosphate/ (accessed 2024-04-09).

[19] Rokosz, K.; Hryniewicz, T.; Dudek, Ł. Phosphate Porous Coatings Enriched with Selected Elements via PEO Treatment on Titanium and Its Alloys: A Review. *Materials* **2020**, *13* (11), 2468. https://doi.org/10.3390/ma13112468.

[20] Babaryk, A. A.; Adawy, A.; García, I.; Trobajo, C.; Amghouz, Z.; Colodrero, R. M. P.; Cabeza, A.; Olivera-Pastor, P.; Bazaga-García, M.; Santos-Gómez, L. dos. Structural and Proton Conductivity Studies of Fibrous π-Ti$_2$O(PO$_4$)$_2$.2H$_2$O: Application in Chitosan-Based Composite Membranes. *Dalton Transactions* **2021**, *50* (22), 7667–7677. https://doi.org/10.1039/D1DT00735A.

[21] Shaaban, Kh. S.; Yousef, E. S.; Mahmoud, S. A.; Wahab, E. A. A.; Shaaban, E. R. Mechanical, Structural and Crystallization Properties in Titanate Doped Phosphate Glasses. *Journal of Inorganic and Organometallic Polymers and Materials* **2020**, *30*, 4655–4663. https://doi.org/10.1007/s10904-020-01574-x.

[22] Voronina, N.; Jo, J. H.; Choi, J. U.; Jo, C.-H.; Kim, J.; Myung, S.-T. Nb-Doped Titanium Phosphate for Sodium Storage: Electrochemical Performance and Structural Insights. *Journal of Materials Chemistry A* **2019**, *7* (10), 5748–5759. https://doi.org/10.1039/C8TA11517F.

[23] Yada, M.; Inoue, Y.; Sakamoto, A.; Torikai, T.; Watari, T. Synthesis and Controllable Wettability of Micro- and Nanostructured Titanium Phosphate Thin Films Formed on Titanium Plates. *ACS Applied Materials & Interfaces* **2014**, *6* (10), 7695–7704. https://doi.org/10.1021/am500974v.

[24] Morra, E.; Giamello, E.; Chiesa, M. EPR Approaches to Heterogeneous Catalysis. The Chemistry of Titanium in Heterogeneous Catalysts and Photocatalysts. *Journal of Magnetic Resonance* **2017**, *280*, 89–102. https://doi.org/10.1016/j.jmr.2017.02.008.

[25] Wu, Y.; Wang, Y.; Huang, D.; Ding, H.; Ren, Y.; Zhang, Y.; Yue, B.; He, H.; Ye, L. Direct Quantification of Oxygen Vacancy on the TiO_2 Surface by 31P Solid-State NMR. *Chem catalysis (Online)* **2023**, *3* (4), 100556–100556. https://doi.org/10.1016/j.checat.2023.100556.

[26] Richard, C.; Alfred-Arulrasa, M.; Ramadas, H.; Mahagamage, P. T.; Defforge, T.; Gaultier, G.; Autret-Lambert, C.; Poirot, N.; Champion, E.; Magnaudeix, A. Synthesis by Solid Route and Physicochemical Characterizations of Blends of Calcium Orthophosphate Powders and Mesoporous Silicon Particles. *Frontiers in Bioengineering and Biotechnology* **2023**, *11*. https://doi.org/10.3389/fbioe.2023.1101513.

[27] Garcia, E. E.; Albitres, G. A. V.; Freitas, D. F. S.; Mariano, D. M.; Mendes, L. C. Zinc and Silver Salts-Containing Lamellar Titanium Phosphate: A Multifunctional Filler. *Materials Sciences and Applications* **2022**, *13* (06), 366–388. https://doi.org/10.4236/msa.2022.136021.

[28] Gerasimova, L. G.; Maslova, M. V.; Shchukina, E. S. Synthesis of Sorption Materials from Low Grade Titanium Raw Materials. *Materials* **2022**, *15* (5), 1922. https://doi.org/10.3390/ma15051922.

[29] Wang, C.; Wang, H.; Shankar, K.; Morozov, E. V.; Hazell, P. J. On the Mechanical Behavior of Steel Wire Mesh Subjected to Low-Velocity Impact. *Thin-Walled Structures* **2021**, *159*, 107281. https://doi.org/10.1016/j.tws.2020.107281.

[30] Liu, Y.; Zhang, K.; Zhang, D.; Dong, W.; Jiang, T.; Zhou, H.; Li, L.; Mao, B. Industrial Stainless Steel Meshes for Efficient Electrocatalytic Hydrogen Evolution. *Journal of energy storage* **2021**, *41*, 102844–102844. https://doi.org/10.1016/j.est.2021.102844.

[31] Chen, C.; Wang, Y.; Ge, F. Construction of Corrosion Resistant Stainless Steel Mesh and the Design for Protecting Optical Window Free from Biofouling. *Ocean Engineering* **2022**, *264*, 112564. https://doi.org/10.1016/j.oceaneng.2022.112564.

[32] Naderi, A.; Zhang, B.; Belgodere, J. A.; Sunder, K.; Palardy, G. Improved Biocompatible, Flexible Mesh Composites for Implant Applications via Hydroxyapatite Coating with Potential for 3-Dimensional Extracellular Matrix Network and Bone Regeneration. *ACS applied materials & interfaces* **2021**, *13* (23), 26824–26840. https://doi.org/10.1021/acsami.1c09034.

[33] Yue, X.; Zhang, L.; Hua, Y.; Wang, J.; Dong, N.; Li, X.; Xu, S.; Neville, A. Revealing the Superior Corrosion Protection of the Passive Film on Selective Laser Melted 316L SS in a Phosphate-Buffered Saline Solution. *Applied surface science* **2020**, *529*, 147170–147170. https://doi.org/10.1016/j.apsusc.2020.147170.

[34] Talha, M.; Ma, Y.; Lin, Y.; Singh, A.; Liu, W.; Kong, X. Corrosion Behavior of Austenitic Stainless Steels in Phosphate Buffer Saline Solution: Synergistic Effects of Protein Concentration, Time and Nitrogen. *New Journal of Chemistry* **2019**, *43* (4), 1943–1955. https://doi.org/10.1039/c8nj04670k.

[35] Cai, B.; Jiang, N.; Tan, P.; Hou, Y.; Li, Y.; Zhang, L.; Zhu, S. The Custom Making of Hierarchical Micro/Nanoscaled Titanium Phosphate Coatings and Their

Formation Mechanism Analysis. *RSC Advances* **2019**, *9* (70), 41311–41318. https://doi.org/10.1039/c9ra08168b.

[36] Pierre, C.; Bertrand, G.; Rey, C.; Benhamou, O.; Combes, C. Calcium Phosphate Coatings Elaborated by the Soaking Process on Titanium Dental Implants: Surface Preparation, Processing and Physical—Chemical Characterization. *Dental Materials* **2019**, *35* (2), e25— e35. https://doi.org/10.1016/j.dental.2018.10.005.

[37] Muthaiah, V. M. S.; Rajput, M.; Tripathi, A.; Suwas, S.; Chatterjee, K. Electrophoretic Deposition of Nanocrystalline Calcium Phosphate Coating for Augmenting Bioactivity of Additively Manufactured Ti-6Al-4V. *ACS Materials Au* **2021**, *2* (2), 132–142. https://doi.org/10.1021/acsmaterialsau.1c00043.

[38] Drevet, R.; Benhayoune, H. Pulsed Electrodeposition for the Synthesis of Strontium-Substituted Calcium Phosphate Coatings with Improved Dissolution Properties. *Materials Science and Engineering: C* **2013**, *33* (7), 4260–4265. https://doi.org/10.1016/j.msec.2013.06.019.

[39] Cotell, C. M.; Sprague, J. A.; Smidt Jr., F. A. Phosphate Coatings. In *Surface Engineering*; ASM International, 1994; pp. 378–404. https://doi.org/10.31399/asm.hb.v05.a0001274.

[40] Yan, G.; Wang, M.; Sun, T.; Li, X.; Wang, G.; Yin, W. Anti-Corrosion Property of Glass Flake Reinforced Chemically Bonded Phosphate Ceramic Coatings. *Materials* **2019**, *12* (13), 2082. https://doi.org/10.3390/ma12132082.

[41] U.S. Department of Energy Office of Scientific and Technical Information. *Ultra-high-temperature ceramic composites: Topics by Science.gov*. www.science.gov. https://www.science.gov/topicpages/u/ultra-high-temperature%2Bceramic%2Bcomposites (accessed 2024-04-13).

[42] Rokosz, K.; Hryniewicz, T.; Kacalak, W.; Tandecka, K.; Raaen, S.; Gaiaschi, S.; Chapon, P.; Malorny, W.; Matýsek, D.; Pietrzak, K.; Dudek, Ł. Phosphate Coatings Enriched with Copper on Titanium Substrate Fabricated via DC-PEO Process. *Materials* **2020**, *13* (6), 1295. https://doi.org/10.3390/ma13061295.

[43] Rokosz, K.; Hryniewicz, T.; Kacalak, W.; Tandecka, K.; Raaen, S.; Gaiaschi, S.; Chapon, P.; Malorny, W.; Matýsek, D.; Pietrzak, K.; Czerwińska, E.; Iwanek, A.; Dudek, Ł. Porous Coatings Containing Copper and Phosphorus Obtained by Plasma Electrolytic Oxidation of Titanium. *Materials* **2020**, *13* (4), 828–828. https://doi.org/10.3390/ma13040828.

[44] Sarraf, M.; Rezvani Ghomi, E.; Alipour, S.; Ramakrishna, S.; Liana Sukiman, N. A State-of-The-Art Review of the Fabrication and Characteristics of Titanium and Its Alloys for Biomedical Applications. *Biodesign and Manufacturing* **2021**, 1–25. https://doi.org/10.1007/s42242-021-00170-3.

[45] Li, B.; Liu, X.; Zhang, X.; Chai, W. Stainless Steel Mesh Coated with Silica for Oil—Water Separation. *European polymer journal/European Polymer Journal* **2015**, *73*, 374–379. https://doi.org/10.1016/j.eurpolymj.2015.10.031.

[46] Sico, J.; Tang, B.; Flores, D.; Mouawad, R.; Punsalan, R.; Gan, Y. X.; Li, M. Fabrication and Characterization of TiO_2 Coatings on 304 Stainless-Steel Substrate for Efficient Oil/Water Separation. *Coatings* **2023**, *13* (11), 1920. https://doi.org/10.3390/coatings13111920.

[47] Muresan, L. M. Corrosion Protective Coatings for Ti and Ti Alloys Used for Biomedical Implants. *Intelligent Coatings for Corrosion Control* **2015**, 585–602. https://doi.org/10.1016/b978-0-12-411467-8.00017-9.

[48] Wijewardhana, T. Dilmi. U.; Ratnayake, A. S. Applicability of Carbothermic Reduction for Upgrading Sri Lankan Ilmenite Ores: Towards Converting Ilmenite into Synthetic Rutile by Mechanical Activation. *Bulletin of the National Research Centre* **2021**, *45* (1). https://doi.org/10.1186/s42269-021-00608-9.

[49] Sri Lanka Export Development Board. *Mineral Resources in Sri Lanka—EDB Blog.* www.srilankabusiness.com. https://www.srilankabusiness.com/blog/mineral-resources-from-sri-lanka.html.

[50] Sampath, A. H. J.; Wickramasinghe, N. D.; de Silva, K. M. N.; de Silva, R. M. Methods of Extracting TiO_2 and Other Related Compounds from Ilmenite. *Minerals* **2023**, *13* (5), 662. https://doi.org/10.3390/min13050662.

[51] Consumer Goods Insights. *Titanium Dioxide (TiO2) Market Size In 2023: Growth Opportunities and Future Outlook 2030.* www.linkedin.com. https://www.linkedin.com/pulse/titanium-dioxide-tio2-market-size-2023-growth (accessed 2024-04-25).

[52] Polaris Market Research. *Titanium Dioxide Market | Global Industry Report, 2032.* Polaris. https://www.polarismarketresearch.com/industry-analysis/titanium-dioxide-tio2-market (accessed 2024-04-25).

[53] Reports and Data. *Top Titanium Dioxide Companies in the World | Reports and Data.* www.reportsanddata.com. https://www.reportsanddata.com/blog/top-titanium-dioxide-companies-in-the-world (accessed 2024-04-25).

[54] Colamarino, G. *TiO2 Industry: Downturn Impacting Global Operating Footprint.* Pcimag.com. https://www.pcimag.com/articles/111809-tio2-industry-downturn-impacting-global-operating-footprint (accessed 2024-04-25).

[55] World Intellectual Property Organization (WIPO). *Production of Titanium and Titanium Dioxide from Ilmenite and Related Applications*. https://www.wipo.int/edocs/pubdocs/en/wipo-pub-1077-23-en-patent-landscape-report-ilmenite.pdf.

[56] Duyvesteyn, W. P. C.; Huls, B. J.; Shrestha, P. L. Processing Ilmenite Ore to TiO_2 Pigment. https://patents.google.com/patent/WO1996024555A1/en (accessed 2024-04-25).

[57] Thambiliyagodage, C.; Wijesekera, R.; Bakker, M. G. Leaching of Ilmenite to Produce Titanium Based Materials: A Review. *Discover Materials* **2021**, *1* (1). https://doi.org/10.1007/s43939-021-00020-0.

[58] Gázquez, M. J.; Bolívar, J. P.; Garcia-Tenorio, R.; Vaca, F. A Review of the Production Cycle of Titanium Dioxide Pigment. *Materials Sciences and Applications* **2014**, *05* (07), 441–458. https://doi.org/10.4236/msa.2014.57048.

[59] Geology Science. *Ilmenite | Physical—Optical Properties, Varieties, Uses, Occurrence*. Geology Science. https://geologyscience.com/minerals/ilmenite/.

[60] Ilmenite | Mineral | Britannica. *Encyclopædia Britannica*; 2020.

[61] King, H. M. *Ilmenite: An ore of titanium | Uses and Properties*. Geology.com. https://geology.com/minerals/ilmenite.shtml.

[62] Woodruff, L. G.; Bedinger, G. M.; Piatak, N. M. Titanium. *Professional Paper* **2017**. https://doi.org/10.3133/pp1802t.

[63] El Khalloufi, M.; Drevelle, O.; Soucy, G. Titanium: An Overview of Resources and Production Methods. *Minerals* **2021**, *11* (12), 1425. https://doi.org/10.3390/min11121425.

[64] Sandamali, K. P. K. *Geological background and Economic Minerals in Sri Lanka*. The Sunday Times Sri Lanka. https://www.sundaytimes.lk/190609/education/geological-background-and-economic-minerals-in-sri-lanka-352593.html.

[65] JICA. *Chapter 2 General Description of Study Area 2.1 Geology 2.1.1 Topography and Geomorphology*. https://openjicareport.jica.go.jp/pdf/11720406_02.pdf.

[66] Premaratne, W. A. P. J.; Rowson, N. A. The Processing of Beach Sand from Sri Lanka for the Recovery of Titanium Using Magnetic Separation. *Physical Separation in Science and Engineering* **2003**, *12* (1), 13–22. https://doi.org/10.1080/1478647031000101232.

[67] Kumara, K. Sri Lankan Scientists Develop a New Process to Produce Titanium Dioxide from Ilmenite | The Sri Lankan Scientist. *The Sri Lankan Scientist*. August 24, 2020. https://scientist.lk/2020/08/24/sri-lankan-scientists-develop-a-non-hazardous-and-environmentally-friendly-process-to-produce-titanium-dioxide-from-ilmenite/.

[68] Wijewardhana, T. Dilmi. U.; Ratnayake, A. S. Applicability of Carbothermic Reduction for Upgrading Sri Lankan Ilmenite Ores: Towards Converting Ilmenite into Synthetic Rutile by Mechanical Activation. *Bulletin of the National Research Centre* **2021**, *45* (1). https://doi.org/10.1186/s42269-021-00608-9.

[69] Sri Lanka Export Development Board. *Industrial Mineral Resources in Sri Lanka | Manufacturing of Industrial Minerals*. www.srilankabusiness.com. https://www.srilankabusiness.com/ceramic-and-porcelain/industrial-minerals-in-sri-lanka.html.

[70] Daily FT. *Lanka's long-neglected treasure, rare earths | Daily FT*. www.ft.lk. https://www.ft.lk/Columnists/lankas-long-neglected-treasure-rare-earths/4-553132 (accessed 2024-04-26).

[71] Volza Grow Global. *Directory of Titanium dioxide rutile Suppliers & manufacturers in Sri Lanka exporting to United States—Volza.com*. www.volza.com. https://www.volza.com/p/titanium-dioxide-rutile/manufacturers/manufacturers-in-sri-lanka/cod-united-states/ (accessed 2024-04-26).

[72] Sampath, A. H. J.; Wickramasinghe, N. D.; de Silva, K. M. N.; de Silva, R. M. Methods of Extracting TiO_2 and Other Related Compounds from Ilmenite. *Minerals* **2023**, *13* (5), 662. https://doi.org/10.3390/min13050662.

CHAPTER 2
DIRECT ACID DIGESTION APPROACH FOR α-TiP SYNTHESIS

2.1 Synthesis of α-Titanium Phosphate via Direct Acid Digestion

2.1.1 Introduction to the Direct Acid Digestion Method

The direct acid digestion method has emerged as a promising technique for the synthesis of α-titanium phosphate (α-TiP) from ilmenite, a naturally abundant titanium-iron oxide mineral.[1] This approach offers several advantages over conventional synthesis routes, including its simplicity, cost-effectiveness, and potential for scalability. The direct acid digestion method involves the dissolution of ilmenite in a concentrated H_3PO_4 solution, followed by the precipitation and purification of the desired α-TiP product.[2]

The direct acid digestion method for synthesizing α-TiP from ilmenite is based on the principle of selective leaching and precipitation. Ilmenite, a mixed oxide of titanium and iron ($FeTiO_3$), is treated with a concentrated H_3PO_4 solution at elevated temperatures. Under these conditions, the iron component of ilmenite is preferentially dissolved, leaving behind a titanium-rich solid residue. This residue, upon further reaction with H_3PO_4, forms α-TiP as the primary product.[2, 3]

The synthesis typically proceeds through the following steps:

(i) Acid Treatment: The process begins with the digestion of ilmenite minerals in a strong acid. Typically, H_3PO_4 is used due to its ability to react with ilmenite to form titanium phosphate. The reaction involves treating ilmenite sand with a high concentration of H_3PO_4 (around 85%) at elevated temperatures (approximately 150 °C) for several hours.[3]

(ii)   Cooling and Settling: After the acid treatment, the mixture is allowed to cool and settle. This step is crucial as it helps in the formation of a precipitate that primarily contains titanium phosphate.[3]

(iii)   Filtration and Washing: The precipitate was then filtered and washed to remove impurities and excess acid. This step ensures that the final product is of high purity and suitable for further applications. [3]

(iv)   Drying and Calcination: The filtered solid was dried and often subjected to calcination. Calcination involves heating the material at high temperatures to induce phase changes and improve the crystallinity of the titanium phosphate. [3]

The direct acid digestion method offers several advantages over traditional synthetic routes, including its relatively simple and cost-effective nature, the use of readily available and inexpensive raw materials (ilmenite and H_3PO_4), and the potential for large-scale production. However, careful control of the reaction parameters, such as the acid concentration, temperature, reaction time, and solid-to-liquid ratios, is crucial for maximizing the yield and purity of the desired α-TiP product.[1, 3]

2.1.2   Optimizing the Direct Acid Digestion Method

The synthesis of α-TiP was carried out using a previously reported direct acid digestion method developed by Palliyaguru et al., in 2019 with a few modifications. The major alteration between the improved method and the method described by Palliyaguru et al. (2019) is the attempt to purify the product α-TiP. In a typical synthesis procedure, 100 g of ilmenite mineral was digested in 800 mL of 85 wt.% H_3PO_4 with vigorous stirring at 150 °C for 4 hours. After the reaction mixture was allowed to cool to room temperature over approximately 24 hours, three distinct layers were observed (Figure 2.1): a dense

layer of unreacted ilmenite at the bottom, a middle white powder precipitate layer (abbreviated as WP) containing the key product α-TiP, and an upper H_3PO_4 leachate layer.
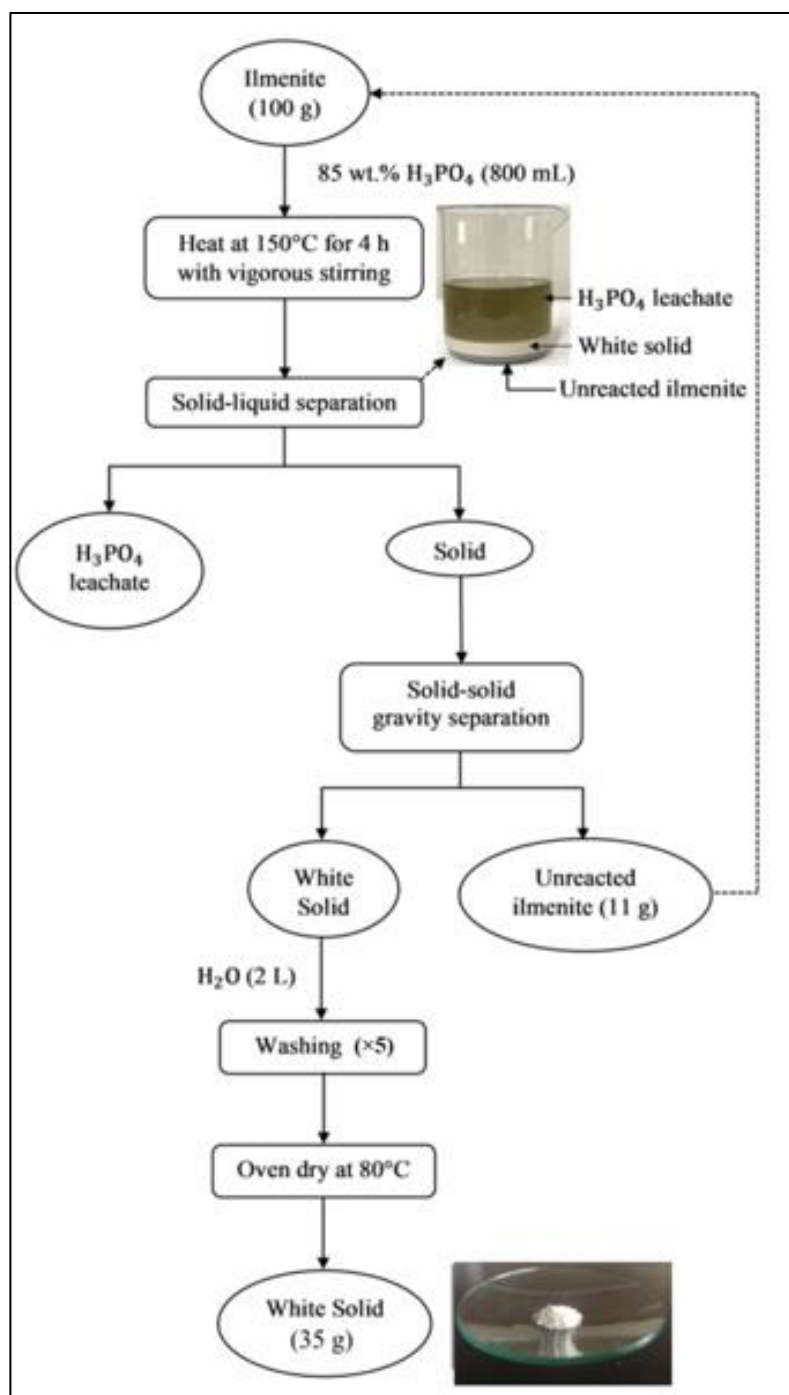
Figure 2.1: Direct digestion of ilmenite with H_3PO_4.

The two upper layers were mechanically separated from the unreacted ilmenite settled at the bottom using a decantation technique. The separated middle WP layer was mixed with 2 L of distilled water and stirred thoroughly for 2 hours at 300 rpm. The mixture was then allowed to resettle for 24 hours. This water-washing step was repeated five times until the WP was free of unreacted ilmenite and the mixture pH reached neutral levels. The purified α-TiP product was oven-dried at 80 °C and stored in a desiccator.

To optimize the synthesis conditions, a series of experiments were conducted to understand the effect of the mass/volume ratio of ilmenite to acid, refluxing time, and concentration of H_3PO_4 on the formation of the desired WP containing α-TiP.

The direct acid digestion method allows for the synthesis of α-TiP from the ilmenite mineral ore via a rather simple and economical approach. Careful control of the reaction parameters is crucial for maximizing the yield and purity of the α-TiP product.

2.1.3   Effect of Ilmenite to Acid Ratio

The ratio of ilmenite to H_3PO_4 plays a crucial role in determining the titanium recovery efficiency of the WP obtained. Experiments were conducted with varying ilmenite-to-H_3PO_4 ratios (w/v) of 1:2, 1:4, 1:6, and 1:8 while keeping the refluxing time constant at 4 hours (Figure 2.2.a). The results revealed that the titanium recovery efficiency of the WP, separated from unreacted ilmenite, reached its maximum when the ilmenite-to-H_3PO_4 ratio was above 1:4 (Figure 2.2.b).
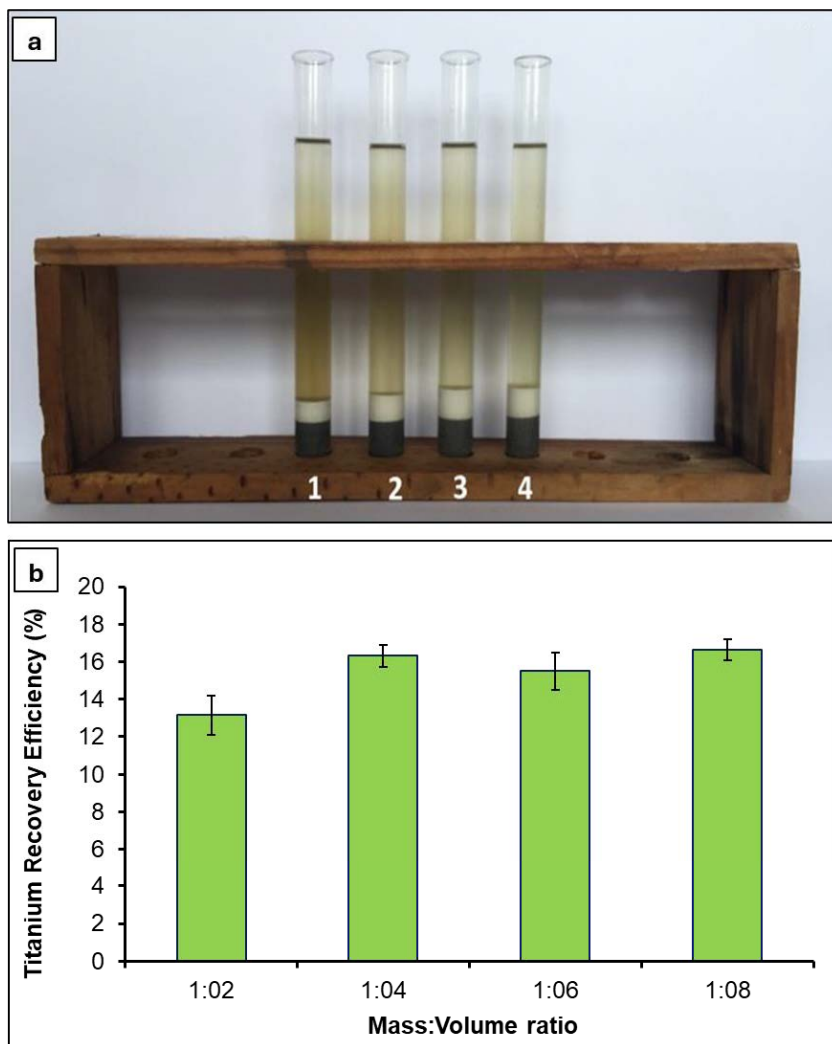
Figure 2.2: Influence of Ilmenite to H_3PO_4 acid ratios on the reaction process. (a) Representation of the solid-liquid layer separation following the reaction between ilmenite and H_3PO_4 (85 wt.%), showcasing variations in mass-to-volume ratios (g: mL) from left to right: 1:2, 1:4, 1:6, and 1:8 at 150 °C for 4 hours; (b) Variation in α-TiP titanium recovery percentage concerning varying ilmenite to H_3PO_4 pulp densities.

However, at a 1:4 ratio, the reaction mixture formed a paste-like consistency, which posed practical difficulties during mixing and gravity settling of the solids due to the lack of a liquid phase. To overcome this issue, additional H_3PO_4 was added until the pulp density reached 125 g L^{-1}, facilitating efficient mixing and improving the reaction conditions.

This observation aligns with previous studies on the dissolution of ilmenite in phosphoric acid. For instance, Wahyuningsih et al. (2014) reported that increasing the acid-to-ilmenite ratio enhanced the dissolution of ilmenite and subsequent titanium extraction. They attributed this behavior to the increased availability of H^+ and the formation of more favorable reaction conditions for the dissolution of ilmenite.

The decision to adjust the pulp density by adding additional H_3PO_4 is a novel approach compared to previous studies. Typically, researchers have employed methods such as increasing the reaction temperature or extending the reaction time to enhance the dissolution of ilmenite and titanium recovery. [5]

Additionally, Palliyaguru et al. (2019) found that the percentage of titanium extracted decreased at temperatures higher than 150 °C due to the hydrolysis of titanium. This observation suggests that increasing the reaction temperature beyond an optimal point can hurt the titanium recovery efficiency. Furthermore, they determined that the optimal acid/ore ratio for ilmenite leaching was 2:1 (w/w) at a reaction time of 3 h.

By adjusting the pulp density through the addition of more acid, as demonstrated in the present study, the desired reaction conditions were maintained without the need for increasing the temperature or extending the reaction time. This approach not only ensures efficient mixing and mass transfer but also avoids the potential drawbacks associated with elevated temperatures, such as hydrolysis of titanium or excessive energy consumption.

Moreover, optimizing the pulp density by adding more acid can potentially reduce the processing time required for the reaction, as evidenced by Palliyaguru et al.'s (2019) finding of an optimal reaction time of 3 h. By maintaining the appropriate pulp density, the reaction kinetics can be enhanced, leading to faster and more efficient titanium extraction.

Therefore, the findings from both the present study and the work of Palliyaguru et al. (2019) support the argument that adjusting the pulp density by adding more acid can provide better control over the reaction conditions, minimize energy consumption associated with temperature increases, and potentially reduce the overall processing time required for efficient titanium recovery from ilmenite.

2.1.4 Influence of Reaction Time

The refluxing time required for achieving maximum titanium recovery was also investigated by conducting experiments at a pulp density of 125 gL^{-1}. The results indicated that the titanium recovery values did not change significantly after 3 hours of refluxing (Figure 2.3). Consequently, a refluxing time of 4 hours was adopted to ensure the optimum formation of the WP.
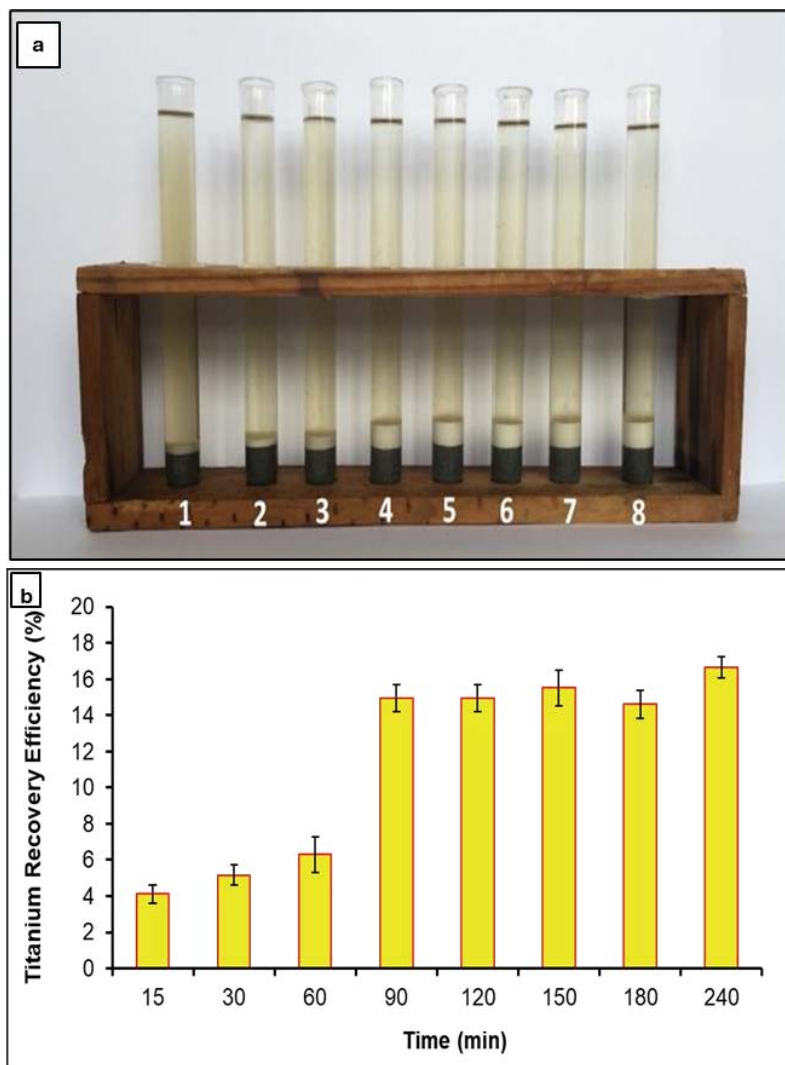
Figure 2.3: Influence of reaction time on the ilmenite and H_3PO_4 reaction process. (a) Visual representation of the solid-liquid layer separation post-reaction between ilmenite and H_3PO_4 (85 wt.%), depicting variations in reaction time (in minutes) from 30 to 240 at 150 °C, with a mass-to-volume ratio of 1:8 (5 g:40 mL) from left to right; (b) Refluxing time of the reaction mixture at an ilmenite to H_3PO_4 pulp density of 125 gL^{-1}.

These findings align with previous studies that have reported the existence of an optimal reaction time for the leaching of ilmenite with phosphoric acid. For instance, Palliyaguru et al. (2019) determined that the optimal reaction time for ilmenite leaching was 3 hours when using an acid/ore ratio of 2:1 (w/w). Similarly, Omidi et al. (2018) observed that increasing the leaching time beyond 4 hours did not significantly improve the dissolution of ilmenite and titanium recovery.

The existence of an optimal reaction time can be attributed to the kinetics of the leaching process and the mass transfer limitations that govern the dissolution of ilmenite.[1, 6] Initially, the dissolution rate is rapid due to the availability of fresh reactive surfaces and a high concentration gradient. However, as the reaction progresses, the formation of reaction products and the depletion of reactants can lead to a decrease in the overall dissolution rate.[1, 7]

By adopting a refluxing time of 4 hours, we have ensured that the leaching process has reached equilibrium or near-equilibrium conditions, maximizing the formation of the desired WP. Extending the refluxing time beyond this point may not significantly improve the titanium recovery but could lead to increased energy consumption and processing costs.

Our decision to adopt a 4-hour refluxing time, slightly longer than the observed optimal time of 3 hours, demonstrates a cautious approach to ensure the complete formation of the WP. This strategy aligns with industrial practices, where slight over-processing is

often preferred to account for potential variations in feedstock composition, and minor process fluctuations, and to ensure consistent product quality.

2.1.5 Impact of Acid Concentration

The influence of H_3PO_4 concentration on titanium recovery was evaluated by conducting experiments at 100 °C for a reaction time of 4 hours, with a pulp density of 125 gL^{-1}. A constant temperature of 100 °C was selected to eliminate the effect of boiling point changes arising from dilution of H_3PO_4, which could potentially affect the final WP yield. The results demonstrated that higher concentrations of H_3PO_4 produced higher recovery efficiencies for titanium (Figure 2.4). This observation aligns with numerous previous studies that have reported a positive correlation between acid concentration and titanium extraction from ilmenite.[1,6,8]
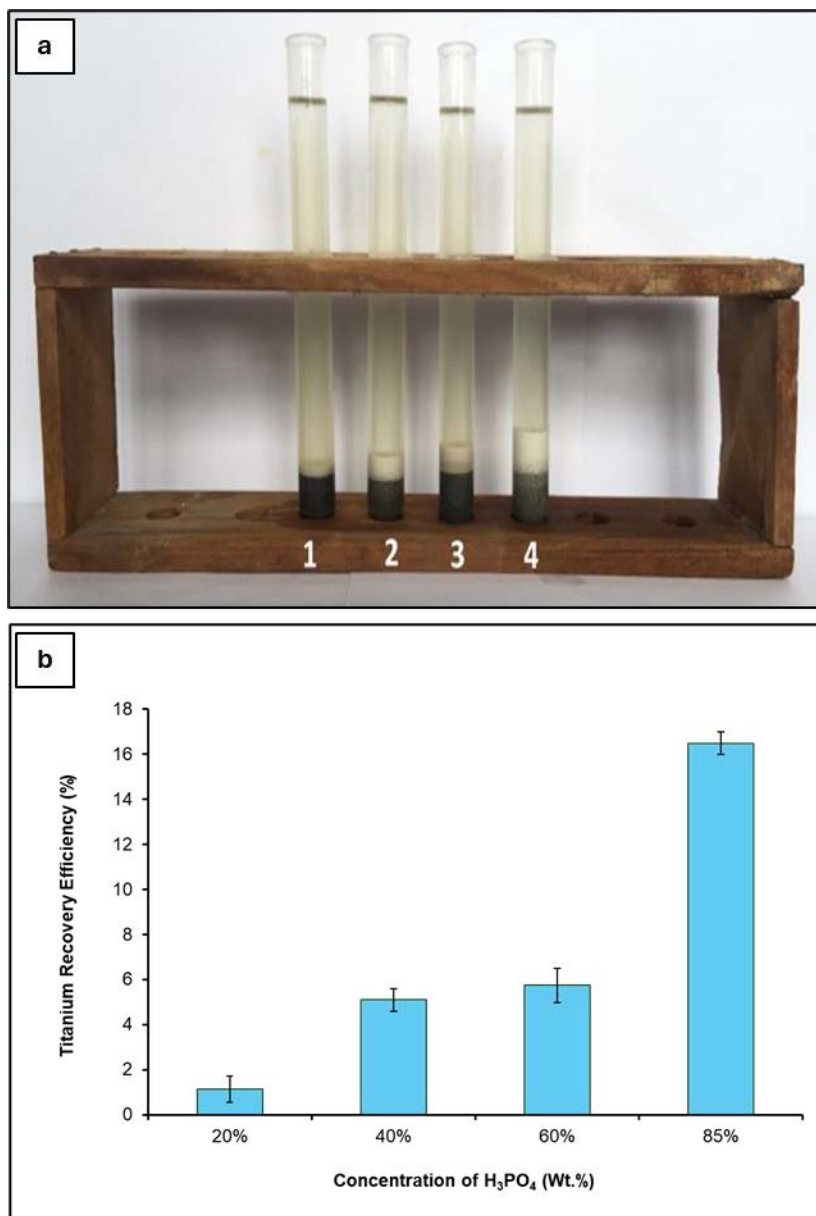
Figure 2.4: Influence of acid concentration on the ilmenite and H_3PO_4 reaction process. (a) Representation of H_3PO_4 concentrations at 20%, 40%, 60%, and 85% at 150 °C, with a mass-to-volume ratio of 1:8 (5 g:40 mL) for 4 hours; (b) H_3PO_4 concentration at a pulp density of 125 gL^{-1}.

The dependence of titanium recovery on acid concentration can be attributed to several factors. First, higher acid concentrations provide a greater abundance of H$^+$, which is

necessary for the dissolution of ilmenite and the subsequent formation of soluble titanium species.[5, 9] Additionally, higher acid concentrations can facilitate the breakdown of the ilmenite structure, exposing more reactive surfaces for leaching.[9]

However, it is important to note that there may be an upper limit beyond which further increases in acid concentration may not significantly enhance titanium recovery or may even have detrimental effects. For instance, Omidi et al. (2018) observed that excessive acid concentrations could lead to the formation of insoluble titanium complexes, hindering the leaching process. Therefore, an optimal acid concentration range must be determined for each specific system and a set of operating conditions.

Under the optimized parameters of a pulp density of 125 gL^{-1}, a refluxing time of 4 hours, and the use of 85 wt.% H_3PO_4, approximately 35 g of dry WP was obtained from 100 g of ilmenite, corresponding to a titanium recovery efficiency of around 17%. While this recovery efficiency may seem relatively low, it is important to consider that we have focused on optimizing a specific set of parameters, and further improvements could potentially be achieved by exploring additional variables or implementing alternative processing techniques.

For instance, a novel approach reported by Palliyaguru et al. (2019) involved the use of a two-stage leaching process, where the initial leaching stage was followed by an oxidative roasting step to enhance the dissolution of unreacted ilmenite. Such innovative techniques, combined with the optimization of process parameters, could potentially lead to higher titanium recovery efficiencies.

Calculations

35 g of white powder (α-TiP) was obtained which contains 17.2% (mass%) titanium.

Therefore, 35 g of white powder contained 6.02 g of titanium.

In this process, 100 g of ilmenite was used with a titanium content is 35.5 g.

Therefore, out of 100 g of ilmenite (Ti content = 35.5%), recovery is 6.02g.

Hence, % recovery was $[\frac{6.02}{35.5} \times 100\%]$ = **17%**

When comes to yield %;

100 g of ilmenite was used in which 35.5 g was present as titanium (mass% of Ti= 35.5)

No. of moles of Ti in 100 g of ilmenite = [35.5 g / 47.9 g mol-1] = 0.74

(Molar mass of Ti = 47.9 gmol^{-1})

If all this Ti in ilmenite is converted to α-TiP through the process, a theoretical mass of α-TiP should be:

0.74 mol x 257.9 g mol^{-1} = 190.8 g (molar mass of α-TiP = 257.9 g mol^{-1})

Obtained 190 g, theoretically should be 190.8 g

Yield % [35 g/190.8 g] x 100 = **18%**

2.1.6   Characterization of the α-TiP Product

XRD analysis confirmed that the WP produced was α-TiP (Figure 2.5.b), which converts to the more stable TiP_2O_7 upon calcination at 800 °C (Figure 2.5.c). This finding is consistent with previous studies that have reported the formation of α-TiP as an intermediate phase during the dissolution of ilmenite in phosphoric acid. The subsequent conversion of α-TiP to the more stable TiP_2O_7 upon calcination at 800 °C is also in agreement with the literature.[1, 5, 6]
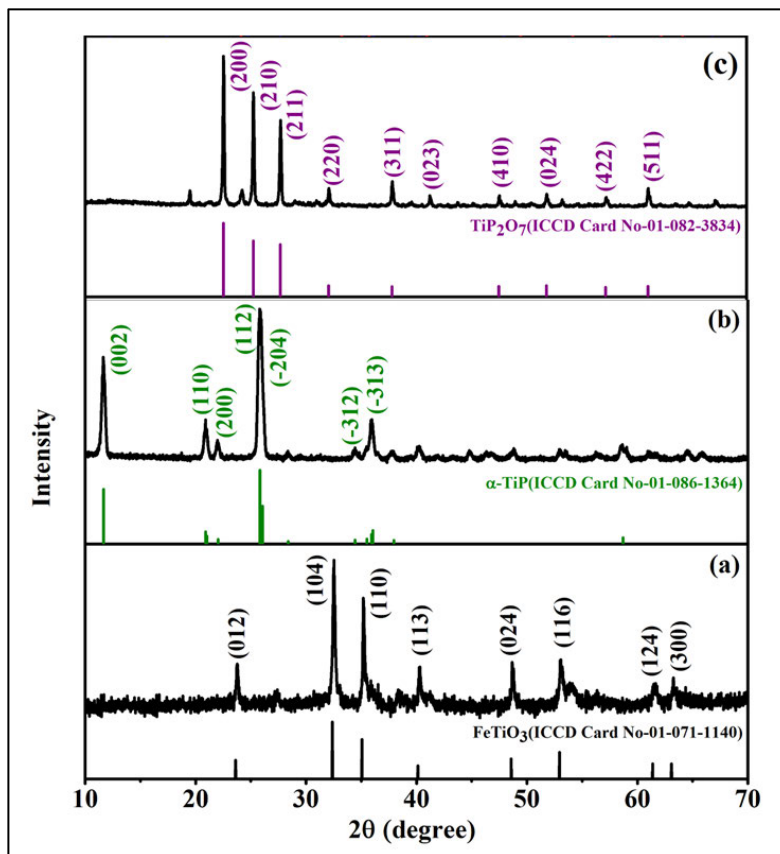
Figure 2.5: X-ray Diffraction (XRD) Patterns of (a) Ilmenite, (b) α-TiP, and (c) TiP_2O_7.

The percentage recovery of titanium in α-TiP from ilmenite (~17%) is relatively low, which is supported by the physical evidence of substantial amounts of unreacted ilmenite

remaining in the bottom of the reaction vessel. Similar observations have been reported by other researchers, where the extent of ilmenite dissolution was found to be influenced by various factors, including acid concentration, temperature, and reaction time.[4, 6]

Further characterization revealed that the WP samples prepared under these conditions contained Fe, Ti, and P with mass percentages of 1.8%, 17.2%, and 27.2%, respectively, in addition to other elements like Mg and V (Table 2.1), which is consistent with the expected impurities present in the ilmenite ore used as the starting material. The presence of iron in the α-TiP product is particularly noteworthy, as it has been reported that iron can partially substitute for titanium in the titanium phosphate structure.[10, 11]

Table 2.1: Percentage of the metal composition of Hi-Ti ilmenite and α-TiP.

	Mass % (n=3)							
	Ti	**Fe**	**P**	**K**	**Mn**	**V**	**Si**	**Mg**
Ilmenite	35.5	20.9	0.8	-	0.5	0.3	0.9	1.1
α-TiP	17.2	1.8	27.2	-	-	0.1	-	1.5

Calculations

With the assumption of 35 g of white powder, which obtained is 100% pure α-TiP (Mw=258.8 g mol-1, Ti wt%=18.5), theoretically, it should contain 6.48 g of titanium.

$[\frac{35\ g}{258\ gmol-1} \times 47.8\ \text{gmol}^{-1}] = 6.48$.

According to the EDAX results, only 6.02 g of titanium was found in α-TiP obtained. Therefore, the purity of α-TiP obtained from was $[\frac{6.02}{35.2} \times 100\%]= \underline{\textbf{88\%}}$.

The yield of WP obtained (18.3 wt.%) is fairly low; nevertheless, the purity of α-TiP is 92.6 wt.%. This high purity can be attributed to the selective precipitation of titanium as α-TiP, while iron remains in the solution as soluble iron phosphate complexes, as proposed by the reaction Equation 1 and supported by literature.[5, 10, 11]

$$3FeTiO_3 + 10H_3PO_4 \rightarrow 3Ti(HPO_4)_2 + 3Fe(H_2PO_4)^{2+} PO_4^{3-} + 9H_2O .... (1)$$

At a temperature of ~150 °C and under refluxing conditions, the oxidation of Fe(II) to Fe(III) takes place. Furthermore, in the presence of concentrated H_3PO_4, Fe(II)/(III) can form various multiligand complexes, such as $Fe(HPO_4)^+$, $Fe(H_2PO_4)^{2+}$, $FeH_5(PO_4)_2^{2+}$, and $FeH_7(PO_4)_3^+$, all of which are soluble in the acidic medium.[12] In general, the reaction can be represented as Equation 2. This property of concentrated phosphoric acid, which enables the separation of titanium and iron through selective precipitation and dissolution, respectively, offers a significant advantage over conventional methods for titanium recovery from ilmenite.

$$Fe^{3+} + H_3PO_4 \rightarrow FeHnPO_4^{n+} + (3-n)H^+ \cdots\cdots\cdots\cdots\cdots\cdots\cdots (2)$$

Compared to the use of strong acids like H_2SO_4 and HCl, the one-pot acid digestion approach using the weak acid H_3PO_4 is more environmentally friendly and safer. The one-pot acid digestion approach using the weak acid H_3PO_4 is more environmentally friendly and safer compared to the use of strong acids like H_2SO_4 and HCl. In contrast, phosphoric acid is a weak acid with a pKa around 2.1, while sulfuric and hydrochloric acids are strong acids that completely dissociate in water. This means phosphoric acid

produces a lower concentration of H$^+$ ions in solution, making it less corrosive and hazardous to handle. Additionally, phosphoric acid is less volatile compared to HCl, reducing the risk of exposure to toxic fumes during the digestion process. The use of phosphoric acid also avoids the production of sulfate waste associated with H$_2$SO$_4$ digestion. One-pot acid digestion using H$_3$PO$_4$ has been demonstrated for the synthesis of biodegradable uronic acid-based surfactants from oligo alginates, semi-refined alginates, and crude brown seaweeds. This cascading one-pot approach facilitates the valorization of biomass while minimizing waste and hazardous chemical usage.[13, 14]

Furthermore, the selective precipitation of titanium as α-TiP simplifies the separation process, eliminating the need for additional steps like solvent extraction or ion exchange, which are often required in conventional methods. Selective precipitation is an effective technique for separating titanium from other metals like Fe, Mg, and Al in steel-making slag leach liquor. By controlling the precipitation conditions, titanium can be selectively precipitated as α-TiP, allowing for its efficient separation from the solution.[15, 16]

References

[1] Thambiliyagodage, C.; Wijesekera, R.; Bakker, M. G. Leaching of Ilmenite to Produce Titanium Based Materials: A Review. Discover Materials 2021, 1 (1). https://doi.org/10.1007/s43939-021-00020-0.

[2] Nguyen, T. H.; Lee, M. S. A Review on the Recovery of Titanium Dioxide from Ilmenite Ores by Direct Leaching Technologies. Mineral Processing and Extractive Metallurgy Review 2018, 40 (4), 231–247. https://doi.org/10.1080/08827508.2018.1502668.

[3] Palliyaguru, L.; Kulathunga, M. U. S.; Kumarasinghe, K. G. U. R.; Jayaweera, C. D.; Jayaweera, P. M. Facile Synthesis of Titanium Phosphates from Ilmenite Mineral Sand: Potential White Pigments for Cosmetic Applications. Journal of Cosmetic Science 2019, 70 (3), 149–159.

[4] Wahyuningsih, S.; Ramelan, A.; Pramono, E.; Djatisulistya, A. Titanium Dioxide Production by HydrochloricAcid Leaching of Roasting Ilmenite Sand. International Journal of Scientific and Research Publications 2014, 4 (11).

[5] Hasan Omidi, M.; Salmani Nuri, O.; Tavakoli, H. Optimization of Ilmenite Dissolution by Synergistic Effect of Oxalic Acid and Hydrochloric Acid for Preparing Synthetic Rutile. International Journal of Nonferrous Metallurgy 2018, 07 (03), 25–38. https://doi.org/10.4236/ijnm.2018.73003.

[6] Mahmoud, M. H. H.; Afifi, A. A. I.; Ibrahim, I. A. Reductive Leaching of Ilmenite Ore in Hydrochloric Acid for Preparation of Synthetic Rutile. Hydrometallurgy 2004, 73 (1–2), 99–109. https://doi.org/10.1016/j.hydromet.2003.08.001.

[7] Reaction Rates and Rate Laws. saylordotorg.github.io. https://saylordotorg.github.io/text_general-chemistry-principles-patterns-and-applications-v1.0/s18-02-reaction-rates-and-rate-laws.html.

[8] Chagnes, A.; Mangold, L.; Halleux, H.; Cote, G. New Insights on Titanium(IV) Speciation to Improve the Purification of Concentrated Phosphoric Acid. The minerals, metals & materials series 2023, 131–140. https://doi.org/10.1007/978-3-031-22761-5_13.

[9] Valdivieso-Ramírez, C. S.; Pontón, P. I.; Dosen, A.; Marinkovic, B. A.; Guerrero, V. H. One-Step Synthesis of Iron and Titanium-Based Compounds Using Black Mineral Sands and Oxalic Acid under Subcritical Water Conditions. Minerals 2022, 12 (3), 306. https://doi.org/10.3390/min12030306.

[10] Essehli, R.; El Bali, B.; Faik, A.; Naji, M.; Benmokhtar, S.; Zhong, Y. R.; Su, L. W.; Zhou, Z.; Kim, J.; Kang, K.; Dusek, M. Iron Titanium Phosphates as High-Specific-Capacity Electrode Materials for Lithium Ion Batteries. Journal of alloys and compounds 2014, 585, 434–441. https://doi.org/10.1016/j.jallcom.2013.09.093.

[11] Petersen, H.; Stegmann, N.; Fischer, M.; Zibrowius, B.; Radev, I.; Philippi, W.; Schmidt, W.; Weidenthaler, C. Crystal Structures of Two Titanium Phosphate-Based Proton Conductors: Ab Initio Structure Solution and Materials Properties. Inorganic Chemistry 2021, 61 (5), 2379–2390. https://doi.org/10.1021/acs.inorgchem.1c02613.

[12] Zhang, T.; Liu, C.-T. Design of Titanium Alloys by Additive Manufacturing: A Critical Review. Advanced Powder Materials 2021, 1 (1). https://doi.org/10.1016/j.apmate.2021.11.001.

[13] Pessel, F.; Noirbent, G.; Boyère, C.; Arnaud, S. P.; Wong, T.; Durand, L.; Benvegnu, T. Cascading One-Pot Synthesis of Biodegradable Uronic Acid-Based Surfactants from Oligoalginates, Semi-Refined Alginates, and Crude Brown Seaweeds. Molecules/Molecules online/Molecules annual 2023, 28 (13), 5201–5201. https://doi.org/10.3390/molecules28135201.

[14] Bonnin, I.; Méreau, R.; Tassaing, T.; De, K. Selective One-Pot Synthesis of Sorbitans (1.4-Sorbitan and 3.6-Sorbitan) from Glucose Via Catalytic Hydrogenation and CO2-Mediated Dehydration. ACS sustainable chemistry & engineering 2024. https://doi.org/10.1021/acssuschemeng.3c08156.

[15] Kim, J.; Azimi, G. Selective Precipitation of Titanium, Magnesium, and Aluminum from the Steelmaking Slag Leach Liquor. Resources, Conservation and Recycling 2022, 180, 106,177. https://doi.org/10.1016/j.resconrec.2022.106177.

[16] Purcell, W.; Sinha, M. K.; Vilakazi, A. Q.; Nete, M. Selective Precipitation Study for the Separation of Iron and Titanium from Ilmenite. Hydrometallurgy 2020, 191, 105,242. https://doi.org/10.1016/j.hydromet.2019.105242.

CHAPTER 3
ALKALI ROASTING ASSISTED α-TiP SYNTHESIS

3.1   Investigating the Alkali Roasting Parameters

An alternative synthetic approach to the direct acid digestion method involves an alkali roasting pretreatment step before acid digestion. In this two-step process, ilmenite is first subjected to alkaline decomposition by reacting with KOH at elevated temperatures, forming a reactive intermediate. This intermediate is subsequently digested in H_3PO_4 to yield the desired α-TiP product.

The alkali roasting pretreatment aims to convert the ilmenite into a more reactive form, facilitating its subsequent conversion to α-TiP. The key parameters governing the alkali roasting step, including the ilmenite-to-KOH molar ratio, roasting temperature, and residence time, significantly influence the nature and reactivity of the intermediate product, ultimately impacting the yield and purity of the final α-TiP.

3.1.1   Alkali Roasting Procedure

The alkaline decomposition of ilmenite was carried out by mixing ilmenite with KOH in a molar ratio of 1:4, based on previous studies demonstrating the effectiveness of this ratio.[1, 2] The mixture was then transferred to a furnace and heated at 800 °C for 4 hours. The resulting green-colored solid was removed from the porcelain crucible and washed with 1 L of distilled water under vigorous stirring at 300 rpm using a magnetic stirrer. This washing step was repeated five times until the excess KOH was removed, and the solution pH became neutral. The resulting brown powder, hereafter referred to as BP, was filtered and oven-dried at 80 °C for 24 hours (Figure 3.1).
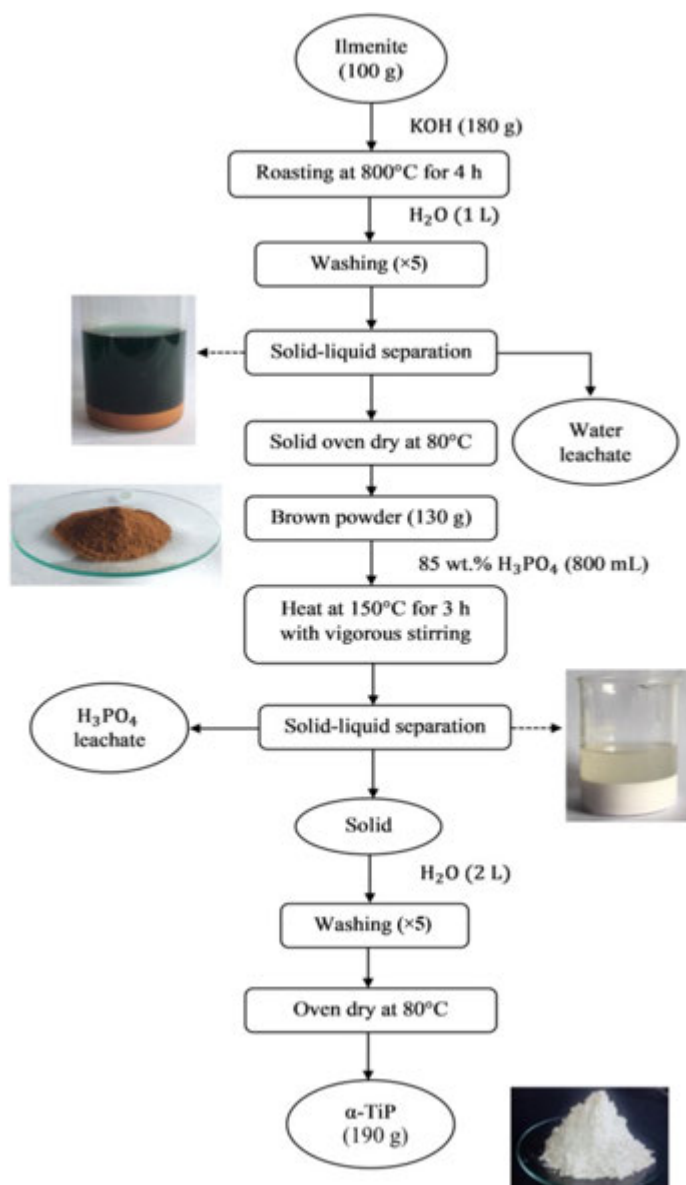
Figure 3.1: KOH roasting followed by the reaction with H_3PO_4.

In the subsequent step, 130 g of the BP intermediate was reacted with 800 mL of 85 wt.% H_3PO_4, corresponding to a solid-to-liquid ratio of 1:8, for 4 hours at 150 °C under refluxing conditions. The obtained white powder, primarily consisting of α-TiP, was washed with 2 L of distilled water five times until the solution pH reached neutrality. The purified α-TiP product was filtered, oven-dried at 80 °C, and stored in a desiccator.

1.3.2 Optimization of Alkali Roasting Parameters

To optimize the alkali roasting process for maximum yield and purity of the α-TiP product, the key control parameters were systematically investigated. These parameters included the ilmenite-to-KOH molar ratio, roasting temperature, residence time in the furnace, and the reaction parameters for the subsequent digestion of the BP intermediate with 85 wt.% H_3PO_4.

While the ilmenite-to-KOH molar ratio was initially set at 1:4 based on previous studies, a range of roasting temperatures from 200 °C to 800 °C was evaluated to determine the optimal temperature for the alkali roasting step. Once an effective roasting temperature of 800 °C was established, experiments were conducted to determine the minimum residence time required to obtain a higher yield of the BP intermediate.

Furthermore, the reaction time for the digestion of the BP intermediate with 85 wt.% H_3PO_4, leading to the formation of α-TiP as the final product, was systematically varied at a fixed solid-to-liquid ratio of 1:8.

3.2   Role of Roasting Temperature

The roasting temperature plays a crucial role in the decomposition of ilmenite in the presence of KOH. In this method, a mixture of ilmenite and KOH (with a Ti/K molar ratio of 1:4) was roasted at different temperatures of 200 °C, 400 °C, 600 °C, and 800 °C for 4 hours. The titanium recovery efficiency of the final WP obtained from the

subsequent acid reaction was analyzed for each roasting temperature, as evidenced by the results presented in Figure 3.2.b.
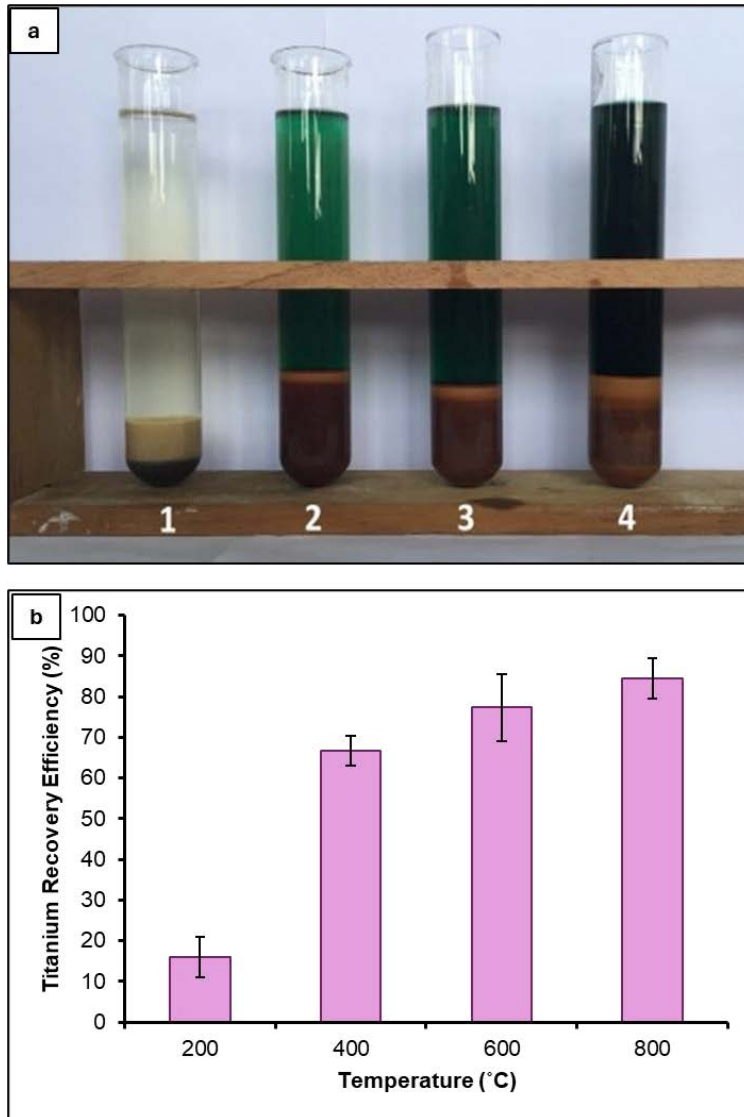
Figure 3.2: Solid/Liquid layer separation of ilmenite and KOH (5 g:8.4 g) roasted mixture mixed with water. (a) Visual representation of left-to-right variation in roasting temperature at 200 °C, 400 °C, 600 °C, and 800 °C; (b) Weight percentage of α-TiP formed with varying roasting temperatures.

At lower roasting temperatures of 200 °C and 400 °C, the titanium recovery efficiency was relatively low. This can be attributed to the incomplete decomposition of ilmenite, which requires higher temperatures to facilitate the desired reactions with molten KOH. Similar observations have been reported in the literature, where the decomposition of ilmenite in the presence of alkali compounds, such as KOH and Na_2CO_3, was found to be highly dependent on the roasting temperature.[3, 4]

A significant increase in the titanium recovery efficiency was observed when the roasting temperature was increased to 600 °C and 800 °C. This can be explained by the fact that at higher temperatures, the molten KOH effectively promotes the decomposition of ilmenite, enabling the desired reactions to proceed more efficiently. The findings are consistent with previous studies that have reported improved titanium recovery from ilmenite when roasted at temperatures above 600 °C in the presence of alkali compounds (Lasheen et al., 2008; El-Hakam et al., 2020; Zaki et al., 2008).[3, 5, 6]

Furthermore, as depicted in Figure 3.2.a the observation of a green color in the water leachate during the washing steps of the BP product, which intensified with increasing roasting temperatures, is indicative of the conversion of manganese present in ilmenite to K_2MnO_4. This conversion can be represented by the following equation.[7]

$$2MnO_2 + 4KOH + O_2 \rightarrow 2K_2MnO_4 + 2H_2O \dots\dots\dots\dots\dots\dots\dots\dots\dots\dots\dots (3)$$

The formation of K_2MnO_4 is a well-documented phenomenon during the alkali roasting of ilmenite and other manganese-containing minerals. The intensity of the green color is directly proportional to the extent of this reaction, which is favored at higher roasting temperatures due to the increased reactivity of the molten KOH.[5, 7]

3.3   Effect of Roasting Duration

After determining the optimal roasting temperature of 800 °C, the effect of roasting duration on the titanium recovery efficiency was investigated. The results presented in Figure 3.3 provide valuable insights into the kinetics of the ilmenite decomposition reaction in the presence of KOH.
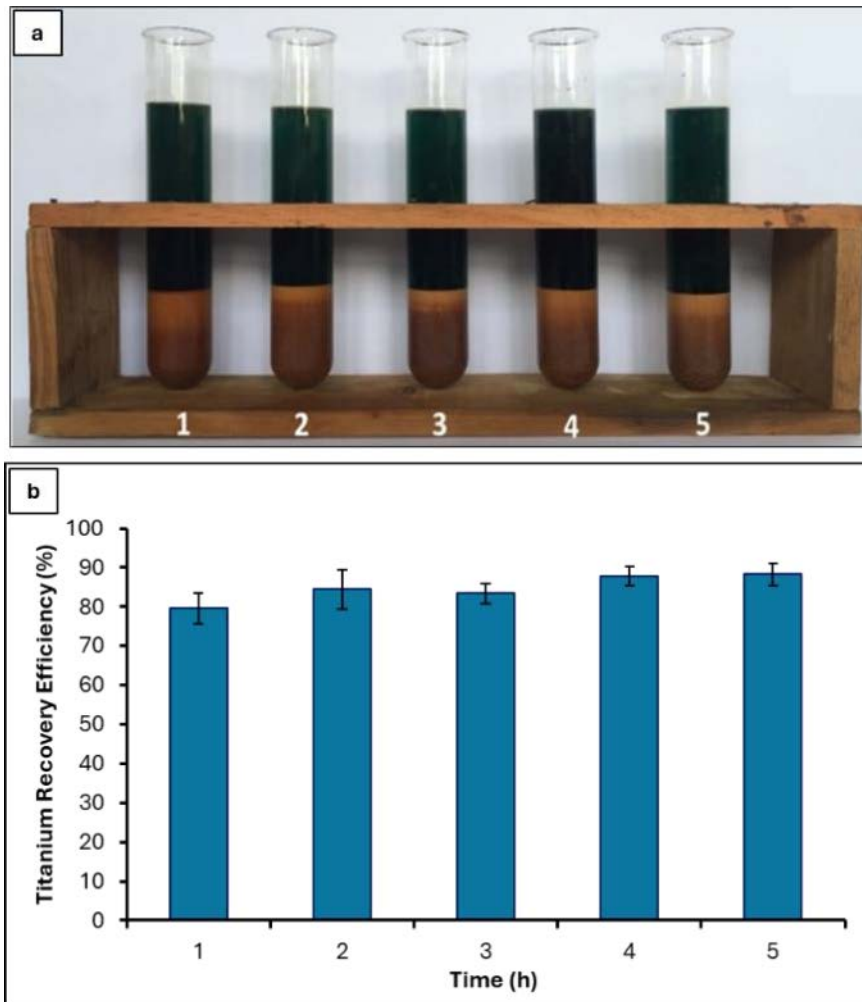
Figure 3.3: Solid/liquid layer separation of ilmenite and KOH (5 g:8.4 g) roasted mixture mixed with water. (a) A photograph depicting the variation of roasting time at 800 °C for 1 h, 2 h, 3 h, and 4 h; (b) Titanium recovery efficiency variation with roasting time at 800 °C using Ilmenite and KOH at a 1:4 molar ratio.

The data revealed that a roasting time beyond 3 hours at 800 °C was sufficient to obtain the maximum titanium recovery efficiency. This observation suggests that the decomposition of ilmenite and the subsequent reactions with KOH reach completion

within this time frame at the optimized temperature of 800 °C. Similar trends have been reported in the literature, where longer roasting durations were found to have a diminishing effect on the titanium recovery efficiency once the reactions reached equilibrium.[8, 9, 10]

Despite achieving the maximum titanium recovery efficiency after 3 hours of roasting, a roasting duration of 4 hours was adopted for the KOH roasting step. This decision was likely made to ensure the complete decomposition of ilmenite and the absence of any residual unreacted material, which could potentially affect the subsequent processing steps or the purity of the final product.

The kinetics of the ilmenite decomposition reaction in the presence of KOH is governed by a complex interplay of various factors, including temperature, KOH concentration, particle size, and the presence of impurities or minor components in the ilmenite ore.[9, 10, 11] At the optimized temperature of 800 °C and with a Ti/K molar ratio of 1:4, the reaction kinetics were favored, enabling the complete decomposition of ilmenite within the 3-4-hour time frame.

It is important to note that while longer roasting durations may not significantly improve the titanium recovery efficiency, they can potentially impact other aspects of the process, such as energy consumption, material handling, and overall process economics. Therefore, the optimal roasting duration should be carefully selected by considering not only the titanium recovery efficiency but also other practical and economic factors.

3.4 Acid Reaction and α-TiP Formation

The acid reaction step, involving the reaction between the BP obtained after the KOH roasting step and concentrated phosphoric acid (85 wt.% H_3PO_4), played a crucial role in the formation of the desired α-TiP product. The rapid completion of this reaction within approximately 30 minutes indicates the high reactivity of the BP with H_3PO_4, facilitated by the prior decomposition of ilmenite during the KOH roasting step (Figure 3.4).
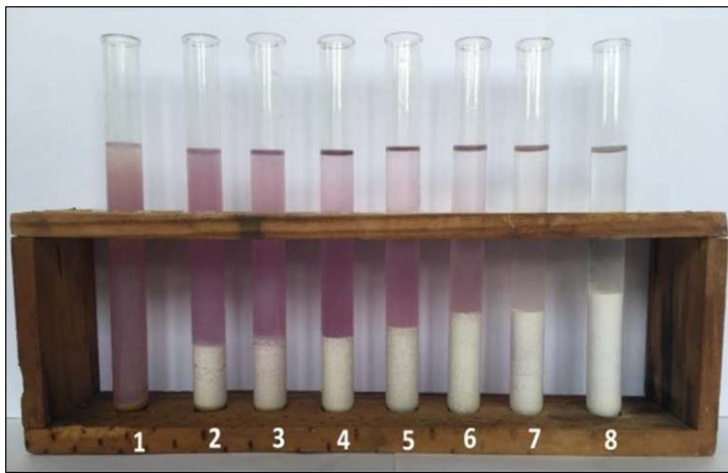
Figure 3.4: reaction between brown powder (BP) and H_3PO_4 (5 g:40 mL) at 150 °C. Variation of reaction time from left to right: 2, 4, 6, 8, 10, 12, 30, and 60 minutes.

The BP consisted primarily of potassium titanate ($KTi_8O_{16.5}$) and Fe_2O_3, formed as a result of the complete decomposition of ilmenite in the presence of molten KOH. The reaction between potassium titanate and H_3PO_4 can proceed through various possible pathways, as represented by equations 4–6.[6, 9, 10]

$$6KTi_8O_{16.5} + 98H_3PO_4 \rightarrow 48Ti(HPO_4)_2.H_2O + 2 K_3(PO_4) + 51H_2O \dots\dots\dots\dots (4)$$

$$4KTi_8O_{16.5} + 66H_3PO_4 \rightarrow 32Ti(HPO_4)_2.H_2O + 2K_2(HPO_4) + 34H_2O \dots\dots\dots\dots (5)$$

$$4\ KTi_8O_{16.5} + 68H_3PO_4 \rightarrow 32Ti(HPO_4)_2.H_2O + 4\ K(H_2PO_4) + 34H_2O \dots\dots\dots\dots\dots (6)$$
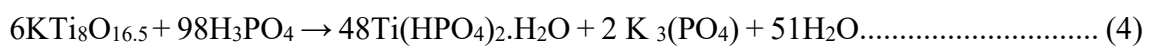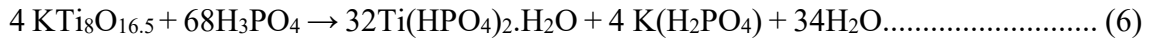
These reactions involve the dissolution of $KTi_8O_{16.5}$ in concentrated H_3PO_4, leading to the formation of titanium phosphate hydrate $[Ti(HPO_4)_2.H_2O]$ and various potassium phosphate compounds, such as $K_3(PO_4)$, $K_2(HPO_4)$, and $K(H_2PO_4)$. The titanium phosphate hydrate is the precursor to the formation of α-TiP during the subsequent drying and calcination steps.

In addition to the reaction with $KTi_8O_{16.5}$, the Fe_2O_3 present in the BP also undergoes a reaction with H_3PO_4, as represented by Equation 7.[10, 12]

$$2Fe_2O_3 + 27H^+ + 7PO_4^{3-} \rightarrow Fe(HPO_4)^+ + Fe(H_2PO_4)^{2+} + FeH_5(PO_4)_2^{2+} + FeH_7(PO_4)_3^+ +$$

$$6H_2O \dots\dots\dots\dots\dots\dots\dots\dots\dots\dots\dots\dots\dots\dots\dots\dots\dots\dots\dots\dots\dots\dots\dots (7)$$
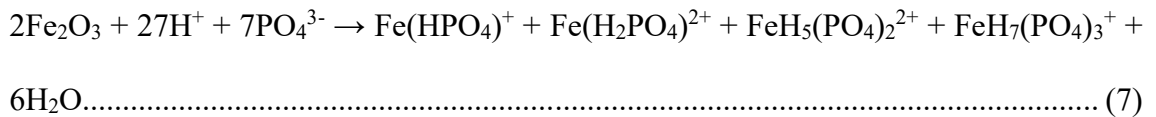
This reaction leads to the formation of soluble iron phosphate complexes, such as $Fe(HPO_4)^+$, $Fe(H_2PO_4)^{2+}$, $FeH_5(PO_4)_2^{2+}$, and $FeH_7(PO_4)_3^+$, which remain in the solution phase. The selective precipitation of titanium as α-TiP and the dissolution of iron as soluble complexes are key aspects of this process, enabling the separation of titanium from iron-containing impurities.

The rapid completion of the acid reaction within 30 minutes can be attributed to the high reactivity of the BP, facilitated by the prior decomposition of ilmenite during the KOH roasting step. The KOH roasting ensures the complete breakdown of the ilmenite

structure, rendering the titanium and iron components more accessible for subsequent reactions with H_3PO_4.

Calculations

One hundred g of ilmenite and 190 g of white powder (α-TiP) were obtained. Titanium mass percentages of ilmenite and white powder are 35.5% and 16.2% respectively. This means that the initial 100 g of ilmenite contains 35.5 g of Titanium and 190 g of White powder is contained 30.8 g (100→ 16.2, ∴ 190→30.8) of Titanium.

Therefore, 30.8 g of Titanium was recovered from 35.5 g. Hence, % recovery was;

$[\frac{30.8}{35.5}× 100\%] = \underline{\textbf{87\%}}$

When comes to yield %;

100 g of ilmenite was used in which 35.5 g was present as titanium (mass% of Ti= 35.5)

No. of moles of Ti in 100 g of ilmenite = [35.5 g / 47.9 g mol-1] = 0.74 (Molar mass of Ti = 47.9 gmol^{-1})

If all this Ti in ilmenite is converted to α-TiP through the process, a theoretical mass of α-TiP should be:

0.74 mol x 257.9 g mol-1 = 190.8 g (molar mass of α-TiP = 257.9 g mol^{-1})

Obtained 190 g, theoretically should be 190.8 g

Yield % [190 g/190.8 g] x 100 = **99.6%**

3.5   Structural and Compositional Analysis of α-TiP

3.5.1   Analysis Procedure

The structural and compositional characteristics of the prepared samples were investigated employing various analytical techniques. X-ray diffraction (XRD) analysis was conducted at room temperature within the angular range of 5° to 80° to ascertain the purity and structural features. CuKα radiation ($\lambda = 1.5406$ Å) was utilized on a Rigaku RINT2200 diffractometer, operating at a scanning rate of 2°/min. Diffractograms were acquired in the 2θ range of 10° to 70°, with a step size of 0.02° and a scan time of 1 s per step. Qualitative phase identification was performed by analyzing the X-ray patterns using pattern processing software coupled with the International Center for Diffraction Data (ICDD) and Powder Diffraction File (PDF) database for standard reference materials. The total iron concentration in the leachates was quantified using a Thermo Scientific iCE 3000 Series Atomic Absorption Spectrometer (AAS). EDXA of the samples was conducted using a Thermo Scientific Niton XL3t GOLDD+ analyzer, employing an incident power of 10 mW. TGA experiments were carried out using a PerkinElmer TGA/DSC SDT650 analyzer under a nitrogen atmosphere, with a constant heating rate of 5 °C/min from 25 °C to 900 °C. UV-Vis spectroscopic measurements were performed on a JASCO V-670 UV-VIS spectrophotometer.

3.5.2 Structure and Composition of α-TiP

The characterization of the WP obtained after the acid reaction step provided insights into the structure and composition of the synthesized product. The XRD analysis confirmed that the product was α-TiP, similar to the product obtained from the direct acid digestion method (Figure 3.5).
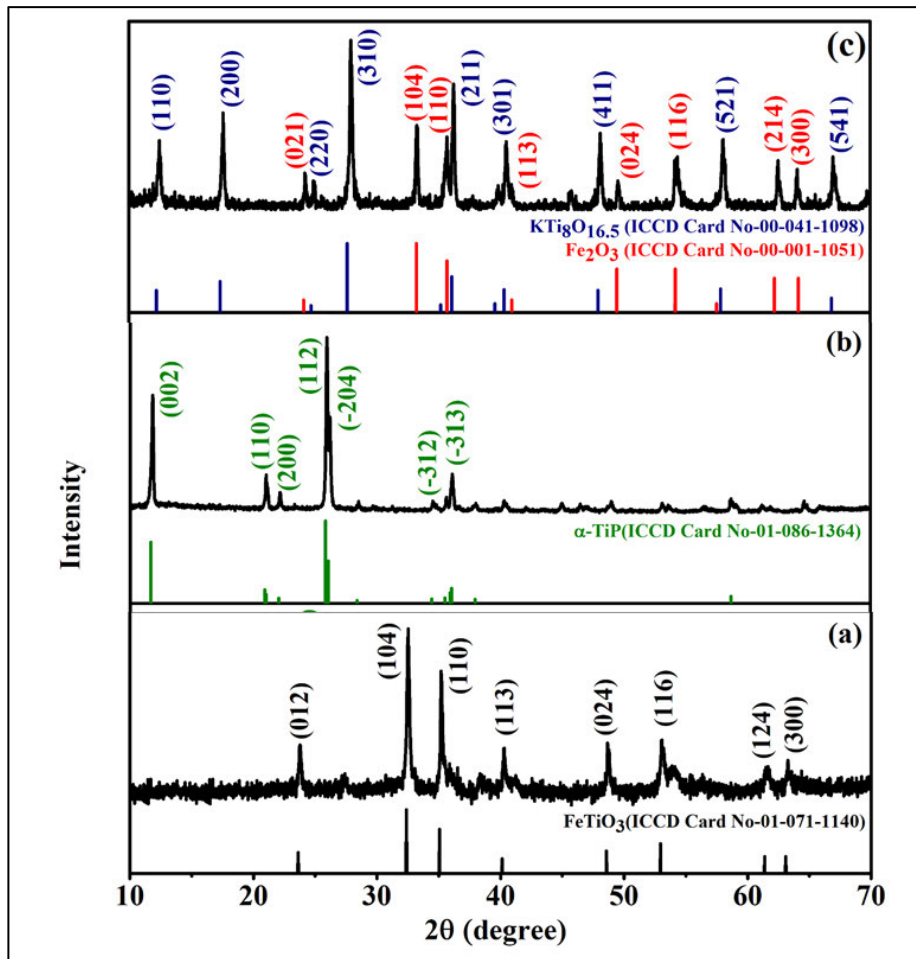
Figure 3.5: XRD patterns of (a) Ilmenite, (b) α-TiP, and (c) KOH roasted ilmenite.

The formation of α-TiP as the primary product in both methods can be attributed to the use of H_3PO_4 as the precipitation medium. The reaction between the soluble titanium species (formed during the decomposition of ilmenite) and H_3PO_4 results in the selective

precipitation of titanium as α-TiP, while other metals remain in solution as soluble phosphate complexes. This selective precipitation behavior of H_3PO_4 has been widely reported in the literature for the separation and recovery of titanium from various titanium-bearing minerals (Mahmoud et al., 2004; Lasheen et al., 2008; Zaki et al., 2008).

Calculations

According to EDAX results, 190 g of white powder contains 30.8 g of titanium.

Theoretically, 190 g of white powder is 100% pure α-TiP, titanium content.

should be [190 g 258 gmol^{-1}× 47.8 gmol] = 35.2 g.

Therefore, the purity of α-TiP was [$\frac{30.8}{35.2}$× 100%] = 88%.

However, the EDAX analysis revealed a higher mass percentage of iron (approximately 3.5%) in the WP obtained from the alkali roasting method compared to the WP from the direct digestion method (1.8% iron). This higher iron content in the WP from the alkali roasting method can be attributed to the KOH roasting step, which completely decomposes ilmenite into potassium titanate and iron oxide. As a result, more iron is available   to co-precipitate with the WP during the subsequent acid reaction step, leading to a higher iron content in the final product.

The co-precipitation of iron with titanium phosphates has been reported in previous studies, particularly when using phosphoric acid as the precipitation medium.[6, 13, 14] The extent of iron co-precipitation is influenced by factors such as the iron concentration, pH, and the presence of other complexing agents or impurities.

Despite the higher iron content, the percentage yield of α-TiP in the product obtained from ilmenite via the alkali roasting method was significantly higher, approximately 99.6 wt.%, compared to the yield of 18.3 wt.% achieved through direct digestion method. This substantial increase in yield can be attributed to the more efficient decomposition of ilmenite facilitated by the KOH roasting step, which ensures a higher availability of soluble titanium species for subsequent precipitation as α-TiP.

However, the purity of α-TiP in the WP obtained from the alkali roasting method was lower, around 87 wt.%, indicating the presence of other elements, especially iron, as impurities. This lower purity can be a trade-off for the higher yield achieved in the alkali roasting method, as the co-precipitation of iron and other impurities becomes more pronounced due to the complete decomposition of ilmenite during the KOH roasting step.

References

[1] Nayl, A. A.; Awwad, N. S.; Aly, H. F. Kinetics of Acid Leaching of Ilmenite Decomposed by KOH. Journal of Hazardous Materials 2009, 168 (2–3), 793–799. https://doi.org/10.1016/j.jhazmat.2009.02.076.

[2] Parirenyatwa, S.; Escudero-Castejon, L.; Sanchez-Segado, S.; Hara, Y.; Jha, A. Comparative Study of Alkali Roasting and Leaching of Chromite Ores and Titaniferous Minerals. Hydrometallurgy 2016, 165 (part 1), 213–226. https://doi.org/10.1016/j.hydromet.2015.08.002.

[3] Parirenyatwa, S.; Escudero-Castejon, L.; Sanchez-Segado, S.; Hara, Y.; Jha, A. Investigation of Molten Salt Phase Formation during Alkali Roasting of Titaniferous Minerals with Sodium and Potassium Hydroxide. Journal for Manufacturing Science and Production 2016, 16 (4). https://doi.org/10.1515/jmsp-2016-0025.

[4] Yustanti, E.; Ode, F. A. F.; Sulistiyono, E. Primary Study of KOH Alkali Fusion—Nitric Acid Leaching Process in Extraction of West Kalimantan Zircon Concentrate. IOP Conference Series: Materials Science and Engineering 2020, 763 (1), 012065. https://doi.org/10.1088/1757-899x/763/1/012065.

[5] Abdelgalil, M. S.; El-Barawy, K.; Ge, Y.; Xia, L. The Recovery of TiO_2 from Ilmenite Ore by Ammonium Sulfate Roasting—Leaching Process. Processes 2023, 11 (9), 2570. https://doi.org/10.3390/pr11092570.

[6] Thambiliyagodage, C.; Wijesekera, R.; Bakker, M. G. Leaching of Ilmenite to Produce Titanium Based Materials: A Review. Discover Materials 2021, 1 (1). https://doi.org/10.1007/s43939-021-00020-0.

[7] Sanchez-Segado, S.; Lahiri, A.; Jha, A. Alkali Roasting of Bomar Ilmenite: Rare Earths Recovery and Physico-Chemical Changes. Open Chemistry 2014, 13 (1). https://doi.org/10.1515/chem-2015-0033.

[8] Indriani Br. Ginting, L.; Manaf, A.; Astuti, W.; Supriyatna, Y. I.; Bahfie, F. Study of Titanium Dioxide (TiO_2) Extraction Process from Ilmenite Banten. IOP conference series. Earth and environmental science 2023, 1201 (1), 012092—012092. https://doi.org/10.1088/1755-1315/1201/1/012092.

[9] Nayl, A. A.; Aly, H. F. Acid Leaching of Ilmenite Decomposed by KOH. Hydrometallurgy 2009, 97 (1–2), 86–93. https://doi.org/10.1016/j.hydromet.2009.01.011.

[10] Liu, Y.; Qi, T.; Chu, J.; Tong, Q.; Zhang, Y. Decomposition of Ilmenite by Concentrated KOH Solution under Atmospheric Pressure. International Journal of Mineral Processing 2006, 81 (2), 79–84. https://doi.org/10.1016/j.minpro.2006.07.003.

[11] Kordzadeh-Kermani, V.; Schaffie, M.; Hashemipour Rafsanjani, H.; Ranjbar, M. A Modified Process for Leaching of Ilmenite and Production of TiO_2 Nanoparticles. Hydrometallurgy 2020, 198, 105,507. https://doi.org/10.1016/j.hydromet.2020.105507.

[12] Galal-Gorchev, H.; Stumm, W. The Reaction of Ferric Iron with Ortho-Phosphate. Journal of Inorganic and Nuclear Chemistry 1963, 25 (5), 567–574. https://doi.org/10.1016/0022-1902(63)80243-2.

[13] BECK, L. W.; SOLTANI, M.; Wang, L. Ferric Phosphate and Methods of Preparation Thereof, September 20, 2010. https://patents.google.com/patent/US20110068295A1/en (accessed 2024-05-06).

[14] Anawati, J.; Azimi, G. Recovery and Separation of Phosphorus as Dicalcium Phosphate Dihydrate for Fertilizer and Livestock Feed Additive Production from a Low-Grade Phosphate Ore. RSC Advances 2020, 10 (63), 38640–38653. https://doi.org/10.1039/d0ra07210a.

CHAPTER 4
PURIFICATION OF SYNTHESIZED α-TiP

4.1   Acid Washing Approaches for Iron Removal

The WP obtained from both the direct acid digestion and alkali roasting methods primarily consists of the desired α-TiP product. However, a considerable amount of co-precipitated iron is present as the main impurity (Table 4.1). The presence of iron impurities can adversely affect the properties and performance of α-TiP in various applications. Therefore, an effective purification strategy is crucial to remove the iron contaminants and obtain a high-purity α-TiP product.

Table 4.1: Percentage of the metal composition of Hi-Ti ilmenite, Brown Powder (BP), α-TiP and purified α-TiP.

	Mass wt.% (n=3)							
	Ti	Fe	P	K	Mn	V	Si	Mg
Ilmenite	35.5	20.9	0.8	-	0.5	0.3	0.9	11.0
Brown powder	26.6	12.5	1.2	4.3	0.1	0.1	0.9	2.5
α-TiP (Method I)	17.2 Yield- 17% Purity-93%	1.8	27.2	-	-	0.1	-	1.5
α-TiP (Method II)	16.2 Yield-87% Purity-88%	3.5	27.5	1.0	-	0.1	0.4	1.8
α-TiP washed with H_3PO_4	18.3 Yield-80% Purity-98%	0.4	28.1	0.1	-	0.1	0.4	1.2
α-TiP washed with HCl	16.2 Yeild-67% Purity-88%	2.5	26.1	0.9	-	-	0.9	-
α-TiP washed with $H_2C_2O_4$	26.8 Yield-82% Purity-84%	0.5	18.5	0.1	-	0.1	0.7	-

Acid-washing techniques have been widely employed for the removal of iron impurities from titanium-based materials. In this study, three different acid-chelating agents were

investigated for their effectiveness in removing iron from the synthesized α-TiP: 85 wt.% H_3PO_4, 20 w/v% $H_2C_2O_4$, and 35 v/v% HCl.

Calculations

Ti mass % of the product obtained via the alkali roasting method was 17.2.

Therefore, 35 g of the product contains [17.2 g/100 g] x 35 g = 6.02 g of Ti

No. of moles of Ti in that 35 g = [6.02 g/47.9 g mol^{-1}] = 0.126 mol

(Molar mass of Ti = 47.9 g mol^{-1})

Mass in the sample as α-TiP is [0.126 g x 257.9 g mol-1] = 32.5 g

(molar mass of α-TiP = 257.9 g mol^{-1})

Hence, out of 35 g (product) only 32.5 g present as α-TiP

% purity ofα-TiP in the product obtained was [32.5 g/35 g]x100 = **92.9**

Ti mass % of the product obtained via the direct digestion method was 16.2.

Therefore, 190 g of the product contain [16.2 g/100 g] x 190 g = 30.8 g of Ti

No. of moles of Ti in that 190 g = [30.8 g/47.9 g mol^{-1}] = 0.643 mol

(Molar mass of Ti = 47.9 g mol^{-1})

Mass in the sample as α-TiP is [0.643 g x 257.9 g mol-1] = 165.8 g

(molar mass of α-TiP = 257.9 g mol^{-1})

Hence, out of 190 g (product) only 165.8 g present as α-TiP

% purity of as □-TiP in the product obtained was [165.8 g/190 g]x100 = **87.3**

4.1.1   Acid Washing Procedure

In a typical acid-washing experiment, 100 g of the as-synthesized α-TiP was mixed with 800 mL of one of the aforementioned acid solutions. For H_3PO_4 and $H_2C_2O_4$, the mixture was refluxed for 2 hours, while for HCl, the mixture was vigorously stirred at room temperature for 2 hours. After the acid treatment, the mixture was allowed to cool, and the white precipitate was separated from the liquid portion using a decantation technique.

The washing cycle was repeated five times, with the iron content in the leachate being monitored after each wash using AAS. This step allowed for the tracking of the iron removal efficiency and the determination of the optimal number of washing cycles required.

After the acid washing steps, the purified WP sample was washed with an excess amount of distilled water until the pH became neutral. The resulting iron-free α-TiP was then dried at 80 °C and stored in a desiccator (Table 4.1). The chemical composition of the purified α-TiP was analyzed using EDAX spectroscopy to confirm the removal of iron impurities.

To ensure the reproducibility and reliability of the results, all experiments were repeated three times, and the average value was reported. Figure 4.1 shows the flowchart developed for the removal of iron from WP.
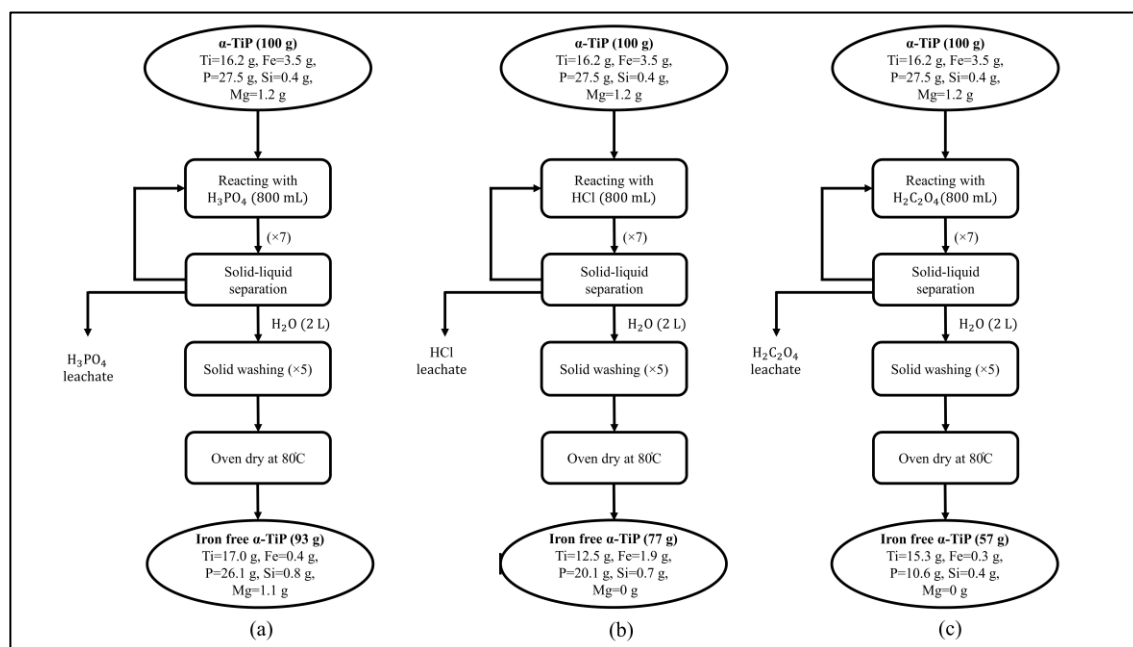
Figure 4.1: Flowchart for the purification of α-TiP through different acid washing cycles. (a) 85 wt.% H_3PO_4, (b) 20 w/v% $H_2C_2O_4$, and (c) 35 v/v% HCl.

4.1.2   Comparison of Acid Washing Agents

The effectiveness of each acid-washing agent in removing iron impurities from the synthesized α-TiP was evaluated based on the iron content in the leachate after each washing cycle and the final iron content in the purified α-TiP product. Through this systematic investigation, the most effective acid-washing approach for obtaining high-purity, iron-free α-TiP was identified. The optimized purification procedure, along with the key parameters and considerations, can be presented in this section.

(i) Washing with H_3PO_4

The removal of iron impurities from the WP obtained via the alkali roasting method, which initially contained approximately 3.5% iron, was attempted through repeated washing cycles with 85 wt.% H_3PO_4. The results demonstrated a significant reduction

in the iron content, from an initial value of 6.3 gL^{-1} to 0.3 gL^{-1} after the fifth washing cycle (Figure 4.2.a). Consequently, the EDAX analysis of the solid WP sample obtained after the final wash revealed a decrease in the iron mass percentage from 3.5% to 0.4%, corresponding to an 88.9% reduction in the final α-TiP product (Figure 4.2.b).
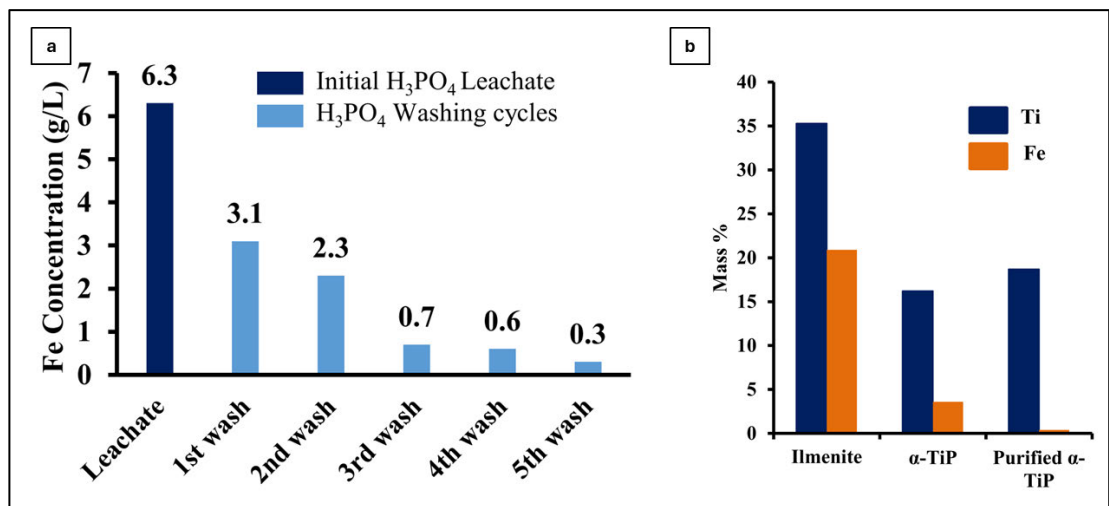
Figure 4.2: Iron variation in leachate with H_3PO_4 concentration. (a) g/L, (b) Mass percentage.

The effective removal of iron impurities can be attributed to the formation of soluble iron phosphate complexes, as represented by Equation 7.[1,2]

$$2Fe_2O_3 + 27H^+ + 7PO_4^{3-} \rightarrow Fe(HPO_4)^+ + Fe(H_2PO_4)^{2+} + FeH_5(PO_4)_2^{2+} + FeH_7(PO_4)_3^+$$
$$+ 6H_2O .... (8)$$
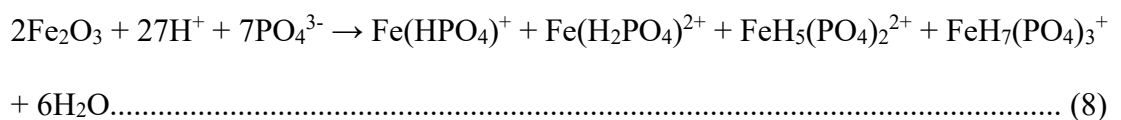
The repeated washing cycles with concentrated H_3PO_4 facilitated the leaching of iron from the solid WP into the liquid phase, effectively reducing the iron content in the

final α-TiP product. This selective leaching of iron is a significant advantage of using H_3PO_4 in the purification process, as it enables the separation of iron impurities from the desired titanium product.

It is noteworthy that the titanium mass percentage in the WP increased from 16.2% to 18.3% after the washing cycles, indicating enrichment of the titanium content in the purified product. This observation further supports the selective leaching of iron impurities, resulting in a higher relative concentration of titanium in the solid phase. Also, it is important to allow sufficient settling time for less dense fine particles of WP during the washing cycles to minimize any potential loss in the final yield of α-TiP. This consideration is crucial for optimizing the purification process and ensuring maximum recovery of the desired product.

Comparing the alkali roasting method with the direct digestion method, we observed a fivefold enhancement in the iron leaching into H_3PO_4 during the alkali roasting method (6.3 gL^{-1} vs. 1.3 gL^{-1}, respectively). This higher leaching efficiency can be attributed to the facile reaction of Fe_2O_3, produced during the KOH roasting step, with H_3PO_4. In contrast, in the direct digestion method, H_3PO_4 has to react with iron present within the ilmenite lattice structure, hindering the leaching process.

After the H_3PO_4 washing cycles, the calculations indicate a yield of 92.5 wt.% for the purified α-TiP product (a drop from the initial 99.6 wt.%), with a purity of 99.8 wt.%, representing an enhancement from the initial purity of 87.3 wt.% to 99.8 wt.% (Table 4.2).

Table 4.2: Percentage yield and purity of α-TiP.

Product	Yield (wt.%)	Purity (wt.%)
α-Ti(HPO$_4$)$_2$·H$_2$O (washed with H$_3$PO$_4$)	92.5	99.8
α-Ti(HPO$_4$)$_2$·H$_2$O (washed with HCl)	76.6	87.1
(TiO)$_2$P$_2$O$_7$ (washed with H$_2$C$_2$O$_4$)	56.7	84.7
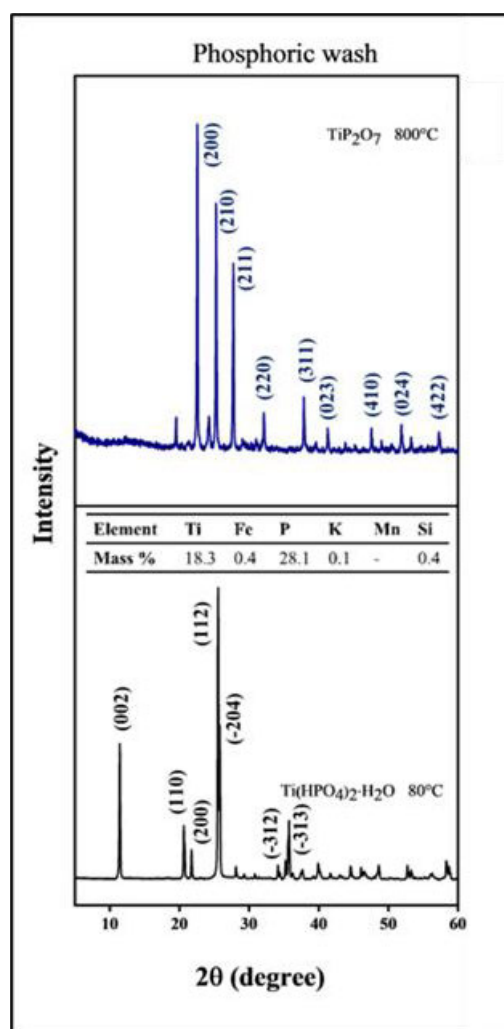
Figure 4.3: XRD patterns and EDAX data of purified α-TiP after H$_3$PO$_4$ acid washing cycles.

(ii) Washing with HCL

The efficiency of iron removal from the WP obtained via the alkali roasting method was also tested using conc. HCl. The choice of HCl as a washing agent is based on its ability to form soluble and stable metal-chloride complexes with metal ions at acidic pH. [3] In this case, iron in the WP reacts with concentrated HCl to form iron-chloride complexes such as $[FeCl_3(H_2O)_3]$, $[FeCl_2(H_2O)_4]^+$, $[FeCl(H_2O)_5]^{2+}$, and $[FeCl_4]^-$, facilitating its separation from the WP.

The results indicated that repeated washing with HCl effectively removed iron from the WP sample, as evidenced by the analysis of iron content in the HCl leachates after each of the five washing cycles (Figure 4.4). However, the amount of iron leached into the HCl solution was relatively low compared to the H_3PO_4 washing process. For example, during the second washing cycle, the amount of iron leached into H_3PO_4 was 2.3 gL^{-1}, whereas the value for HCl was about 0.5 gL^{-1}.
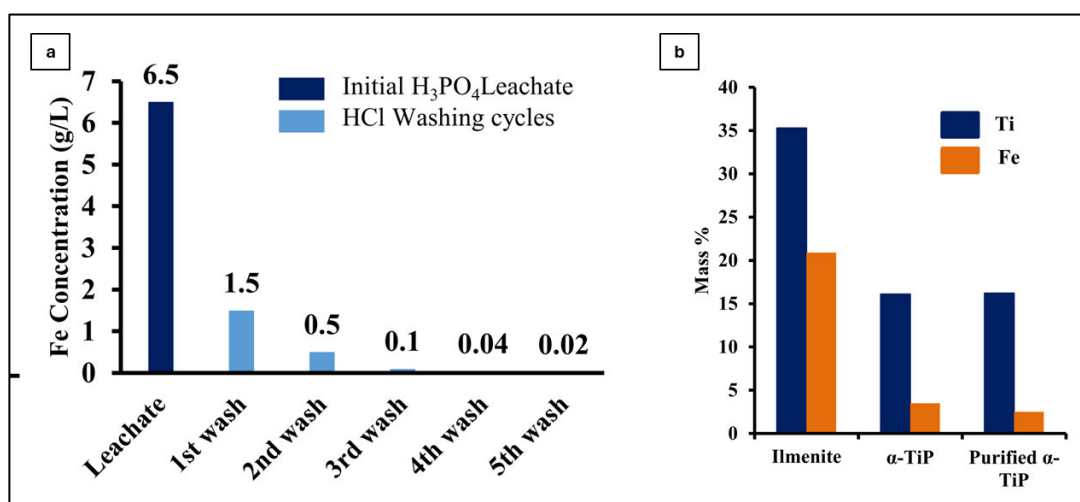
Figure 4.4: Iron variation in leachate with HCl concentration. (a) g/L, (b) Mass percentage.

The EDAX analysis of the solid WP samples produced after the HCl washing cycles indicated that the initial iron mass percentage of 3.5% was reduced to 2.5%, representing a drop of approximately 28.6% (Figure 4.5). In comparison, the H_3PO_4 washing process achieved an 88.9% reduction in iron content, suggesting a higher efficiency in removing iron impurities from the WP.

Element	Ti	Fe	P	K	Mn	Si
Mass %	16.2	2.5	26.1	0.9	-	0.9
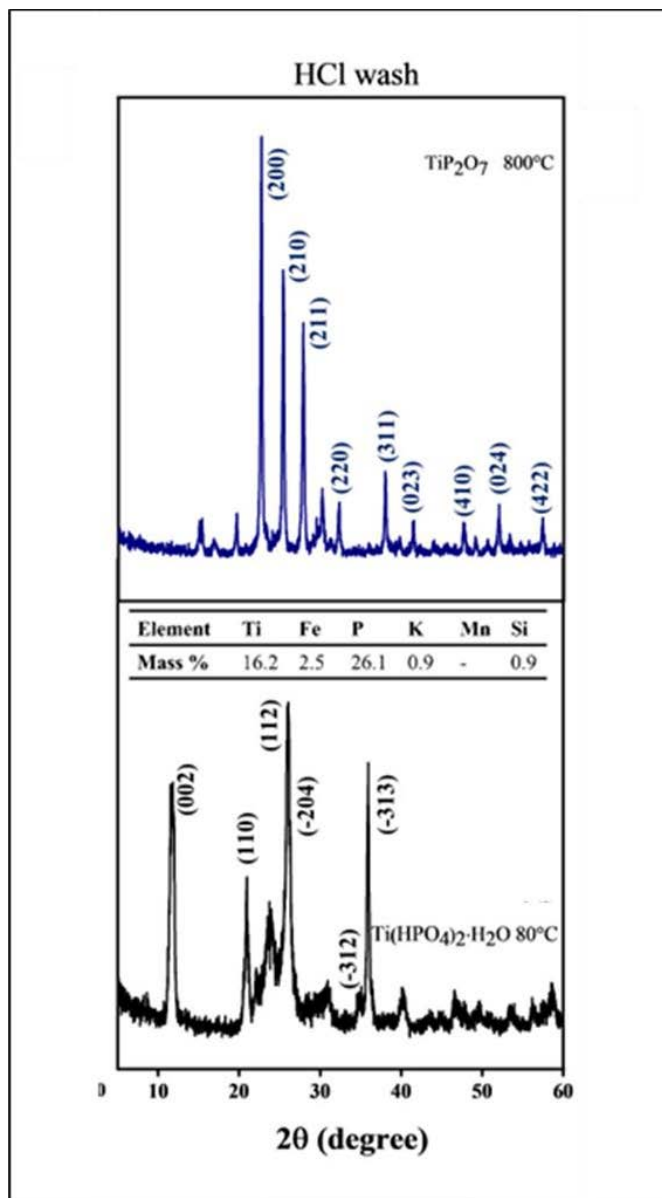
Figure 4.5: XRD patterns and EDAX data of purified α-TiP after HCl acid washing cycles.

Interestingly, the EDAX data revealed that concentrated HCl not only leached iron from the WP but also leached an appreciable amount of titanium into the liquid phase. This observation can be explained by a possible reaction between α-TiP and HCl, as represented by Equation 9.

$$Ti(HPO_4)_2 + 2HCl + H_2O \rightarrow TiOCl_2 + 2H_3PO_4 .... (9)$$

The leaching of titanium is evident from the EDAX data of the HCl-purified WP, in which the titanium mass percentage remained unchanged from its initial value of 16.2% (Figure 4.5). In contrast, one would expect to observe a higher value closer to the theoretical value of 18.5% for titanium in α-TiP, indicating that a significant amount of titanium was lost during the HCl washing process.

Despite the leaching of titanium, the XRD patterns recorded for the HCl-purified WP samples confirmed the chemical identity of the product as α-TiP, which thermally transformed to TiP_2O_7 upon heating to 800 °C.[4, 5]

The calculations indicated that after the HCl washing cycles, a yield of 76.6 wt.% could be obtained, a drop from the initial value of 99.6 wt.%, with a purity of 87.1 wt.% as α-TiP, which is almost unchanged from the initial purity of 87.3 wt.%.

(iii) Washing with $H_2C_2O_4$

In addition to H_3PO_4 and HCl, $H_2C_2O_4$ was investigated as a potential chelating agent for the removal of iron from the WP samples. Oxalic acid is widely recognized as an effective chelating agent for iron removal in various applications.[6, 7]

The washing procedure employed for $H_2C_2O_4$ was similar to that used for H_3PO_4 (Figure 4.1), and the iron content leached into the liquid phase was measured (Figure 4.6.a). The results indicated a significant reduction in the iron content, from an initial value of 2.5 g L-1 to 0.003 g L-1 after the fifth washing cycle, suggesting the effective removal of iron from the WP.
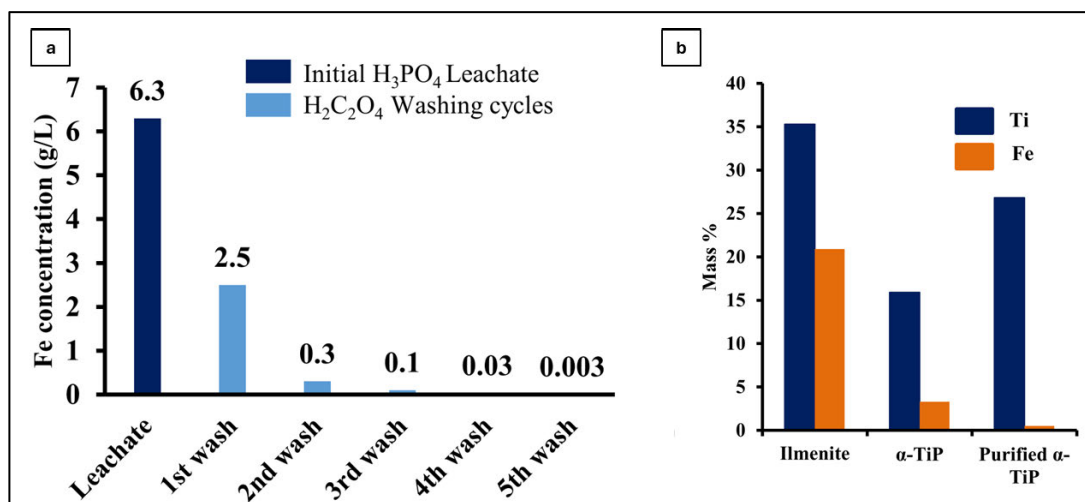
Figure 4.6: Iron variation in leachate with $H_2C_2O_4$ concentration. (a) g/L, (b) Mass percentage.

The EDAX data of the solid WP prepared after washing with $H_2C_2O_4$ further confirmed the efficient removal of iron, with a reduction from 3.5% to 0.5% in the mass percentage, corresponding to an 85.7% decrease (Figure 4.6.b). Notably, during

the $H_2C_2O_4$ washing process, the titanium mass percentage increased from 16.2% to 26.8%, indicating enrichment of the titanium content in the purified product.

Interestingly, the XRD pattern of the WP obtained after the $H_2C_2O_4$ washing cycles revealed that α-TiP underwent a chemical transformation to an unknown compound, which could not be identified based on the XRD data. However, upon calcining the ample at 800 °C for 4 hours, the compound formed was identified as titanyl pyrophosphate $(TiO)_2P_2O_7$ based on the XRD pattern.[8, 9]
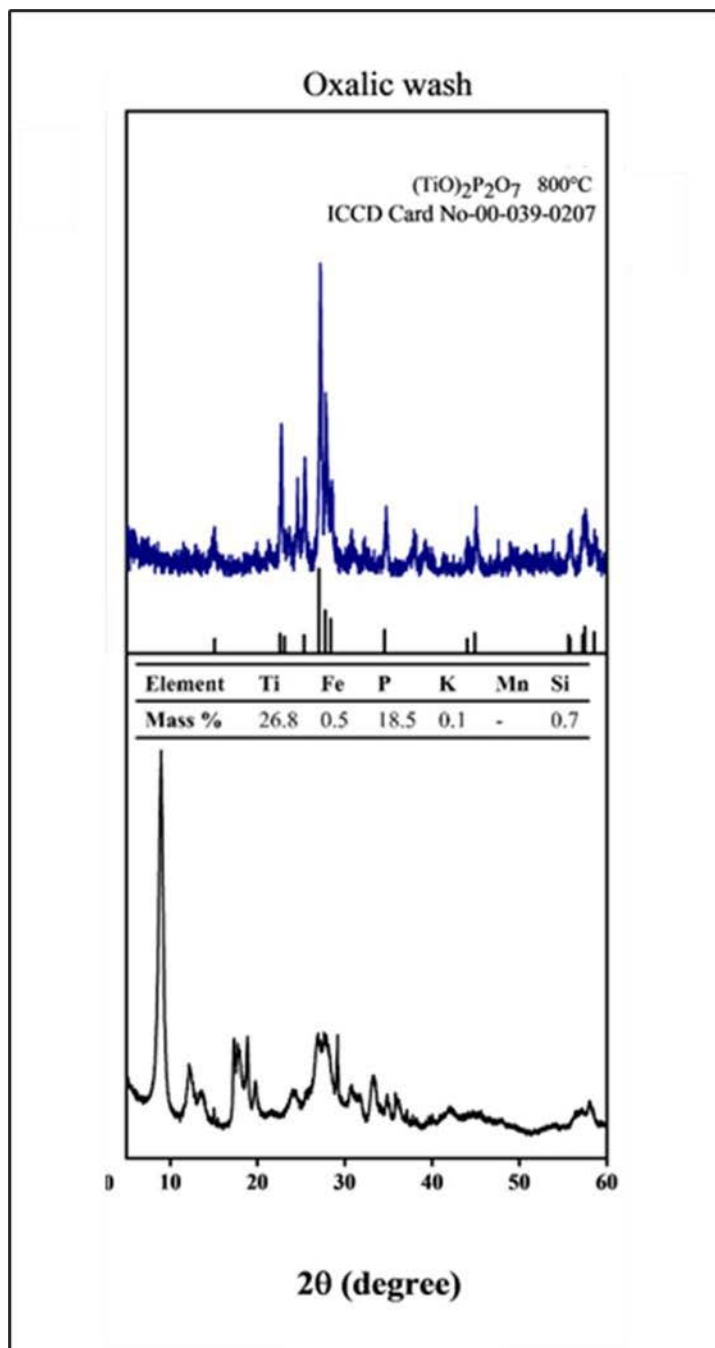
Figure 4.7: XRD patterns and EDAX data of purified α-TiP after $H_2C_2O_4$ acid washing cycles.

The proposed possible reaction between α-TiP and $H_2C_2O_4$ under atmospheric conditions is represented by Equation 10:

$$4Ti(HPO_4)_2 + 2H_2C_2O_4 + O_2 \rightarrow 2(TiO)_2P_2O_7 + 4H_3PO_4 + 4CO_2 \dots\dots\dots\dots\dots (10)$$

The titanium mass percentage achieved in the final product (26.8%) is close to the theoretical value of 31.8% in $(TiO)_2P_2O_7$, and the level of iron impurity in the final product (0.5%) is comparable to that obtained after the H_3PO_4 washing process (0.4%).

The formation of titanyl pyrophosphate $(TiO)_2P_2O_7$ during the $H_2C_2O_4$ washing process is an interesting observation, as it suggests the potential for chemical transformations or modifications of the α-TiP structure in the presence of chelating agents like oxalic acid. While the mechanism of this transformation is not fully elucidated, it could be related to the complexation of titanium with oxalate ions and the subsequent oxidation and condensation reactions leading to the formation of $(TiO)_2P_2O_7$.

Importantly, the yield of the final product obtained after the $H_2C_2O_4$ washing cycles could not be accurately determined due to the chemical transformation of α-TiP to $(TiO)_2P_2O_7$. However, the purity of the final product, containing 0.5% iron and 26.8% titanium, is comparable to that obtained after the H_3PO_4 washing process.

4.2 Thermal Stability and Phase Transformations

4.2.1 Thermogravimetric Behavior

TGA was performed to investigate the thermal stability and decomposition behavior of the α-TiP obtained via different methods and purification processes. The TGA curves, coupled with the corresponding Differential Scanning Calorimetry (DSC) curves, provide valuable insights into the phase transformations occurring during heating.

For the α-TiP obtained via the direct digestion method and the alkali roasting method (with H_3PO_4 and HCl washing), the TGA curves reveal a two-stage decomposition process (Figure 4.8). The initial weight loss observed around 200 °C corresponds to the loss of surface and crystal water, which is also evident in the DSC curves as an endothermic peak. This observation is consistent with previous reports on the dehydration behavior of α-TiP.[10, 11]
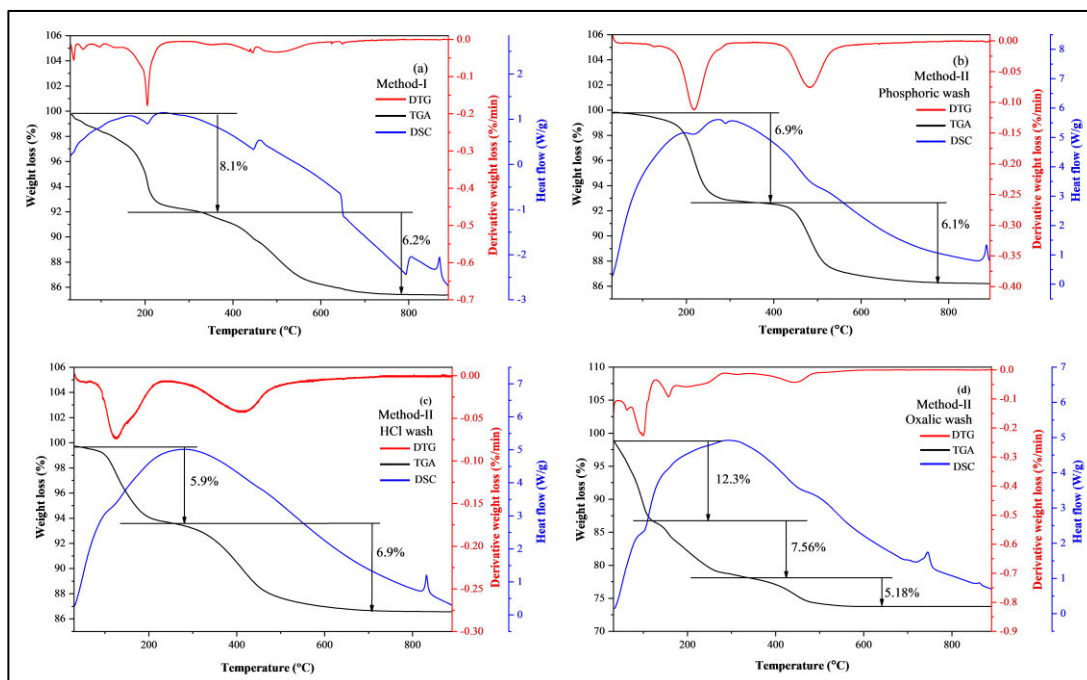
Figure 4.8: TG-DTG and DSC curves of α-TiP obtained via (a) Direct digestion method, and purified α-TiP from (b) H_3PO_4, (c) HCl, and (d) $H_2C_2O_4$ washing processes in alkali roasting method.

The second weight loss, observed between 400 °C and 500 °C, can be attributed to the pyrophosphorization process, resulting in the conversion of α-TiP into the layered TiP_2O_7 phase. This transformation involves the condensation of the phosphate groups and the elimination of water molecules, leading to the formation of the pyrophosphate structure.

The DSC curves of α-TiP exhibit an exothermic peak around 850 °C, which corresponds to the phase transition of the layered TiP_2O_7 to the cubic TiP_2O_7 phase. [10] This phase transformation is associated with the rearrangement of the pyrophosphate units and the formation of a more stable, high-temperature cubic structure.

In contrast, the α-TiP subjected to $H_2C_2O_4$ washing cycles shows a different thermogram with three decomposition stages. This behavior suggests the elimination of water/hydroxyl groups during the decomposition process, leading to the formation of the titanyl pyrophosphate $(TiO)_2P_2O_7$ phase, as confirmed by the XRD analyses.[11]

The observations regarding the thermal decomposition behavior of α-TiP are in line with previous studies on the thermal transformations of titanium phosphate materials.[8, 9, 10, 11] The formation of the layered TiP_2O_7 phase and its subsequent transformation to the cubic TiP_2O_7 phase at higher temperatures are well-documented phenomena for α-TiP.

The unique three-stage decomposition behavior observed for the α-TiP subjected to $H_2C_2O_4$ washing cycles can be attributed to the chemical transformation of α-TiP to titanyl pyrophosphate $(TiO)_2P_2O_7$, as evidenced by the XRD analyses. The presence of oxalate ions during the washing process likely influenced the structure and composition of the titanium phosphate material, leading to the formation of $(TiO)_2P_2O_7$ upon thermal treatment.

The TGA and DSC analyses provide valuable information about the thermal stability and phase transformation behavior of the α-TiP obtained via different syntheses and purification methods. These insights are crucial for understanding the thermal processing requirements and the potential applications of these materials, where their high-temperature stability and phase transformations may play a significant role.

4.2.2   Structural Changes Upon Heating

The structural changes occurring during the heating process were further investigated using X-ray diffraction (XRD) spectroscopy techniques, providing valuable insights into the phase transformations and structural modifications of the titanium phosphate compounds.

For the α-TiP obtained from the direct digestion method and the alkali roasting method (with H_3PO4 and HCl washing), the XRD patterns spectra confirmed the thermal transformation of α-TiP to the more stable TiP_2O_7 phase upon calcination at 800 °C.[12] This transformation is consistent with the observations from the TGA and DSC

data, which showed the pyrophosphorization process and the phase transition of the layered TiP_2O_7 to the cubic TiP_2O_7 phase at higher temperatures.

The conversion of α-TiP to TiP_2O_7 involves the condensation of phosphate groups and the elimination of water molecules, leading to the formation of the pyrophosphate structure.[10, 11] The XRD patterns provide direct evidence of this structural transformation, confirming the phase evolution and the rearrangement of the pyrophosphate units into a more stable, high-temperature cubic structure.

In the case of the WP obtained after $H_2C_2O_4$ washing, the XRD pattern initially indicated the formation of an unknown compound upon washing. However, after calcination at 800 °C for 4 hours, the XRD pattern matched the titanyl pyrophosphate $(TiO)_2P_2O_7$ phase.[9, 10]

The formation of $(TiO)_2P_2O_7$ can be attributed to the chemical transformation of α-TiP in the presence of oxalate ions during the $H_2C_2O_4$ washing process. A possible reaction involving the complexation of titanium with oxalate ions was proposed, followed by oxidation and condensation reactions, leading to the formation of the titanyl pyrophosphate phase.

These findings highlight the importance of thermal treatment and characterization techniques in understanding the phase transformations and structural changes that occur during the synthesis and purification processes of titanium phosphate compounds. The XRD analyses provide direct evidence of the structural evolution, enabling the

identification of the intermediate and final phases formed under different reaction conditions and thermal treatments.

Furthermore, the structural information obtained from these techniques is essential for elucidating the reaction mechanisms and the influence of various purification processes on the final product composition and structure. This knowledge is crucial for optimizing the synthesis and purification procedures, as well as for tailoring the properties of the titanium phosphate materials for specific applications.

References

[1] Liu, Y.; Qi, T.; Chu, J.; Tong, Q.; Zhang, Y. Decomposition of Ilmenite by Concentrated KOH Solution under Atmospheric Pressure. International Journal of Mineral Processing 2006, 81 (2), 79–84. https://doi.org/10.1016/j.minpro.2006.07.003.

[2] Galal-Gorchev, H.; Stumm, W. The Reaction of Ferric Iron with Ortho-Phosphate. Journal of Inorganic and Nuclear Chemistry 1963, 25 (5), 567–574. https://doi.org/10.1016/0022-1902(63)80243-2.

[3] Das, G. K.; Pranolo, Y.; Zhu, Z.; Cheng, C. Y. Leaching of Ilmenite Ores by Acidic Chloride Solutions. Hydrometallurgy 2013, 133, 94–99. https://doi.org/10.1016/j.hydromet.2012.12.006.

[4] Parirenyatwa, S.; Escudero-Castejon, L.; Sanchez-Segado, S.; Hara, Y.; Jha, A. Comparative Study of Alkali Roasting and Leaching of Chromite Ores and Titaniferous Minerals. Hydrometallurgy 2016, 165 (part 1), 213–226. https://doi.org/10.1016/j.hydromet.2015.08.002.

[5] Costantino, U.; A. La Ginestra. On the Existence of Pyrophosphates of Tetravalent Metals Having a Layered Structure. Thermochimica acta 1982, 58 (2), 179–189. https://doi.org/10.1016/0040-6031(82)87080-9.

[6] Taxiarchou, M.; Panias, D.; Douni, I.; Paspaliaris, I.; Kontopoulos, A. Removal of Iron from Silica Sand by Leaching with Oxalic Acid. Hydrometallurgy 1997, 46 (1–2), 215–227. https://doi.org/10.1016/s0304-386x(97)00015-7.

[7] Blesa, M. A.; Marinovich, H. A.; Baumgartner, E.; Maroto, G. Mechanism of Dissolution of Magnetite by Oxalic Acid-Ferrous Ion Solutions. Inorganic Chemistry 1987, 26 (22), 3713–3717. https://doi.org/10.1021/ic00269a019.

[8] Bamberger, C. E. Fruits of Serendipity in Research of Titanium Compounds: From "Sodium Tianide" to Titanium Nitride Whiskers. Powder diffraction 1988, 3 (4), 240–241. https://doi.org/10.1017/s0885715600013543.

[9] Maslova, M.; Ivanenko, V.; Gerasimova, L.; Larsson, A.-C.; Antzutkin, O. N. Synthesis of Titanium Phosphates from Unconventional Solid Precursor and Their Ion-Exchange and Electrochemical Properties. Journal of materials science 2021, 56 (16), 9929–9950. https://doi.org/10.1007/s10853-021-05876-4.

[10] Benhamza, H.; Barboux, P.; Bouhaouss, A.; Josien, F.-A.; Livage, J. Sol— Gel Synthesis of $Zr(HPO_4)_2 \cdot H_2O$. Journal of materials chemistry 1991, 1 (4), 681–684. https://doi.org/10.1039/jm9910100681.

[11] Colón, G.; Sánchez-España, J. M.; Hidalgo, M. C.; Navío, J. A. Effect of TiO_2 Acidic Pretreatment on the Photocatalytic Properties for Phenol Degradation. Journal of Photochemistry and Photobiology A-chemistry 2006, 179 (1–2), 20–27. https://doi.org/10.1016/j.jphotochem.2005.07.007.

[12] Palliyaguru, L.; Kulathunga, M. U. S.; Kumarasinghe, K. G. U. R.; Jayaweera, C. D.; Jayaweera, P. M. Facile Synthesis of Titanium Phosphates from Ilmenite Mineral Sand: Potential White Pigments for Cosmetic Applications. Journal of cosmetic science 2019, 70 (3), 149–159.

CHAPTER 5

ADVANCED FABRICATION AND APPLICATIONS OF TITANIUM PHOSPHATE FOR STAINLESS STEEL MESHES

5.1   Background and Significance

In the realm of materials science and engineering, the development of novel composites with enhanced properties continues to drive technological progress across various sectors. One such innovation that has garnered significant attention is the fabrication of α-titanium phosphate (α-TiP) on stainless steel mesh (S.S.M.). This chapter delves into the intricacies of the fabrication process, the unique properties of the resulting material, its potential applications, and the broader implications for industry and research.

Titanium phosphate, particularly its alpha form; α-TiP, has long been recognized for its remarkable chemical and thermal stability. When combined with the structural integrity and durability of stainless-steel mesh, it creates a compo/site material that synergizes the benefits of both components. The significance of this innovation lies in its potential to address challenges in various industrial applications where resistance to extreme conditions, antimicrobial properties, and catalytic activity are paramount.

5.2   Fabrication process

The fabrication of α-TiP on S.S.M. is characterized by its simplicity and cost-effectiveness, making it an attractive option for large-scale industrial production. The process can be broken down into several key stages:

5.2.1 Ilmenite decomposition

The process begins with the decomposition of ilmenite (FeTiO3), a naturally occurring mineral that serves as the primary source of titanium. This process involves the use of environmentally benign chemicals to avoid the release of harmful byproducts. The decomposition of ilmenite typically occurs through high-temperature treatment in the presence of a suitable reductant, leading to the formation of titanium dioxide (TiO2) and iron oxides. This step is crucial because it ensures the availability of high-purity titanium, which is essential for the subsequent synthesis of α-TiP.

5.2.2 α-TiP Synthesis

Two primary methods are employed for the synthesis of titanium phosphate:

5.2.2.1 Direct acid digestion method

This method involves the direct reaction of titanium-containing compounds, such as TiO_2, with phosphoric acid (H_3PO_4). The reaction parameters, including temperature, acid concentration, and reaction time, are carefully controlled to maximize the yield and purity of α-TiP. The resulting α-TiP is typically obtained as a fine powder, which can be further processed for coating applications.

5.2.2.2 Novel two-step alkali roasting method

This innovative approach involves an initial alkali roasting step, where ilmenite is mixed with potassium hydroxide and heated to a high temperature. This step facilitates the formation of a titanium-alkali complex, which is subsequently treated with phosphoric acid to yield α-TiP. This method offers advantages in terms of higher yield and purity,

and the process parameters can be optimized to further enhance the quality of the final product.

5.2.3   Optimization of the Reaction Parameters

A critical aspect of the fabrication process is the fine-tuning of the reaction parameters to achieve the following:

- High α-TiP yield

- High purity of the final product

- Maximal titanium recovery from the initial ilmenite

Optimization involves systematic variations in factors such as temperature, ilmenite to phosphoric acid ratio, reaction time, and reagent concentration. For example, maintaining an optimal ilmenite to phosphoric acid ratio of 150°C during the acid digestion process can significantly influence the crystallinity and phase purity of α-TiP. Similarly, controlling the concentration of phosphoric acid is essential to prevent the formation of secondary phases and impurities.

5.2.4   Purification

The synthesized TiP underwent a purification process using three different acids: phosphoric acid (H3PO4), hydrochloric acid (HCl), and oxalic acid (H2C2O4). Each acid serves a specific purpose in removing different types of impurities. The purification protocol involves multiple washing and filtration steps to ensure the high purity of the final α-TiP product.

5.2.5 Coating process

The final stage involves the fabrication and coating of α-TiP on stainless steel mesh. The fabrication method is a dip coating method. This process is optimized to achieve a larger surface area, which is crucial for many of the potential applications of the material. The coating technique likely involves careful control of factors such as the TiP concentration, the ratios of TiP and other compounds, coating temperature, dipping number, and drying conditions. The mesh is typically dipped in a slurry of α-TiP, followed by controlled drying and sintering to ensure uniform coating and strong adhesion. The fabrication process has been optimized after several experiments to a very simple method that needs very lesser and inexpensive chemicals and less preparation time.
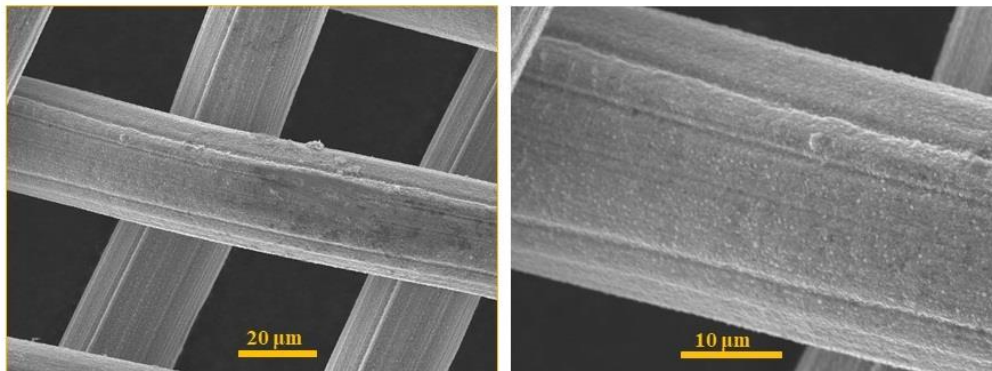
Figure 5.1 SEM images of the bare stainless-steel mesh before α-TiP coating.
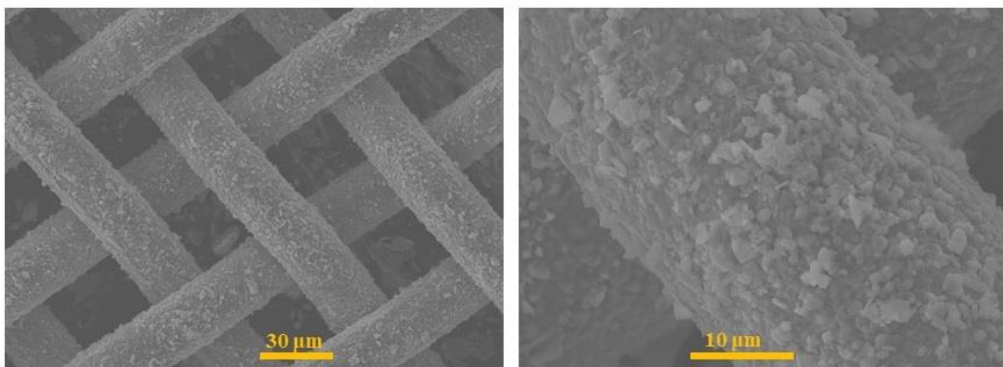
Figure 5.2 SEM images of the stainless-steel mesh after α-TiP coating.

5.3   Properties of α-TiP-Coated S.S.M.

The resulting composite material has a range of remarkable properties that make it suitable for diverse applications.

5.3.1   Fabrication of different surface structures on S.S.M using α-TiP variations

5.3.1.1   Different sizes of α-TiP on S.S.M

The particle size of the TiP is there in microscale which is synthesized from the direct acid digestion method and alkali roasting method. But when during the purification process with phosphoric acid, five washing cycles were done to remove iron.

In this five-step purification cycle, the particle size of the synthesized TiP which is prepared from direct acid digestion method and alkali roasting method, will be reduced to nanoscale from macro scale.

Hence from each step, we can receive different particle sizes of TiP without changing the chemical identity of TiP.

Using those different sizes of TiP which were prepared at each cycle, then TiP fabrication was done separately as shown in figure 5.3.
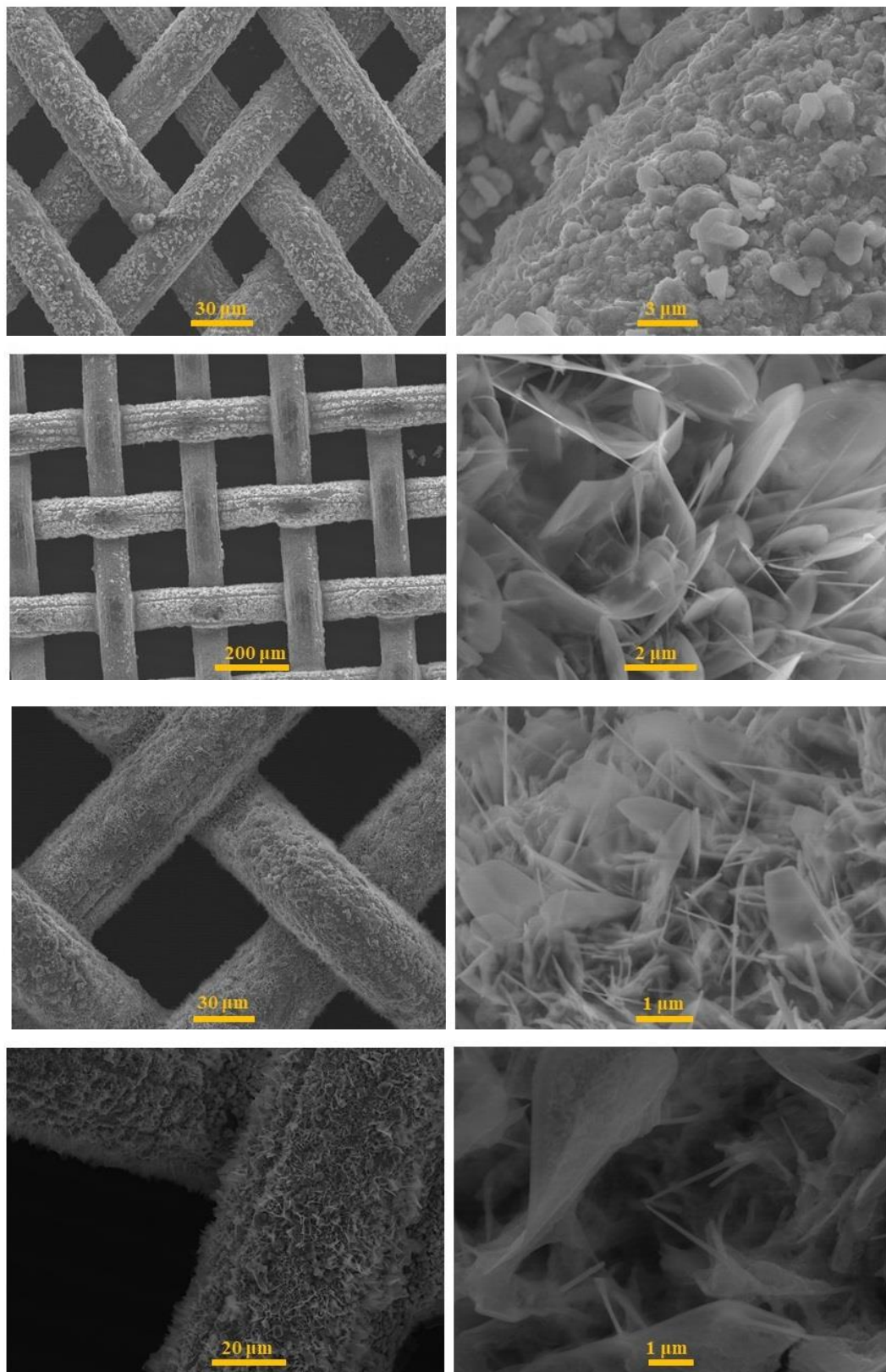
Figure 5.3 SEM images of fabrication of S.S.M from different particle sizes of TiP.

5.3.1.2 Fabrication of mixtures of TiP/ other materials on S.S.M

The fabrication of α-TiP on stainless steel mesh, particularly with unique combinations of TiP with different materials such as metal oxides; shows a significant enhancement in the surface structure along with increasing surface area.
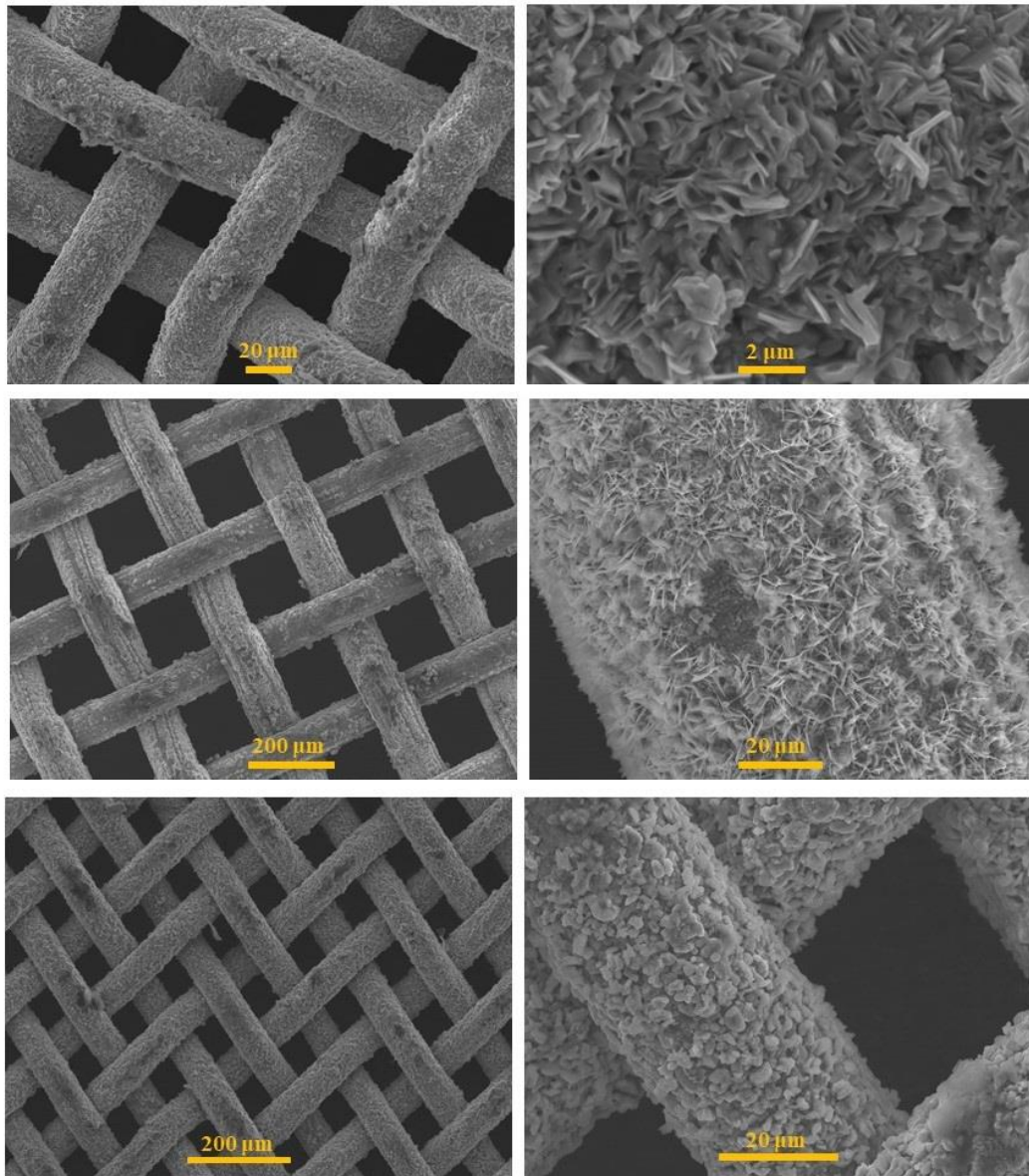
Figure 5.4 SEM images TiP coated S.S.M with different TiP/ metal oxides mixtures.

5.3.2   Increased surface area

The optimized fabrication process results in a coating with a large surface area. This characteristic is crucial for applications involving catalysis, adsorption, or ion exchange, where maximizing the available reactive surface area is key to efficiency. The increased surface area is achieved through the formation of a porous TiP layer, which provides numerous active sites for interactions.

5.3.3   Robust adhesive strength

The TiP coating demonstrated exceptional adherence to the stainless-steel mesh substrate. This strong attachment persists even under challenging conditions such as ultrasonic environments, high-speed fluid flow, and mechanical vibrations. The robust adhesive strength is attributed to the formation of chemical bonds between the TiP and the oxide layer on the stainless-steel surface
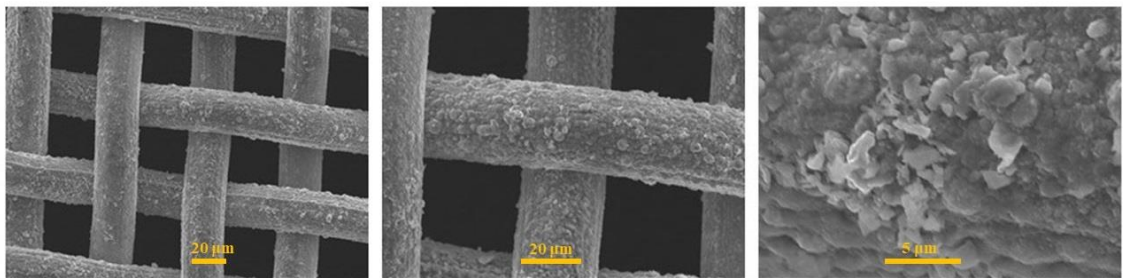
Figure 5.5 SEM images TiP coated S.S.M after exposing to an ultrasonication condition for 1 hour.

5.3.4 Resistance to Extreme Chemical Environments

One of the most striking properties of the TiP-coated S.S.M. is its stability under both highly acidic and strongly basic conditions. The material is resilient when exposed to concentrated hydrochloric acid (HCl) and saturated sodium hydroxide (NaOH) solutions. This chemical resistance is due to the inherent stability of the titanium phosphate structure, which remains intact under extreme pH conditions, making it suitable for applications in harsh chemical environments.
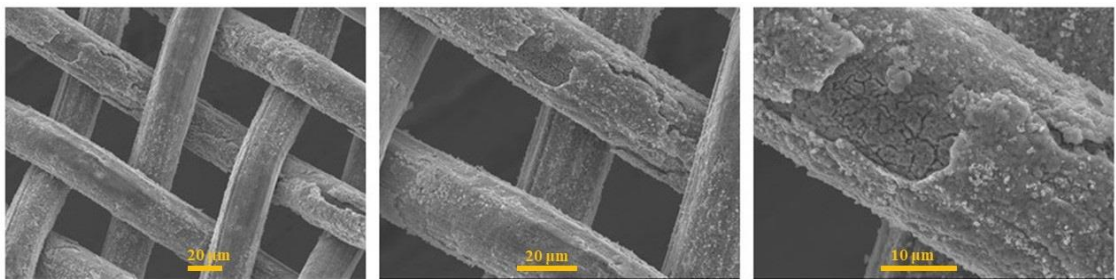
Figure 5.6 SEM images Bare/ un coated S.S.M after exposing to concentrated hydrochloric acid for 1 hour.
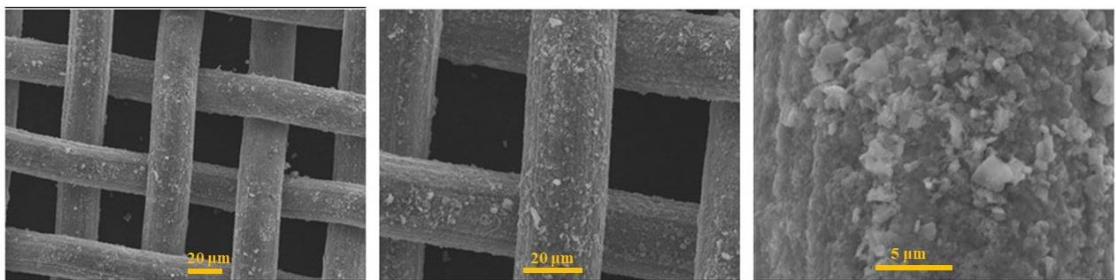
Figure 5.7 SEM images TiP coated S.S.M after exposing to concentrated hydrochloric acid for 1 hour.

5.3.5 Excellent Thermal Stability

The integrity of the coating is maintained even after exposure to temperatures as high as 850°C. This high-temperature stability is particularly noteworthy, as it broadens the

potential applications to include high-temperature catalysis, exhaust systems, and industrial furnace components. The thermal stability is attributed to the strong covalent bonds within the TiP lattice, which prevent degradation at elevated temperatures.

5.4   Enhanced Functionality with TiO_2 Layer

Building upon the impressive properties of TiP-coated S.S.M., have developed a method to fabricate an additional thin layer of TiO_2 on the surface. This innovation further expands the potential applications of the material
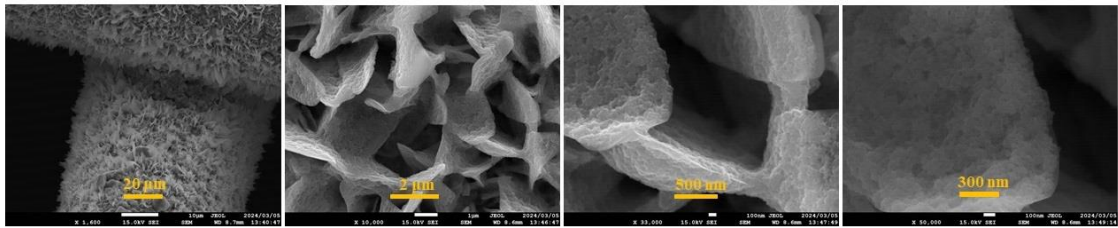
Figure 5.8 SEM images of TiP-coated S.S.M., after fabrication an additional thin layer of TiO_2 on the TiP surface.

5.4.1   Increased surface area

The TiO_2 layer provides an additional increase in the overall surface area of the material, potentially enhancing its performance in catalytic and adsorption applications. The anatase phase of TiO_2 is known for its high surface area and active sites, which can further improve the effectiveness of various processes.

5.4.2   Antivirus/ Antimicrobial Properties

Perhaps one of the most exciting aspects of the combination of TiP and TiO_2 layers is its ability to kill viruses, bacteria, and fungi, even in dark conditions. Figure 5.8 and tbale 5.1 show the antibacterial and antivirus activity comparison by using bare mesh, and TiP mesh with TiO_2 layer. The TiP mesh clearly shows it has very strong antibacterial and antiviral activity in both UV light irradiation and dark conditions. These results strongly prove the antibacterial and antivirus properties of TiP mesh which can be applied to make a better solution against bad odors and biofilm production.

	Mean Infectious Titer (pfu/sample)* [2]		
	0 hours	4 hours	
		Dark Place	0.25mW/cm2
Unprocessed Mesh	2.8*10^6	$2.5*10^6$	$1.9*10^6$
TiP Mesh		$2.7*10^1$	$1.7*10^1$

Table 5.1 Antiviral performance evaluation test using bacteriophage.
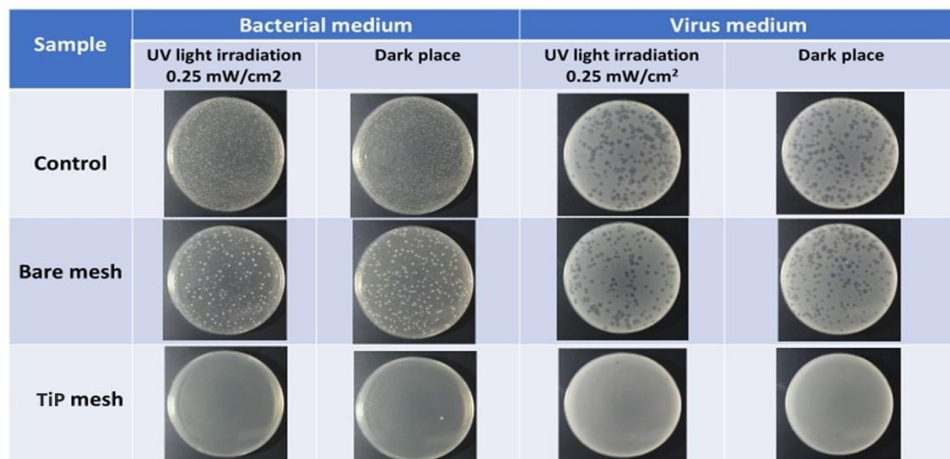

Figure 5.8 Comparison of Antimicrobial And Antivirus Activity.

5.4.3   Proposed Mechanism for the Catalytic Effect

Titanium phosphate is also sometimes referred to as "phosphate titania" or "lightless catalyst[1]. Surprisingly, the TiP mesh has the capability of performing this action even under dark conditions. The mechanism by which TiP mesh decomposes bacteria could be different from that of a general photocatalyst[2]. The TiP mesh has a structure where the surface of a stainless-steel mesh is coated with a nano-structured titanium phosphate, and then an extremely thin film of titanium oxide is applied on TiP of that. However, the technique employed during the manufacturing process is different from the previously reported techniques.

Moreover, the TiP we use has cation exchange capabilities. This ion exchange capability could also allow it to react under conditions without light[3]. As an alternative suggestion, it is possible that the ion exchange characteristics of titanium phosphate generate hydrogen peroxide, which in turn deodorizes and sterilizes due to its expected polarization properties. Regarding the decomposition mechanism, detailed studies have not been done yet and many aspects remain unclear.

Since the outermost layer is titanium oxide, it has high general photocatalytic performance, and the effect of decomposing chemicals with UV irradiation is naturally present. In TiP mesh, an extremely thin titanium oxide film is formed on the nanostructure of titanium phosphate, making it even more reactive than simple titanium phosphate. Therefore, at present, we assume the following two reasons for its high effectiveness: the ion exchange capability of the underlying titanium phosphate influences the charge transfer to the thin titanium oxide film, thereby enhancing the oxidative action of the surface titanium oxide and there are both areas where the titanium phosphate is exposed and areas covered by titanium oxide on the surface, and in multi-step decomposition

reactions, each has complementary actions. In either scenario 1 or 2, it is highly likely that UV irradiation can self-clean the surface of the titanium phosphate, restoring its performance.

5.5 Potential Applications

The unique combination of properties exhibited by the TiP-coated S.S.M., especially with the additional anatase TiO_2 layer, opens up a wide range of potential applications across various industries:

5.5.1 Automotive Industry

The material's high thermal stability and resistance to harsh conditions make it suitable for use in vehicle components such as exhaust systems, catalytic converters, and heat shields. The antimicrobial properties could also be leveraged in air filtration systems for vehicle cabins, ensuring a cleaner and healthier environment for passengers.

5.5.2 HVAC Systems

Commercial air-conditioning systems could benefit from the antimicrobial properties of the material, potentially reducing the spread of airborne pathogens and improving indoor air quality. The durability of the coating ensures long-term effectiveness even in the challenging environments of HVAC systems, where temperature fluctuations and moisture levels can degrade conventional materials.

5.5.3 Water Treatment

Owing to its large surface area, chemical resistance, and antimicrobial properties, this material is highly suitable for water purification and circulation systems. It can be used in filtration membranes, adsorption columns, or as a substrate for advanced oxidation

processes in water treatment plants. Antimicrobial properties also help prevent biofouling, which is a common issue in water treatment systems.

5.5.4 Medical Equipment

The resistance of a material to extreme conditions and its antimicrobial properties make it an excellent candidate for use in medical devices and equipment. Potential applications include surgical instruments, implants, and surfaces in healthcare facilities where maintaining a sterile environment is crucial. TiP coatings can also be applied to medical textiles, such as wound dressings and bandages, to prevent infections.

5.5.5 Catalysis and Chemical Manufacturing

The combination of high surface area, thermal stability, and chemical resistance positions this material as a promising substrate for heterogeneous catalysts. This method could find applications in petrochemical processing, fine chemical synthesis, and environmental remediation. The unique properties of the TiP and TiO2 layers can enhance the efficiency and selectivity of catalytic processes, leading to improved yields and reduced energy consumption.

5.6 Challenges and Future Research Directions

While the use of α-TiP in S.S.M. technology shows great promise, several areas warrant further investigation:

5.6.1 Scalability

Research into scaling up the production process while maintaining the desirable properties of a material is crucial for industrial adoption. This involves developing cost-

effective and efficient manufacturing techniques that can be applied on a commercial scale. Pilot-scale studies and collaboration with industry partners can facilitate the transition from laboratory research to large-scale production.

5.6.2 Long-term Stability

Studies on the long-term stability of coatings under various real-world conditions would provide valuable data for potential applications. This includes assessing the material's performance under different environmental conditions, such as varying temperatures, humidity levels, and exposure to chemicals. Long-term durability tests can help in understanding the material's lifespan and maintenance requirements.

5.6.3 Environmental impact

Comprehensive life cycle assessments of the material, from production to disposal or recycling, would be beneficial for evaluating its overall environmental sustainability. This includes assessing the energy consumption, resource usage, and potential environmental impacts associated with each stage of the material lifecycle. Sustainable production practices and recycling strategies can be developed to minimize the material's ecological footprint.

5.6.4 Customization for Specific Applications

Research into tailoring the properties of the coating (e.g., porosity, surface chemistry) for specific applications could expand its utility across different industries. This involves developing methods to control the microstructure and surface properties of the TiP and TiO_2 layers to suit the requirements of particular applications. For example, modifying

the pore size distribution and surface functional groups can enhance a material's performance in terms of adsorption and catalysis.

References

[1] リン酸チタニア化合物，厚生労働科学研究費補助金（化学物質リスク研究事業） 分担研究報告書.

[2] Abdullah H, Khan MM, Ong HR, Yaakob Z. Modified TiO_2 photocatalyst for CO_2 photocatalytic reduction: an overview. Journal of CO2 Utilization 2017, 22:15-32. https://doi.org/10.1016/j.jcou.2017.08.004.

[3] Sahu BB, Parida K. Cation exchange and sorption properties of crystalline α-titanium (IV) phosphate. Journal of colloid and interface science 2002, 248(2):221-30. https://doi.org/10.1006/jcis.2001.7818.

[4] Wang, C.; Wang, H.; Shankar, K.; Morozov, E. V.; Hazell, P. J. On the Mechanical Behavior of Steel Wire Mesh Subjected to Low-Velocity Impact. Thin-Walled Structures 2021, 159, 107281. https://doi.org/10.1016/j.tws.2020.107281.

[5] Liu, Y.; Zhang, K.; Zhang, D.; Dong, W.; Jiang, T.; Zhou, H.; Li, L.; Mao, B. Industrial Stainless Steel Meshes for Efficient Electrocatalytic Hydrogen Evolution. Journal of energy storage 2021, 41, 102844–102844.

[6] Chen, C.; Wang, Y.; Ge, F. Construction of Corrosion Resistant Stainless Steel Mesh and the Design for Protecting Optical Window Free from Biofouling. Ocean Engineering 2022, 264, 112564. https://doi.org/10.1016/j.oceaneng.2022.112564.

[7] Naderi, A.; Zhang, B.; Belgodere, J. A.; Sunder, K.; Palardy, G. Improved Biocompatible, Flexible Mesh Composites for Implant Applications via Hydroxyapatite Coating with Potential for 3-Dimensional Extracellular Matrix Network and Bone Regeneration. ACS applied materials & interfaces 2021, 13 (23), 26824–26840. https://doi.org/10.1021/acsami.1c09034.

[8] Yue, X.; Zhang, L.; Hua, Y.; Wang, J.; Dong, N.; Li, X.; Xu, S.; Neville, A. Revealing the Superior Corrosion Protection of the Passive Film on Selective Laser Melted 316L SS in a Phosphate-Buffered Saline Solution. Applied surface science 2020, 529, 147170–147170. https://doi.org/10.1016/j.apsusc.2020.147170.

[9] Talha, M.; Ma, Y.; Lin, Y.; Singh, A.; Liu, W.; Kong, X. Corrosion Behavior of Austenitic Stainless Steels in Phosphate Buffer Saline Solution: Synergistic Effects of Protein Concentration, Time and Nitrogen. New Journal of Chemistry 2019, 43 (4), 1943–1955. https://doi.org/10.1039/c8nj04670k.

[10] Pierre, C.; Bertrand, G.; Rey, C.; Benhamou, O.; Combes, C. Calcium Phosphate Coatings Elaborated by the Soaking Process on Titanium Dental Implants: Surface Preparation, Processing and Physical—Chemical Characterization. Dental Materials 2019, 35(2), e25— e35. https://doi.org/10.1016/j.dental.2018.10.005.

[11] Rokosz, K.; Hryniewicz, T.; Kacalak, W.; Tandecka, K.; Raaen, S.; Gaiaschi, S.; Chapon, P.; Malorny, W.; Matýsek, D.; Pietrzak, K.; Dudek, Ł. Phosphate Coatings Enriched with Copper on Titanium Substrate Fabricated via DC-PEO Process. Materials 2020, 13(6), 1295. https://doi.org/10.3390/ma13061295.

[12] Sarraf, M.; Rezvani Ghomi, E.; Alipour, S.; Ramakrishna, S.; Liana Sukiman, N. A State-of-The-Art Review of the Fabrication and Characteristics of Titanium and Its Alloys for Biomedical Applications. Biodesign and Manufacturing 2021, 1–25. https://doi.org/10.1007/s42242-021-00170-3.

CHAPTER 6
CONCLUSIONS

This study presents a novel and efficient route (alkali roasting method) for the preparation of high-yield and high-purity α-TiP from ilmenite ore, outperforming the previously reported direct digestion method, which involved direct digestion of ilmenite with concentrated H_3PO_4. The key findings and conclusions are as follows:

1. The novel alkali roasting method involves a two-step process: (i) initial roasting of ilmenite with KOH at 800 °C for 4 hours, and (ii) subsequent acid digestion of the roasted product with conc. H_3PO_4 to produce a white precipitate identified as α-TiP.

2. The alkali roasting method achieved a remarkably high α-TiP yield of approximately 99.6 wt.%, a significant improvement over the 18 wt.% yield obtained from the direct digestion method. However, the as-synthesized α-TiP contained approximately 3.5% iron as a major impurity.

3. To further purify the α-TiP, five acid washing cycles were performed using iron-chelating acids: concentrated H_3PO_4, conc. HCl, and saturated $H_2C_2O_4$. These washing steps effectively reduced the iron content in the final product.

4. The H_3PO_4 washing cycles yielded α-TiP with a purity of 99.8 wt.% and a yield of 92.5 wt.%, demonstrating exceptional iron removal efficiency, with the iron content reduced from 3.5% to 0.4%.

5. The HCl washing cycles were less effective, producing α-TiP with a purity of 87.1 wt.% and a yield of 76.6 wt.%. Additionally, undesirable leaching of titanium from the α-TiP structure was observed during the HCl washing process.

6. The $H_2C_2O_4$ washing cycles led to the chemical transformation of α-TiP into the relatively unexplored titanyl pyrophosphate phase, $(TiO)_2P_2O_7$. After calcination at 800 °C, this phase was obtained with a purity of 84.7 wt.% and a yield of 56.7 wt.%.

7. Thermogravimetric analysis revealed a two-stage decomposition process for α-TiP, involving initial water loss and subsequent pyrophosphorization to form the layered TiP_2O_7 phase, which further transformed into cubic TiP_2O_7 upon heating to 850 °C. The $(TiO)_2P_2O_7$ phase exhibited a three-stage decomposition behavior, suggesting the elimination of water/hydroxyl groups during the heating process.

8. The fabrication of α-TiP on stainless steel mesh was successfully done in a very simple and cost-effective way which needs very lesser and inexpensive chemicals with less preparation time.

09. The fabrication of α-TiP on stainless steel mesh, particularly with the addition of a TiO_2 layer, represents a significant advancement in materials science and engineering. Its unique combination of properties, including robust adhesion, resistance to extreme conditions, and high surface area, position it as a versatile material with potential applications across numerous industries.

10. As research in this field progresses, we anticipate further refinements in the fabrication process, a deeper understanding of the material's properties, and the development of novel applications. The ongoing experiment results suggest that this technology is poised for commercialization, potentially leading to transformative impacts in sectors ranging from automotive and environmental technology to healthcare and chemical manufacturing.

11. The success of this innovation also highlights the importance of interdisciplinary research in materials science, combining principles from chemistry, physics, and engineering to create materials with properties that exceed the sum of their parts. As we continue to face global challenges in areas such as energy efficiency, environmental protection, and public health, materials such as α-TiP in S.S.M. offer promising solutions and inspire further innovations in the field of advanced materials.

CHAPTER 7
RECOMMENDATIONS

While this study presents a novel and efficient method for the high-yield and high-purity extraction of α-titanium phosphate (α-TiP) from ilmenite ore, several areas can be further explored and optimized for future research and industrial applications:

1. Process optimization: The KOH roasting step and the subsequent acid digestion conditions, such as temperature, time, and reagent concentrations, can be further optimized to maximize the yield and purity of the desired α-TiP product.

2. Scale-up and industrial implementation: The developed method should be scaled up and evaluated for its feasibility and economic viability in industrial-scale operations. Factors such as cost-effectiveness, energy consumption, and environmental impact should be thoroughly assessed.

3. Alternative roasting agents: In addition to KOH, the potential of other roasting agents or combinations thereof can be explored for improved titanium recovery and reduced impurity levels in the final product.

4. Leaching and purification strategies: While the acid washing cycles effectively removed iron impurities, the development of more efficient and environmentally friendly leaching and purification strategies could be investigated. This may include the exploration of alternative chelating agents, selective precipitation techniques, or the application of membrane separation processes.

5. Characterization and applications of $(TiO)_2P_2O_7$: The formation of the relatively unexplored titanyl pyrophosphate phase, $(TiO)_2P_2O_7$, during the oxalic acid washing process presents an opportunity for further characterization and investigation of its potential applications in various fields, such as catalysis, energy storage, and advanced materials.

6. Integration with value-added product development: The purified α-TiP and $(TiO)_2P_2O_7$ obtained from this study could be further explored for their potential applications in the development of value-added products, such as pigments, catalysts, or functional materials.

7. Life cycle assessment and sustainability: A comprehensive life cycle assessment should be conducted to evaluate the environmental impact and sustainability of the proposed method, taking into account factors such as resource consumption, energy usage, and waste management.

8. Techno-economic analysis: A detailed techno-economic analysis should be performed to assess the economic feasibility and potential profitability of the developed method, considering factors such as capital and operating costs, product value, and market demand.